MPLP X

Book of Abstracts

2026

Table of contents

Monday
August 24

Monday	Tuesday	Wednesday	Thursday	Friday	Saturday	Sunday
27	28	29	30	31	1	2
3	4	5	6	7	8	9
10	11	12	13	14	15	16
17	18	19	20	21	22	23
24	25	26	27	28	29	30
31	1	2	3	4	5	6

Precision Measurement with Atom Interferometry

Mingsheng Zhan[1,2,3,*]
[1]*Wuhan Institute of Physics and Mathematics, Innovation Academy for Precision Measurement Science and Technology, Chinese Academy of Sciences, Wuhan 430071, China*
[2]*Hefei National Laboratory, Hefei 230088, China*
[3]*Wuhan Institute of Quantum Technology, Wuhan 430206, China*

*E-mail: mszhan@apm.ac.cn

Atoms are the core basic structure level of matters. They serve as bridges connecting microcosmic and macroscopic phenomena, as well as classical - quantum correspondence. Laser cooled and coherently controlled atoms offer unique advantages in demonstrating wave-particle duality. On one hand, when these atoms are manipulated via high-precision optical tweezers to form a single-atom array, they constitute the core of an atom quantum computer and work as a platform for multi-body physics study. Meanwhile, when atoms undergo coherent manipulation to form a matter-wave interferometer, they can be utilized for precision measurements in fundamental physics experiments, as well as for applications in quantum sensing and metrology as atomic quantum interference devices (AQUIDs).

In this talk I will address these issues by presenting recent experimental progress in my group in precise atomic coherence control of a ^{85}Rb-^{87}Rb dual-species sysytem [1]. It includes magic-intensity optical dipole traps [2], heteronuclear single atom arrays with second order coherence time [3], quantum gates with fidelity greater than 99.995% [4], quantum entanglement of heteronuclear atoms [5], coherently forming a single ultracold molecule in an optical trap [6] and defect-free preparation of heteronuclear single atom arrays of arbitrary configurations [7]. I will also outline the development of long-baseline dual-species atom interferometers (AIs), including the Wuhan 10-meter fountain AI [8], the Chinese Space Station AI [9-11], and the planned Zhaoshan long-baseline Atom Interferometer Gravitation Antenna (ZAIGA) [12]. The progress with the interferometers in quantum test of the Einstein's weak equivalence principle [13-14] and a wide variety of AQUIDs will be discussed.

References

[1] M. S. Zhan, *Physics (in Chinese)* **44**, 518 (2015); *ibid*. **51**, 92 (2022).
[2] J. H. Yang et al., *Phys. Rev. Lett.* **117**, 123201 (2016).
[3] R. J. Guo et al., *Phys. Rev. Lett.* **124**, 153201 (2020).
[4] C. Sheng et al., *Phys. Rev. Lett.* **121**, 240501 (2018).
[5] Y. Zeng et al., *Phys. Rev. Lett.* **119**, 160502 (2017).
[6] X. D. He et al., *Science* **370**, 331 (2020).
[7] C. Sheng et al., *Phys. Rev. Lett.* **128,** 083202 (2022).
[8] L. Zhou et al., *Gen. Relativ. Gravit.* **43**, 1931 (2011).
[9] M. He et al., *npj Microgravity* **9**, 58 (2023).
[10] J.T. Li et al., *Nat. Sci. Rev.* **12**(4), nwaf012 (2025).
[11] D.F. Zhang et al., *Sci. Adv.* (in press, 2026); arXiv:2603.22981.
[12] M. S. Zhan et al., *Int. J. Mod. Phys. D* **29**, 1940005 (2020).
[13] L. Zhou et al., *Phys. Rev. Lett.* **115**, 013004 (2015).
[14] L. Zhou et al., *Phys. Rev. A* **104**, 022822 (2021).

Synchrotron Radiation Facility SKIF: project implentation status, research program, and infrastructure development

Y.V. Zubavichus, E.B. Levichev

Synchrotron Radiation Facility SKIF, Koltsovo, Novosibirsk Region, Russia

E-mail: ya.v.zubavichus@srf-skifaser.nsc.ru

Synchrotron Radiation Facility SKIF is a novel large-scale research facility being currently constructed in the Science City of Koltsovo, 15 km apart from Novosibirsk. The 3 GeV electron storage ring designed by specialists from the Budker Institute of Nuclear Physics SB RAS (Novosibirsk) augmented with advanced superconducting undulators will provide the record low emittance of 75 pm·rad to serve the beamlines with ultrabright photon beams [1]. Construction of SKIF is generally complete (Fig. 1). Full commissioning of the complex is expected by the end of 2026. The normal user operation should start in 2027.

Detailed technical specifications of the accelerator complex as well as seven first-priority beamlines are given. X-ray techniques implemented at the first-priority beamlines of SKIF are discussed within the context of SKIF research program.

Principles of the SKIF user policy are briefly outlined, including the system for the submission and expert evaluation of beamtime proposals. Infrastructure development program of SKIF aimed at the construction of second-priority beamlines (30 in total) is envisaged.

Fig. 1 Digital model of SKIF (left) and real aerial photo of the construction site as of mid of July, 2026

Authors thank the Russian Ministry of Science and Higher Education for the partial financial support within the SKIF governmental order.

References

[1] A.V. Bukhtiyarov et al., Cryst. Rep. **67**, 690 (2022).

I parallel

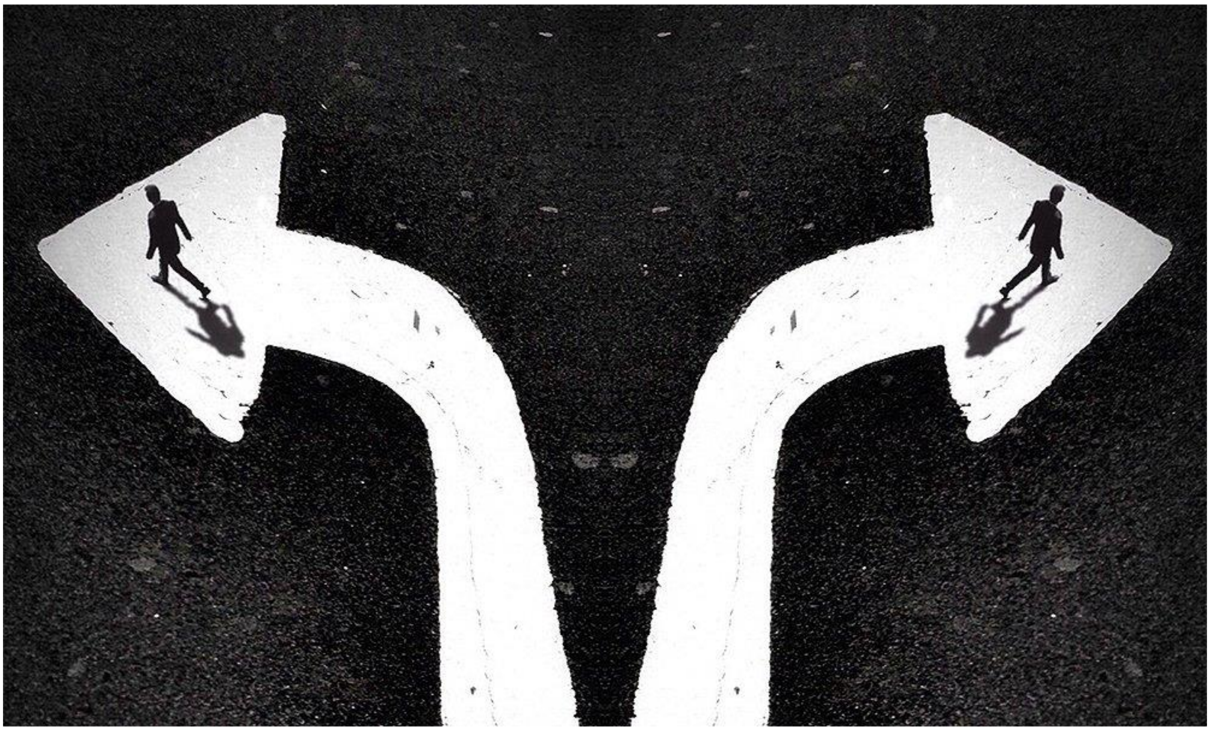

Extreme Ultraviolet Frequency Comb and Its Applications

Linqiang Hua[1,2], **XiaoJun Liu**[1,2]
[1]*Innovation Academy for Precision Measurement Science and Technology, Chinese Academy of Sciences, Wuhan 430071, China*
[2]*University of Chinese Academy of Sciences, Beijing 100080, China*
Email: hulq@apm.ac.cn, xjliu@apm.ac.cn

VUV/XUV frequency comb technique have opened a shared frontier bridging precision spectroscopy and ultrafast science since their first demonstration in 2005 [1-2]. In this talk, we will present the realization of a VUV/XUV frequency comb system via intra-cavity high-harmonic generation (HHG) at the Innovation Academy for Precision Measurement Science and Technology, Chinese Academy of Sciences. After years of systematic optimization, we have realized stable operation of this VUV/XUV system featuring high output power, long continuous runtime, and controllable transverse mode shaping [3-4]. Enabled by this high-performance source, we aim to explore new frontiers across atomic, molecular, and even nuclear physics [5].

References

[2] R. J. Jones et al., Phys. Rev. Lett. **94**, 193201 (2005).
[3] C. Gohle et al., Nature **436**, 234–237 (2005).
[4] M. Zhu et al., Opt. Lett. **49**, 3757 (2024).
[5] R. Xiao Opt. Lett. **50**, 5153 (2025).
[6] T. Xin et al., National Science Review **12**, 1 (2025).

Three-photon laser excitation of Rydberg atoms for quantum information

I.I. Ryabtsev[1, 2], **I.I. Beterov**[1, 2], **N.N. Bezuglov**[1, 3], **E.A. Yakshina**[1, 2], **G. Suliman**[1, 2], **D.B. Tretyakov**[1], **V.M. Entin**[1], **K. Miculis**[4, 5]
[1]*Rzhanov Institute of Semiconductor Physics SB RAS, 630090 Novosibirsk, Russia*
[2]*Novosibirsk State University, 630090 Novosibirsk, Russia*
[3]*Saint-Petersburg State University, 199034 Saint-Petersburg, Russia*
[4]*Institute of Atomic Physics and Spectroscopy, University of Latvia, LV-1004 Riga, Latvia*
[5]*National Research Nuclear University MEPhI, Moscow, 115409 Russia*
E-mail: ryabtsev@isp.nsc.ru

Three-photon excitation of Rydberg states is of interest for performing quantum gates on single neutral atoms trapped in optical dipole traps [1] and for improving the sensitivity of quantum sensors of electric fields based on electromagnetically induced transparency at Rydberg excitation of alkali-metal atoms in optical gas cells [2]. Three-photon excitation can be implemented in a star-like geometry with a zero sum of the wave vectors of the three laser beams. In this case, both the recoil effect during laser excitation and the residual Doppler effect are suppressed [3].

In our experiments, we investigated the features of three-photon excitation $5S_{1/2}\rightarrow 5P_{3/2}\rightarrow 6S_{1/2}\rightarrow nP_{3/2}$ of Rydberg states of ultracold Rb atoms. The first experiments were performed with disordered mesoscopic ensembles of Rydberg atoms in a magneto-optical trap with their detection by the method of selective field ionization with the number of atoms resolution [1,4-7]. The spectra [1,4-6] and the time dynamics [7] of three-photon excitation of states with the principal quantum number n=37-120 were studied using the radiation of three cw single-frequency lasers.

We then moved on to experiments with single Rb atoms in arrays of optical dipole traps. Optical pumping and single-qubit quantum gates with individual addressing were demonstrated [8,9], and three-photon laser excitation of a single Rb atom in an optical dipole trap was realized [10]. Excitation to the Rydberg state was detected optically by the disappearance of resonant fluorescence. After narrowing the laser line widths, coherent Rabi oscillations were observed for the first time during three-photon excitation of a single Rb atom [11].

To describe the experiments, a theoretical model was constructed that revealed a number of new features of three-photon excitation that make it possible to improve the fidelity of quantum gates and individual addressing of single Rb atoms in trap arrays [12]. It was shown that with strong laser excitation at the second step with the Rabi frequency Ω_2 and moderate excitation at the first and third steps with the Rabi frequencies Ω_1 and Ω_3, the three-photon Rabi frequency is determined by the expression $\Omega=\Omega_1\Omega_3/\Omega_2$. If we form three exciting laser beams in such a way that the spatial distributions of $(\Omega_1\Omega_3)$ and Ω_2 are identical, then Ω becomes independent of the position of the atom within the laser beams, even for very tightly focused beams. This was confirmed by analytical and numerical simulations of Rabi oscillations at three-photon excitation. For two-photon excitation, a strong decrease in the contrast of two-photon Rabi oscillations was observed in the numerical simulation as the waist radius decreased. The work on implementing this idea is in progress.

This work was supported by the Russian Science Foundation (project 23-12-00067-П, https://rscf.ru/project/23-12-00067-П/).

References

[1] I.I.Ryabtsev et al., Physics − Uspekhi **59**, 196 (2016).
[2] I.I.Ryabtsev, et al., Radiophysics and Quantum Electronics **67**(1), 1 (2024).
[3] I.I. Ryabtsev et al., Phys. Rev. A **84**, 053409 (2011).
[4] V.M.Entin et al., JETP **116**(5), 721 (2013).
[5] E.A.Yakshina et al., Quantum Electronics **48**(10), 886 (2018).
[6] E.A.Yakshina et al., JETP **130**(2), 170 (2020).
[7] D.B.Tretyakov et al., Quantum Electronics **52(**6), 513 (2022).
[8] I.I.Beterov et al., JETP **132**(3), 341 (2021).
[9] I.I.Beterov et al., Quantum Electronics **51**(6), 464 (2021).
[10] I.I.Beterov et al., JETP **137**(2), 246 (2023).
[11] I.I.Beterov et al., Zh. Eksper. Teor. Fiz. **166**, 535 (2024), English translation: arXiv: 2410.01703.
[12] N.N. Bezuglov et al., Phys. Rev. A **112**, 063103 (2025).

Experimental investigation of photon frequency shift in stimulated emission

P.L. Chapovsky[1,2,3]
[1]*Institute of Automation and Electrometry, SB RAS, Novosibirsk, Russia*
[2]*Institute of Laser Physics, SB RAS, Novosibirsk, Russia*
[3]*Iternational Tomography Center, SB RAS, Novosibirsk, Russia*
E-mail: pavel.chapovsky@gmail.com

Einstein introduced stimulated emission of electromagnetic radiation by atoms in his 1916 paper on Planck distribution for blackbody radiation spectrum. In subsequent papers, Einstein postulated identical characteristics of photons incident on an atom and photons produced by stimulated emission. In modern quantum electrodynamics, stimulated emission of a photon occurs in the state of the incident photon, with conservation of energy, wave vector, and phase of the photon wave function. These fundamental laws of stimulated emission require experimental verification.

In this report, we discuss the experiments [P.L. Chapovsky, arXiv:2504.11802 (2025); JETP, **168**, 55 (2025)] on testing the conservation of photon energy in stimulated emission. The experiments investigate the beat frequency of the amplified radiation with the radiation incident on an optical amplifier using Mach-Zehnder interferometer. The principle scheme of the experiment is shown in Fig.1a. The incident radiation was generated by a semiconductor laser (Toptica, Germany) with a wavelength of 780 nm and a linewidth of 0.5 MHz. Light amplification is performed by a semiconductor tapered amplifier (Eagleyard Photonics, Germany). Acousto-optic modulators (AOM) shift the frequencies of the optical beams in two arms of the Mach-Zehnder interferometer by 76 MHz and 76 MHz + 0.11 Hz.

The optical beat signals at the output of the Mach-Zehnder interferometer (Fig.1b) are detected and approximated by a harmonic function using the least-squares method. This yields the optical beat frequencies without an amplifier and with the amplifier in one arm of the interferometer. It was found that the frequency of the amplified radiation is shifted relative to the frequency of the radiation incident on the amplifier by $\Delta\nu = (+640 \pm 80)$ μHz. In relative units, this small frequency shift is equal to

$$\Delta\nu/\nu = (+1.7 \pm 0.2) \cdot 10^{-18}\,.$$

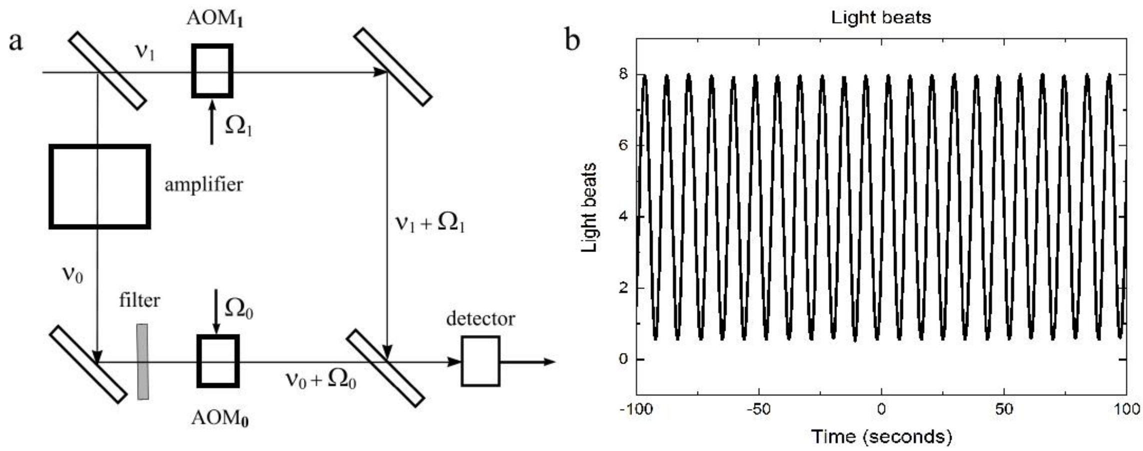

Fig. 1. a – Mach-Zehnder interferometer with tapered amplifier in one arm. b – Fragment of optical beats at the frequency 0.11 Hz.

In this report, we discuss possible origins of the observed frequency shift in stimulated emission of radiation. We discuss also a few future applications of the developed experimental technique for precise detection of radiation frequency variations in optical phenomena.

Nuclear Optical Clocks

S.M. Ignatovich[1], O.N. Prudnikov[1,2*], A.V. Taichenachev[1,2*], V.I. Yudin[1,2,3]

[1]*Institute of Laser Physics, Laser Physics Department, 630090, Novosibirsk, Russia*

[2]*Novosibirsk State University, Physics Department, 630090, Novosibirsk, Russia*

[3]*Novosibirsk State Technical University, 630073, Novosibirsk, Russia*

*E-mail:*taichenachev@mail.ru*

As is well known [1], time and frequency are the most accurately measured physical quantities. Modern optical frequency standards (atomic optical clocks) based on ensembles of ultracold atoms in optical lattices and single ions in radio-frequency traps have achieved relative instability and frequency uncertainty at the level of 10^{-18} (and even slightly better) [2–5].

However, in light of recent experimental achievements and theoretical analysis, it seems highly likely that the next decisive step in improving the metrological characteristics of quantum frequency standards will be made based on the transition in the nucleus of the 229Th isotope between the ground and low-lying isomeric states with an energy of 8.4 eV. As is known (see [7] and references therein), the first indications of the existence of a low-lying isomeric state in thorium-229 were obtained back in the 1970-s. The first proposal to excite the isomeric state of thorium-229 by optical photons using the electron bridge mechanism belongs to E.V. Tkalya [8]. The pioneering proposal to create an ultra-precise optical clock based on this transition was made by E. Pike and C. Tamm in [9]. The main idea of this work was that the frequency of the transition in the nucleus is significantly less sensitive to changes in external conditions compared to the frequency of any transition in the electron shell of the atom. Even then, it was noted that it was possible to directly excite the transition with radiation from an ultrastable laser or a femtosecond laser comb and detect the transition by fluorescence or by changes in the hyperfine splitting frequency. Various options for precision spectroscopy of the transition were discussed: in radiofrequency traps using laser cooling or in transparent crystals ($Th0_2$, ThF_4). In [10], a realistic estimate of the relative uncertainty of the frequency standard based on laser-cooled $^{229}Th^{3+}$ ions in a trap was given at a level of 10^{-19}. The possibility of achieving similarly high metrological characteristics in solid-state nuclear clocks was investigated in [11]. In this talk, we briefly review the latest advances in optical clocks based on the ground-isomeric state transition in the thorium-229 nucleus. A short prehistory of the search for optical nuclear transition as well as pioneering proposals to use this transition for nuclear optical clocks [7-9] are present. Recent experimental observations of direct laser excitation of this transition [12] are discussed in detail. We also outline the main challenges that need to be addressed on the way to creating nuclear-optical clocks with a relative uncertainty of the order of 10^{-19} – 10^{-20}. Particular attention is focused on our proposal on the two-photon optical nuclear clock [13].

This work is performed within the state assignment FWGU-2026-0013.

References

[1] F. Riehle, Frequency Standards: Basics and Applications (Wiley-VCH, Weinheim, 2005).
[2] N. Hinkley et al., Science **341**, 1215 (2013).
[3] N. Huntemann et al., Phys. Rev. Lett. **116**, 063001 (2016).
[4] S.M. Brewer et al., Phys. Rev. Lett. **123**, 033201 (2019).
[5] A. Aeppli et al., Phys. Rev. Lett. **133**, 023401 (2024).
[6] H.N. Hausser et al., arXiv:2402.16807 (2024).
[7] E.V. Tkalya, Phys. Usp. **46**, 315 (2003).
[8] E.V. Tkalya, JETP Lett. **55**, 211 (1992).
[9] E. Peik et al., Europhys. Lett. **61**, 181 (2003).
[10] C.J. Campbell et al., Phys. Rev. Lett. **108**, 120802 (2012).
[11] G.A. Kazakov et al., New J. Phys. **14**, 083019 (2012).
[12] J. Tiedau et al., Phys. Rev. Lett. **132**, 182501 (2024); R. Elwell et al., Phys. Rev. Lett. **133**, 013201 (2024); C. Zhang et al., Nature **633**, 63 (2024).
[13] V.I. Yudin et al., JETP Lett. **121**, 365-374 (2025).

Research and Application of Miniaturized Single-ion Optical Clock

Xueren Huang[1,2], Jian cao[1,2] Yi Yuan[1,2], Xuanjian Wang[1,2], Jian cao[1,2]
Xinyue Guo[1,2], Huitao Ren[1,2], Hualin Shu[1,2]

[1]*Innovation Academy for Precision Measurement Science and Technology, Chinese Academy of Sciences, Wuhan 430071, China*

[2]*University of Chinese Academy of Sciences, Beijing 100080, China*

Email: hxueren@apm.ac.cn,

Time and frequency rank among the physical quantities with the highest attainable measurement precision to date., Recently atomic clocks based on optical transitions have surpassed the performance of cesium clocks by two orders of magnitude,.High precision optical clocks demonstrate broad application prospects in the field of precision measurement.

Firstly,In this talk, I will report a robust, compact, and transportable optical clock (TOC-729-2) based on a trapped single 40Ca+ion with a systematic uncertainty of 1E-17, This TOC was constructed in a volume of 0.33 m3 excluding the controlling electronics in 19-in. racks. After being moved 1200 km away by express delivery, With the TOC uptime of 92% in 35-day period, the absolute frequency of the 729 nm Clock transition of $^{40}Ca^{+}$ was measured using a satellite link to International Atomic Time (TAI) to provide traceability to the SI second, and the absolute frequency result is 411 042 129 776 400.15(22) Hz, corresponding to a relative uncertainty of 5:3 E-16.

Secondly, We will introduce the deployment of a compact and transportable optical clock (TOC) to a timekeeping institution and steering an active hydrogen maser (HM) to generate an optical time scale (OTS), realizing the upgrade of the local time scale. This steering experiment with a deployable optical clock marks a significant advancement, demonstrating that a timing accuracy below 100 ps per month can be achieved feasibly in various timekeeping institutions.

References

[1] J. Cao, et al., Applied Physics Letters **120**(5), (2022).
[2] Y. Wei, et al., Phys. Rev. Lett. **133**(033001) (2024).
[3] Y. Yuan et al., Physical Review Applied **21**(4) (2024).
[4] X. Wang et al., Applied Physics B **131**(225) 001-008 (2025).
[5] Y. Yuan et al., Metrologia **63**(025003) 2026.

Precision Laser Spectroscopy via Coulomb Crystals

Wen-cui Peng, Sheng-Guo He, Xin Tong
Innovation Academy for Precision Measurement Science and Technology, Chinese Academy of Sciences, Wuhan 430071, People's Republic of China
E-mail: tongxin@wipm.ac.cn

Ion-trapped atomic and molecular ions, cooled via direct laser cooling or sympathetic cooling, form ordered Coulomb crystals. Benefiting from long trapping and state lifetimes in nearly perturbation-free environments, such crystals serve as excellent platforms for high-precision laser spectroscopy. Here, we present high-precision spectroscopic measurements of trapped Be^+ and HD^+ ions based on Coulomb crystal systems for fundamental physics research.

We measured the magnetically insensitive ground-state hyperfine transition of Be Coulomb crystals in a linear Paul trap using microwave-driven state transfer [1]. After high-order Zeeman correction across a ±0.5 mT magnetic field range, the hyperfine structure constant *A* was determined to be −625.008 840(35) MHz with a relative precision of 5.6×10^{-8}, yielding a nuclear Zemach radius of 4.03(5) fm via the point-nucleus approximation.

We also develop a novel method that integrates the quantum state preparation of polar molecular ions [2] and the detection of spatially resolved fluorescence for the high-precision spectroscopy of HD^+ ions [3]. This method suppresses common-mode noise arising from fluorescence fluctuations and reduces the state redistribution induced by blackbody radiation. We achieve the first measurement of the HD^+ $(0, 0)\rightarrow(6, 1)$ rovibrational transition at 303.3965067(20) THz, consistent well with QED predictions. This Coulomb crystal-based technique enables precise determinations of fundamental physical constants and promising explorations of higher-order QED effects.

References

[1] Z. Ao, W. Bai, Q. Zhang, W. Peng, X. Tong, Phys. Rev. A **113**, 042822 (2026).
[2] Y. Zhang et al. Phys. Rev. A **107**, 043101 (2023).
[3] Q. Zhang et al. Phys. Rev. A **112**, 32801 (2025).

Research on the Interference Coupling Model of Optical Fiber Microcavity and Multi-Parameter Sensing Technology

Shuang Wang[1,2], Hongyu Liu[1], Penghui Dai[1], Tianxiang Sun[1], Xueyi Wu[1], Lu Tian[1], Xiaoshuang Dai[1], Junfeng Jiang[1] and Tiegen Liu[1]

[1]*State Key Laboratory of Precision Measurement Technology and Instruments, Tianjin University, Tianjin 300072, China*

[2]*School of Electronic Science and Technology, Hainan University, Haikou 570228, Hainan, China*

E-mail: shuangwang@tju.edu.cn

To address the discrepancy between the theoretical and actual spectra for micro-electro-mechanical system (MEMS) optical fiber composite micro-cavity sensors [1-2], we analyze the interference effects within the micro-cavity, incorporating the multi-beam interference effects within the sensitive chip and the coupling coefficients. A spectral model for MEMS-based optical fiber composite micro-cavity sensors is established, providing a theoretical foundation for early-stage chip design and significantly reducing fabrication costs.

Employing beam transport iteration, this work divides light passing through interfaces into equal reflection and transmission beams until the intensity decays to a set threshold. Spectral simulations are conducted from the perspectives of coupling coefficients and multi-beam interference. The reliability of the theoretical formulas is validated, and the impact of spectral overlap on experimental results is confirmed. Based on Fresnel equations, Gaussian beam propagation characteristics, and the ABCD matrix, the model treats light within the cavity as multi-beam interference, with separate reflection and transmission calculations to derive the total electric field. And the results are shown in Fig. 1(a)-(d).

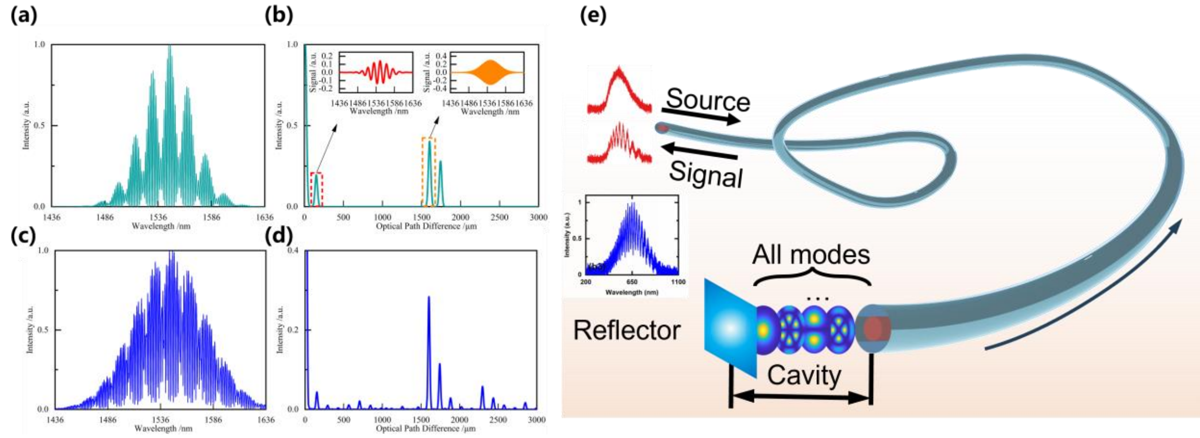

Fig. 1 (a) Spectrum under the classical model, (b) Frequency spectrum under the classical model, (c) Spectrum under the coupling model, (d) Frequency spectrum under the coupling model, (e) Multimode decoherence model

In addition, to resolve the longstanding ambiguity in the theoretical description of multimode Fabry-Perot (FP) interferometry a theoretical analysis is performed on the multimode fiber FP interference model based on the previous research [3] as shown in Fig. 1(e). Experimental verification confirms that, due to the decoherence effect, the end face of the multimode fiber, when serving as a reflecting surface, produces FP interference only for short cavities. We present a theoretical method for improving the coherent-regime SNR, which provides a scheme for optical fiber sensing. Its applications in temperature-pressure sensing, vibration detection, localization, and energy monitoring are then discussed.

This work was supported by National Natural Science Foundation of China 62575206 and Tianjin Natural Science Foundation 24JCYBJC00140.

References

[1] Wang X, et al. Photonics Research **9**(4) 521-529 (2021).
[2] Chen X, et al. Optics Communications **506** 127580 (2022).
[3] Xuan Wu, et al, Opt. Express **21**, 14487-14499 (2013).

Exploration of fiber-based and fiber-coupled photonic devices at cryogenic temperatures down to 4 K

B. Nyushkov[1], I. Novikov[1], N. Golovin[1], K. Savinov[1], A. Krivetsky[1], M. Radchenko[1], V. Boldyrev[1], A. Dmitriev[1], I. Korel[1], and A. Vostretsov[1]
[1]*Novosibirsk State Technical University*
E-mail: nyushkov@corp.nstu.ru

Research into characteristics of photonic elements and devices under cryogenic conditions advances photonics technologies in metrology, quantum computing, and space instrumentation. Until now, research at ultra-low temperatures (<10 K) has been limited to a few elements, such as photodiodes, fibers, and fiber gratings [1-3]. Our work expands the range of such cryogenic devices.

We conducted thermal cycling (across the 4–300 K temperature range) of fiber splitters coupled uniquely with fiber Bragg gratings to form a cryogenic spectral demultiplexer. We propose using this demultiplexer with cryogenic photodiodes as a multichannel cryogenic photonic interface for driving superconducting qubits. Our experiment is the first proof-of-concept for such an all-optical cryogenic demultiplexer. Earlier, only an optoelectronic demultiplexer had been reported for this purpose [3].

We demonstrate the first all-cryogenic Er-doped fiber laser operating at 4 K. Stable continuous-wave and gain-switched regimes are achieved at this temperature. We reveal that upon cooling, the slope efficiency increases notably, most probably due to the suppression of the phonon-mediated depletion of the upper laser level [4]. Figure 1 displays the fiber laser mounted on the cryostat's cold finger, alongside the laser's power characteristics at temperatures of 298 K and 4 K. Changes in the lasing wavelength and intermode frequency were investigated across the 4–300 K temperature range. Thermal cycling in this range confirmed the reproducibility of the laser performance.

Through this study, we tested a complex experimental setup – a two-stage, pulse-tube helium sorption refrigerator upgraded with fiber-optic vacuum feedthroughs and photonic instrumentation. It allows further in-depth cryogenic studies of various photonic devices even at temperatures <4 K.

(a)

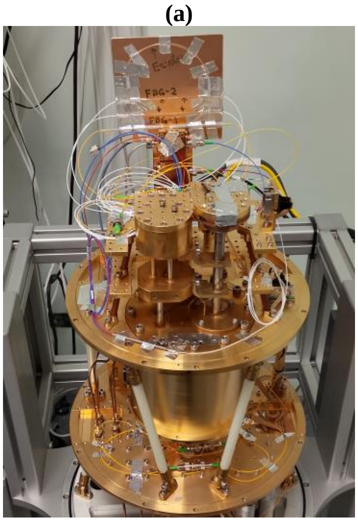

(b)

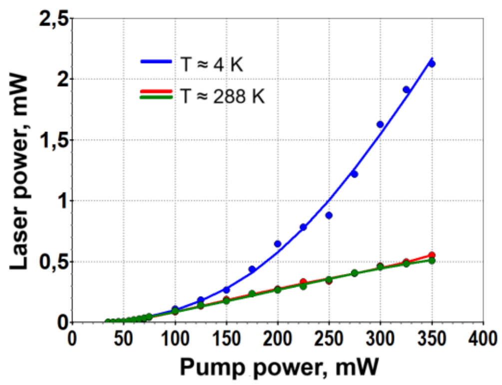

Fig. 1 (a) - a photo of the fiber laser mounted on the cryostat's cold finger, (b) - the laser's power characteristics measured at temperatures of 298 K and 4 K.

This work was supported by the Ministry of Science and Higher Education of the Russian Federation (project FSUN-2026-0007).

References

[1] R. Martins et al., J. Lightwave Technology **33**, 2511 (2015).
[2] L. Marcon et al., Sensors **22**, 4009 (2022).
[3] T. Nakamura et al., Optica Quantum **3**, 221 (2025).
[4] A.M. Smirnov et al., ACS Photonics **5**, 5038 (2018).

Development of flexible and portable coherent Raman scattering spectrum instrument in optical fiber format

Junfeng Jiang[1], Jinchao Dou[1], Wei Cheng[1], Genming Dong[1], Xiaoshuang Dai[1], Jie Du[1], Shuang Wang[1], Kun Liu[1], Hengfeng Yan[2], Youjian Song[1]

[1]*State Key Laboratory of Precision Measurement Technology and Instruments, School of Precision Instrument and Opto-Electronics Engineering, Tianjin University,* Tianjin, China

[2]*Inno Laser Technology*

E-mail: jiangjfjxu@tju.edu.cn

Coherent Raman scattering (CRS) microspectroscopy is a label-free detecting method for chemical materials and biological samples through the vibrational modes of the chemical bonds [1-3]. CRS microspectroscopy requires two ultrashort laser pulses with wavenumber difference matching the resonant frequency of the vibrational mode and phase matching [4-6]. Conventional ultrashort laser spatial configuration is used, however, it is complicated and hard for maintenance, which prevent the system from spread application. Fiber-based ultrafast laser sources have advantages of low cost, compact, and excellent stability. Optical fiber transmission is another important issue for CRS field application. Conventional solid core optical fiber transmission for high peak power ultrashort pulse delivery is troublesome because of dispersion and nonlinear effects.

We developed a CRS fiber format configuration in source, transmission and probe. First, a dual-wavelength tunable fiber picosecond laser source is demonstrated. A fiber-based optical parametric oscillators (FOPO) is synchronously pumped by an electrically-controlled tunable mode-locked fiber laser (TMFL), which can realize a wavelength output range over 270 nm. Second, a hollow-core anti-resonance fiber (HC-ARF) with transmission band in the excitation wavelength band of coherent Raman scattering is developed. Third, based on the specially manufactured HC-ARF, a microsphere-based fiber focusing probe is fabricated, and the piezoelectric-driven scanning of the optical fiber probe is developed.

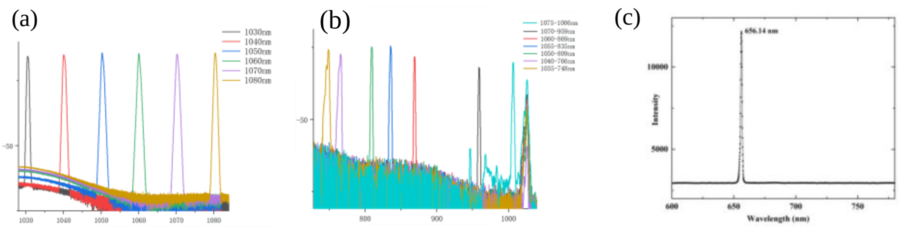

Fig. 1 (a)TMFL tunable spectra, (b) FOPO tunable spectra, (c) CARS signal from cyclohexane sample

Dual-wavelength tunable fiber picosecond laser source consists of three main parts: TMFL, optical power amplifiers, and a FOPO. A self-made tunable filter is introduced into the cavity to achieve tunable narrowband mode-locking with ps-level duration. A Yb-doped fiber is used as the gain medium and mode-locking operation is ensured by a SESAM. A time delay compensation module is used to satisfy the synchronous pump condition. The amplified pulse is coupled into the FOPO by a customized wavelength division multiplexer to produce parametric oscillation based on FWM in a photonic crystal fiber. To enhance the spectral resolution of the output signal, an additional 260-m PM780 fiber was introduced to achieve passive dispersive filtering. The FOPO covers the range from 740 nm to 1006 nm. We design and fabricate the HC-ARF with air core diameter 24.98 μm and micro tube diameter 8.58 μm to cover the wavelength range from 740 - 1100 nm. Silica microsphere is fixed in HC-ARF for focusing based on the photonic nanojet effect, which make output spot diameter 1.75 μm at 1074 nm. We measured Raman spectrum of cyclohexane at 2853 cm^{-1} with the system sucessfully.

This work was supported by National Key Research and Development Program of China (No. 2022YFF0706000).

References

[1] J. X. Cheng et al., J Phys Chem B. **827**, 108 (2003).
[2] A. Zumbusch et al., Phys. Rev. Lett. **4142**, 82 (1999).
[3] I. Kazuki et al., Nat. Commun. **306**, 16 (2025)

Fiber Optic Tapers as Passive Optical Power Limiters

A. Lavrova [1,2], A. Ponosova [1], E. Borisova[1], and V. Makarov [1,3,2]
[1]*Russian Quantum Center, Skolkovo, Moscow 121205, Russia*
[2]*National University of Science and Technology MISiS, Moscow 119049, Russia*
[3]*Vigo Quantum Communication Center, University of Vigo, Vigo E-36310, Spain*
E-mail: an_lav_rova@mail.ru

Optical power limiters (OPL) are essential for protecting sensitive components in high-power laser systems and optical communication systems [1]. An all-fiber passive limiter offers low insertion loss below the threshold and strong attenuation above it, safeguarding system integrity without disrupting normal operation. The existing solutions suffer from slow response times, limited spectral bandwidth, or vulnerability to high-power illumination [2].

Here we develop and investigate a fiber optic taper (tapered fiber) as an OPL. It consists of a section of optical fiber whose radius gradually decreases to a minimum over a transition zone, maintains this minimum value over a defined length (the waist), and then gradually returns to its original value [3]. When high-power radiation propagates through the taper, a significant intensity increase can occur in the constricted region, leading to nonlinear optical effects, material degradation, and eventual fiber breakage. Although standard silica fibers have a low third-order nonlinearity, the reduction of the mode-field radius and the increase in refractive index contrast (e.g., by using an air cladding) dramatically enhance the nonlinear parameter [4]. For a 10-mm taper optimized at a wavelength of 1.55 μm, this makes the onset of effects such as stimulated Brillouin scattering (SBS), self-phase modulation (SPM), and four-wave mixing (FWM) likely, with threshold powers on the order of tens to hundreds of watts.

In this study, we experimentally investigate three fiber taper samples. The tapers are fabricated from standard SMF-28 fiber using a Fujikura FSM-100P fusion splicer with the following parameters: a transition zone length of 1 mm, a waist length of 1 mm, and a waist diameter of 50 μm. We measure the dependence of the taper transmittance on the input power of continuous-wave radiation at 1550 nm. At input powers between 2.6 W and 4.5 W, we obtain an irreversible reduction in transmittance, which is not consistent with theoretical predictions. Since the threshold power for nonlinear effects is much higher, we suppose that the fabrication process induces internal defects, which cause other limiting mechanisms, such as local overheating and material degradation. These findings indicate the need for a more detailed study of the necessary conditions for fiber tapers to function as optical power limiters.

References

[1] Dong G. et al., Physica D: Nonlinear Phenomena **216** (1), 90–94 (2006).
[2] Ponosova A. et al., PRX Quantum. **3**(4) (2022).
[3] Love J.D., IEE Proceedings-J. **138** (5) 343-354 (1991).
[4] Воронин В. Г., Наний О. Е. Основы нелинейной волоконной оптики : учебное пособие / В. Г. Воронин, О. Е. Наний. — М. : Университетская книга, 2011. — 128 с. : табл., ил. ISBN 978-5-91304-212-5

II parallel

Active Space Experiments and Their Laboratory Modeling on Large-Scale Plasma Devices

M.E. Gushchin[1]

[1]*Federal Research Center A.V. Gaponov-Grekhov Institute of Applied Physics of the Russian Academy of Sciences*

E-mail: mguschin@ipfran.ru

Laboratory facilities for modeling space plasma phenomena have been developed worldwide since the early 1970s, and today the field of "laboratory simulation of space plasmas" is considered mature and well-established. For space plasma modeling, specialized, large-scale plasma chambers are preferred. Powerful lasers and electrical discharges—pulsed, high-frequency, and direct current—are used to simulate space plasma phenomena and space plasma objects. Several plasma devices are successfully used in Russia for space plasma modeling, the largest of which are the Krot (IAP RAS) and KI-1 (ILP SB RAS). Currently, the priority task is to improve the quality of modeling and its predictive potential through the use of new diagnostics and the implementation and adaptation of new numerical models verified using reliable laboratory data.

Active experiments involve the injection of charged particle flows, neutral matter, and plasma from spacecraft, as well as the excitation of intense electromagnetic fields by spacecraft antennas and specialized ground-based transmitters. Such experiments are conducted in the Earth's upper atmosphere, ionosphere, and magnetosphere by using satellites, rockets and ground-based infrastructure. These experiments provide invaluable information about the state of the geophysical environment and its response to external influences. Today, there is a significant surge of interest in active experiments worldwide, conducted primarily by the United States, the European Union, China, and Russia.

At the current level of scientific and technological development, laboratory simulation based on similarity rules can significantly facilitate the preparation of active experiments, assist in the selection of their parameters, and the interpretation of results—including both past experiments and future missions. The talk covers issues related to both the capabilities and prospects of laboratory modeling of active experiments on large-scale plasma devices, as well as the challenges of such modeling. Recent international and domestic active experiments are examined, including plasma injections from the ISS, radiofrequency ionospheric plasma stimulation from spacecraft (the Ionosphere-M constellation), and ground-based HF heating facilities such as SURA.

Author thanks Russian Science Foundation for the financial support (project No 24-12-00459).

Laser plasma experiments to model geophysical processes and phenomena

I.F. Shaikhislamov, A.A. Chibranov, A.E. Ivanov, A.G. Berezutsky, V.G. Posukh, M.V. Loginov, P.A. Trushin, M.S. Rumenskikh, Yu.P. Zakharov, I.B. Miroshnichenko
Institute of laser physics SB RAS, Novosibirsk, Russia
E-mail: ShaikhislamovIldar@yandex.ru

Laboratory modeling of various phenomena in space plasmas represents an important method for studying the physics of the corresponding processes. Despite significant advances in space observations and computational results, experimental research continues to play a significant role, providing information inaccessible by other means. In the 1970s–1980s, an extensive series of studies on the expansion of laser plasma in a magnetic field was carried out, largely aimed at reproducing active space experiments, including barium cloud releases within the AMPTE program. From the mid-1990s, thanks to the advent of more powerful laser systems, a new stage began, receiving the names "Laboratory Astrophysics with Lasers" and "High-Energy-Density Laboratory Astrophysics". One of the central directions of this field became the laboratory realization of collisionless shock waves. The use of laser plasma for achieving shocks in a laboratory has a long history; however, substantial achievements in this area have only been reached in recent years. Experiments conducted at the KI-1 facility of the ILF SB RAS remain leading in this domain in terms of the realized parameters and obtained results.

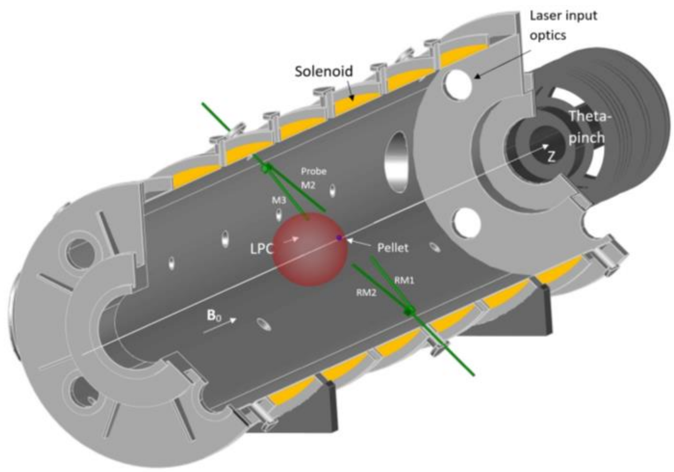

Fig. 1 KI-1 laser plasma Facility

In our previous study, a directed super-Alfvén flow of laser plasma propagating in magnetized hydrogen plasma was investigated [1]. A similar physical setup was implemented at the LAPD, where laser plasma expanded across a magnetic field into an extended and relatively homogeneous background plasma [2]. These experiments demonstrated magnetosonic solitons and pre-shock structures resembling a low-Mach collisionless shock wave. In the present work we report results of experiments with spherical plasma clouds, which is much more relevant to geophysical processes related to artificial plasma releases. Obtained measurements show new effects related to finite Larmore radius of ions and spherical geometry of experiments.

References

[1] I. F. Shaikhislamov et al., Plasma Physics Reports **41**, 5 (2015).
[2] D. B. Schaeffer et al. Phys. Plasmas **24**, 041405 (2017).

Aerographite target for laboratory astrophysical research

D.S. Amonsky, A.V. Kovalenko, A.D. Malakhov
Institute of Laser Physics Research, RFNC-VNIIEF, Sarov

E-mail: dmitryamonsky@yandex.ru

A creation of spherical clouds of laser plasma is of interest for a laboratory modeling of explosive space phenomena. In this work it is proposed to use a spherically expanding cloud of plasma formed by irradiating an aerographite target with a density lower than the critical density for the wavelength of the laser radiation. It has been demonstrated experimentally that with sufficiently high laser radiation power it is possible to form a quasi-spherical cloud of expanding fully ionized carbon plasma with controlled parameters. At an absorbed laser radiation energy of ~ 10 kJ in a time of ~ 2 ns, a target with a density of ~ 6 mg/cm^3 and a radius of ~ 1.5 mm has produced a nearly spherical plasma cloud with a front expansion velocity of more than 1000 km/s.

Searching for observable biosignatures in exoplanetary atmospheres

D.V. Bisikalo[1,2]
[1]*National center for physics and mathematics, Sarov*
[2]*Institute of astronomy, Moscow*
E-mail: Bisikalo@inasan.ru

The challenge of searching for biomarkers in exoplanetary atmospheres is one of the most intriguing issues not only in astrophysics but in science as a whole. This report presents a brief overview of potential atmospheric biomarkers in the context of the search for extraterrestrial life [1]. Current understanding suggests that N_2–O_2-dominated atmospheres serve as indicators of biological activity [2, 3]; therefore, it is worthwhile to investigate them more thoroughly. It is concluded that NO molecule is of greatest interest for the detection of an N_2–O_2 atmosphere using modern spectroscopic methods [4]. Special attention is paid to the possibility of detecting NO with the spectrographs of the SPEKTR-UF Russian space mission [5], scheduled for launch in 2031.

This work was supported by the Russian Science Foundation (project 22-12-00364-p).

References

[1] Bisikalo D. et al., FIZMAT. **2**(4), 213-252 (2024).
[2] Lammer H. et al., Astrobiology. **19(**7) 927–950 (2019).
[3] Sproß L. et al., Astronomy Reports. **65** (4) 275–296.l (2021).
[4] Tsurikov G. et al., Astronomy Reports. **68**, 1406–1422 (2024).
[5] Sachkov M. et al., Proceedings of the SPIE. **13093**(130933F) (2024).

Spectroscopy of exoplanet atmospheres with the Spektr-UF space telescope

G. Tsurikov[1], D. Bisikalo[2,1], V. Shematovich[1], A. Zhilkin[1]
[1]*Institute of astronomy of the RAS, Moscow*
[2]*National Center for Physics and Mathematics, Sarov*
E-mail: tsurikov@inasan.ru

The Spektr-UF space telescope, being developed in Russia, is designed to obtain images and spectra of space objects in the ultraviolet (UV) spectral range (115–310 nm), which is inaccessible for observation by ground-based telescopes. Exoplanetary research occupies a key place in the telescope's scientific program. Spektr-UF is planned to be used to address several particularly pressing issues in exoplanet research, including: a) estimation of space weather parameters around solar-type stars based on observations of the atmospheres of hot exoplanets [1,2]; b) searching for spectral lines of biosignature molecules in the atmospheres of terrestrial-type exoplanets [3]. This work presents the capabilities of Spektr-UF for addressing these issues.

Interpreting transit absorptions in the atmospheres of hot exoplanets may allow us to estimate space weather parameters (stellar wind and extreme radiation fluxes) around other stars [1,2]. The paper presents estimates of the detection limits for the HI Lyα spectral line (the strongest indicator of interaction between planetary and stellar winds [2]) in the atmospheres of hot exoplanets using Spektr-UF. For this purpose, the results of modeling transit absorptions in this line from [2], as well as the Spektr-UF exposure calculator [4], are used. According to the calculation results, it is shown that the limiting distances for reliable $>3\sigma$ detection of this spectral line are: a) 20 pc when using a vacuum ultraviolet echelle spectrograph (VUVES, R = 50000); b) 150 pc when using a long-slit spectrograph (LSS, R = 1000, allows to detect of the integrated absorption in the spectral line). A list of planetary systems with solar-type stars has been compiled for determining space weather parameters using Spektr-UF. This list includes 12 planetary systems for the VUVES spectrograph and 180 exoplanets for the LSS spectrograph. Determining space weather parameters for these planetary systems after the launch of Spektr-UF will enable forecasting of extreme solar events (coronal mass ejections and superflares) that could impact satellite and civil infrastructure.

An important indicator of biological activity on a terrestrial-type planet is the presence of an N_2-O_2-dominant atmosphere. The search for molecules - indicators of such an atmosphere (potential biomarkers) on exoplanets will be the main issue of the Spektr-UF scientific program. The most promising and reliable biomarker for searches with Spektr-UF is nitric oxide [4]. This study explores the possibility of detecting spectral lines of this molecule (γ-bands, 203–248 nm) in exoplanet atmospheres using Spektr-UF. The obtained results demonstrate that the Spektr-UF spectrograph can detect NO on typical super-Earths and mini-Neptunes located in the habitable zone of G- and early K-type stars that are more active than the Sun. The detection limits for this molecule extend up to 40 pc. A list of 11 exoplanets - candidates for NO detection using the Spektr-UF instrument is presented. Detecting NO on these exoplanets will allow us to identify their N_2-O_2 atmospheres and determine their possible habitability.

Authors thank Russian Science Foundation (project 22-12-00364-p) for their supports.

References

[1] V. Shematovich et al., FIZMAT. **1**, 20 (2023).
[2] I. Shaikhislamov et al., FIZMAT. (2026). In press.
[3] G. Tsurikov et al., Astron. Rep. **68**, 12 (2024).
[4] G. Tsurikov et al., Proc. of SPIE. **13093**, 12 (2024).

Water vapor in the atmospheric radiative balance. Continuum absorption by water vapor.

I. Ptashnik
V.E.Zuev Institute of Atmospheric Optics, SB RAS
E-mail: piv@iao.ru

Water vapor is the strongest greenhouse gas in Earth's atmosphere, accounting for up to 70% of all solar radiation absorbed by atmospheric gases [1]. Its effect doubles the radiative forcing — a measure of changes in the Earth-atmosphere radiation balance — caused by any other factor, such as absorption by other gases, aerosols, surface, etc. The absorption of electromagnetic radiation by water vapor results from both hundreds of thousands of spectral lines of the water molecule, whose parameters are already fairly well known [2], and from the weakly selective, so-called continuum absorption. The nature of this continuum absorption has been studied for over 100 years and is still not fully understood [3]. This report reviews the research conducted over the past 25 years, which has shown that a significant portion of the water vapor's continuum absorption is due to water dimers, that is, two water molecules linked by a weak hydrogen bond [4-8].

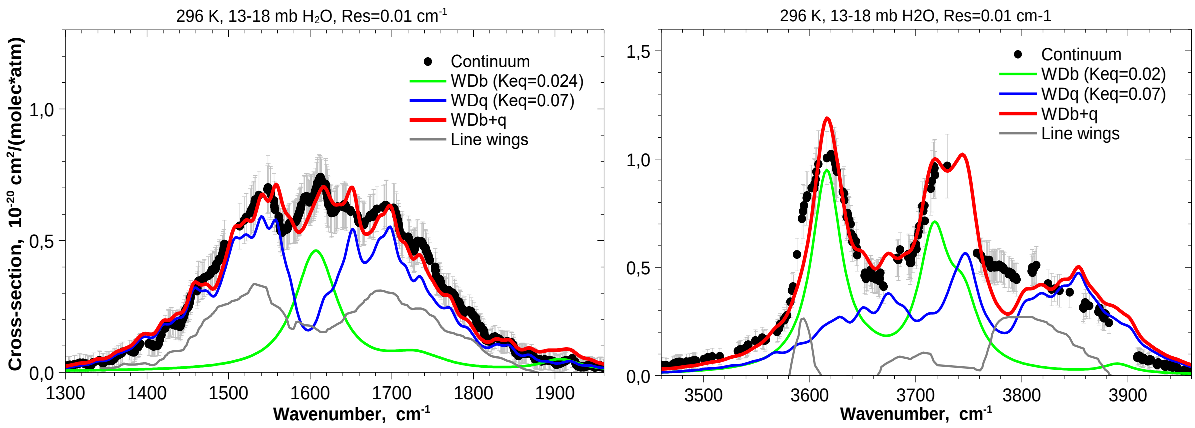

Fig. 1 Examples of the experimental continuum absorption (dots) in two water vapour near-IR bands obtained at 296 K compared to the water dimer model [7] (red line) including contribution of bound dimers (green) and some effective contribution of quasibound dimers (blue), part of which can be tentatively attributed to wings of water monomer lines (grey) [8].

Apart from the true bound water dimers, contribution of quasibound dimers was also identified in the detected spectra of the water vapour continuum absorption, as well as possible contribution of water monomer line wings [5-8].

This work was partly supported by the Ministry of Science and Higher Education of the Russian Federation (Program of the Basic Scientific Investigations, budget funds for IAO SB RAS).

References

[1] J. Kiehl et al., Bull. Am. Meteorol. Soc. **78,** 197 (1997).
[2] I. Gordon et al. J. Quant. Spectrosc. Radiat. Transf., **277**, 107949 (2022).
[3] K. Shine, et al., Surv. Geophys. **33**, 535 (2012).
[4] I. Ptashnik. J. Quant. Spectrosc. Radiat. Transf. **109**, 831 (2008).
[5] I. Ptashnik et al., J. Quant. Spectrosc. Radiat. Transf. **112**, 1286 (2011).
[6] E. Serov et al., J. Quant. Spectrosc. Radiat. Transf. **193**, 1 (2017).
[7] I. Ptashnik et al., J. Quant. Spectrosc. Radiat. Transf. **228**, 97 (2019).
[8] A. Simonova et al., J. Quant. Spectrosc. Radiat. Transf. **329**, 109198 (2024).

Influence of planetary magnetic fields on extended helium tails of WASP-69b

M. Rumenskikh[1,2], M.P. Golubovsky[1,2], S.S. Sharipov[1], I.F. Shaikhislamov[1,2]
[1]*Institute of Laser Physics SB RAS, Novosibirsk, Russia*
[2]*Institute of astronomy RAS, Moscow, Russia*
E-mail: marina_rumenskikh@mail.ru

The atmospheres of hot Jupiters, intensely irradiated by their host stars, undergo hydrodynamic escape that extends beyond the Roche lobe, occasionally producing extended cometary tails detected in observations. A key objective in contemporary exoplanet research is the indirect determination of planetary magnetic fields, as numerical modeling demonstrates that field strength critically shapes atmospheric morphology—sufficiently strong fields can suppress mass loss rates and inhibit tail formation, thereby enabling an estimate of the upper limit on a planet's magnetic field strength based on the observational presence or absence of escaping tails.

Transit spectroscopy in the metastable helium triplet at 10830 Å has emerged as a powerful diagnostic tool for probing exoplanetary plasmaspheres, delivering reliable measurements of composition, temperature, density, and evidences of plasma interactions between stellar and planetary winds. Unlike the commonly used Lyman-α line, which suffers from interstellar absorption and geocoronal contamination, the helium line remains largely unaffected by these distortions, providing a cleaner observational window for characterizing escaping atmospheres and, importantly, for inferring magnetic field properties through their imprint on atmospheric structure.

We employ a three-dimensional MHD model to simulate transit absorption signatures of WASP-69 b in the 10830 Å helium line, specifically investigating how planetary magnetic fields and system parameters manifest in observable spectral features. Our results confirm that magnetic fields substantially alter the geometry and dynamics of escaping atmospheres, and that transit observations in the helium line can serve as an effective method for constraining planetary magnetic field strengths through their influence on mass outflow patterns and tail morphology.

This work was supported by National center of physics and mathematics.

Online Session

Will quantum computers replace classical ones and is there an alternative to parallel computing?

V. Zadkov
Institute of Spectroscopy of the Russian Academy of Sciences, Troitsk-Moscow, Russia

Nowadays, nanoelectronics technologies allow mass-production of chips with a resolution of a few nanometers and with atomic resolution at the laboratory level. At this rate, the elementary logic gates that make up these chips will soon consist of hundreds or even dozens of atoms, so that these devices will no longer obey the laws of classical physics and their quantum nature will dominate. Such quantum logic devices are used to create a quantum computer.

This talk highlights the main directions of development in the modern field of quantum simulators and computers, and briefly discusses the state of prototype development. The answers to the questions about the advantages of quantum computers over classical ones and whether quantum computers will replace classical ones are given. However, intensive inclusion of Russia in the international quantum technology race, for which Russia spends essential budget, has a very unclear result in the end.

By contrast, an alternative paradigm is proposed for creating chips based on classical information, which is trasferred by a flood of electrons passing through a narrow slit of a superconducting metal ring (so called rapid single-flux logic devices, RSFQ logic). This technology was demonstrated back in 1983-1985 in the USSR, under grant by Profs. Likharev and Koshelets who launched the first mega-grant in the USSR ($5 million per year) for the implementation of this project. It was successfully completed and all basic principles of RSFQ logic and devices based on it were demonstrated and implemented.

Already in 2010, RSFQ chips had clock speeds up to 1 GHz, and energy consumption was only a fraction of pico Joule. These RSFQ-devices were used in special applications (fast Fourier transform, image processing, etc.). Also, personal RSFQ-based teraflop table-size computer at 100kUS dollars and a power consumption of about 1 kW was proposed for mass production! Important is that the production technologies of such chips do not require nanometer resolution, and the computer itself does bot requires a separate power plant for its operation and a huge cooling complex for the utilization of dissipated energy.

Such technologies could become the basis for supercomuters, which differ in their paradigm of the element base and software from those that are actively promoted worldwide. Their potential is higher both in terms of operating speed and consumption by several orders of magnitude. At the same time, computers themselves remain linear (i.e. they do not use parallelism). The latter is especially important because most numerical calculation tasks cannot be parallelized.

Measuring quantum properties of light at low intensity for any statistics.

G. Leuchs[1,2,3], **Hans Dang**[2,3], **Sebastian Luff**[2,3], **Nikolay Kalinin**[1], **Thomas Dirmeier**[2,3], **Martin Fischer**[1], **Markus Sondermann**[1,2], **Mojdeh. S. Najafabadi**[1], **Luis L. Sanchez-Soto**[1,4,5]
[1]*Max Planck Institute for the Science of Light, Erlangen, Germany*
[2]*Friedrich-Alexander-Universität Erlangen-Nürnberg, Germany*
[3]*University of Ottawa, Canada*
[4]*Universidad Complutense de Madrid, Spain*
[5]*Chapman University, Orange CA, USA*
E-mail: gerd.leuchs@fau.de

Naïvely one might expect, that sufficient attenuation of any light field will eventually lead to measurable quantum effects. This naïve expectation is true (!) even for thermal light when comparing measurements of different types of correlation functions:

(1) the auto correlation function obtained by measuring an intensity time series with a single detector and calculating the correlation function numerically yielding $g^{(2)}_{auto}(\tau)$, and

(2) the Hanbury Brown & Twiss type cross correlation function, $g^{(2)}_{cross}(\tau)$, for which the signal beam is first split, then measured with two detectors, finally correlating the two different measured intensity signals.

For efficient detectors, the difference between $g^{(2)}_{auto}(\tau)$ and $g^{(2)}_{cross}(\tau)$ can only be explained considering a true quantum effect: the projection associated with a quantum measurement.

More mathematically speaking, by comparing $g^{(2)}_{auto}(\tau)$ and $g^{(2)}_{cross}(\tau)$ one recovers the commutator of the quantum field operators. The curves were measured experimentally for different states of light [1]. Fig. 1 shows the theoretical expectation.

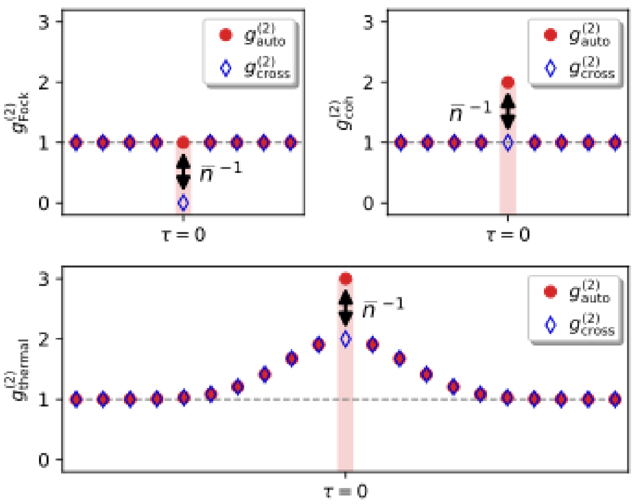

Fig. 1 The two different intensity correlation functions differ only at $\tau = 0$ under the condition that the width of the time bin is chosen to be equal to $\frac{1}{2b}$, with b being the bandwidth of the detector. Upper left diagram: perfect Fock state with exactly one single photon per time bin. Upper right diagram: coherent state. Lower diagram: thermal light.

References

[1] H. Dang et al., **arXiv:2601.18870** (2026).

Tuesday
August 25

Monday	Tuesday	Wednesday	Thursday	Friday	Saturday	Sunday
27	28	29	30	31	1	2
3	4	5	6	7	8	9
10	11	12	13	14	15	16
17	18	19	20	21	22	23
24	25	26	27	28	29	30
31	1	2	3	4	5	6

Equivalence Principle test with 10-meter atom interferometer

Lin Zhou[1,2], Chuan He[1], Lu Zhou[1,3], Si-Tong Yan[1], Jun-Jie Jiang[1,3], Jia-Qi Lei[1,3], Run-Dong Xu[1], Zhuo Hou[1,3], Zhi-Xin Li[1,3], You-Meng Hu[1,3], Jia-Ming Wei[1,3], , Jin Wang,[1,2,4] and Ming-Sheng Zhan[1,2,4]

[1]*State Key Laboratory of Magnetic Resonance and Atomic and Molecular Physics, Innovation Academy for Precision Measurement Science and Technology, Chinese Academy of Sciences-Wuhan National Laboratory for Optoelectronics, Wuhan 430071, China*

[2]*Hefei National Laboratory, Hefei 230088, China*

[3]*School of Physical Sciences, University of Chinese Academy of Sciences, Beijing 100049, China*

[4]*Wuhan Institute of Quantum Technology, Wuhan 430206, China*

E-mail: lzhou@apm.ac.cn, mszhan@apm.ac.cn

The equivalence principle (EP) serves as a cornerstone of general relativity. High-precision quantum tests of the EP not only provide a crucial means to verify the applicability of existing theories but also offer an important window for exploring new physics beyond the Standard Model. To this end, we have established a 10-meter atom interferometer in Wuhan, dedicated to EP tests and related fundamental physics research.

Based on this apparatus, we have developed a series of core techniques, including a dual-species cold-atom fountain of ^{85}Rb and ^{87}Rb, four-wave double-diffraction Raman transition (4WDR) atom interferometer, and shear-phase readout. By integrating these techniques, we have achieved a cold-atom fountain with a launch height of 12 m, and obtained atom-interference fringes with a maximum free-evolution time of 2T=2.86 s, corresponding to a single-shot gravity measurement resolution of 4.1E−11 g.

In terms of EP tests, we carried out a mass test with ^{85}Rb and ^{87}Rb using the 4WDR scheme in 2015, reaching an accuracy of order 3E−8. On this basis, we further developed the 4WDR-e method to realize joint mass-and-energy test, and respectively constrained the violation parameters for the mass term and the energy term to the order of E-10. Currently, we are advancing a joint mass-and-energy test with a target precision of E-12, and have made progress in key technologies such as dual-species ultracold-atom source preparation, optical lattice acceleration, and Large-momentum-transfer technique. The differential measurement resolution of our dual-species atom interferometer has reached 4.5 E-12 .

References:

[1] L. Zhou et al., Phys. Rev. Lett. **115**, 013004 (2015).
[2] L. Zhou et al., Phys. Rev. A **104**, 022822 (2021).
[3] L. Zhou et al., Front. Phys. **10**, 1039119 (2022).

Study of Systematic Shifts in an Atom Interferometer-Gravimeter

D.N. Kapusta[1], K.N. Adamov[1,3], A.E. Bonert[1], A.N. Goncharov[1,2], M.A. Nelin[1,2], K. E. Rekhtin[1,3], A.V. Taichenachev[1,3], V.I. Yudin[1,2,3], O.N. Prudnikov[1,3]
[1]*Institute of Laser Physics SB RAS, 630090, Novosibirsk, Russia*
[2]*Novosibirsk State Technical University, 630073, Novosibirsk, Russia*
[3]*Novosibirsk State University, 630090, Novosibirsk, Russia*
E-mail: dmitriikapusta@mail.ru

Compact quantum gravimeters based on the interference of ultracold atoms [1] are designed for absolute measurements of the gravitational acceleration g and currently attract significant interest. They are characterized by a short duration of the interferometric sequence (on the order of a few to tens of milliseconds), enabling a high repetition rate (tens to hundreds of hertz) [2, 3], as well as low sensitivity to vibrations and certain sources of systematic shifts. Consequently, they are successfully employed in highly dynamic environments, such as airborne and marine gravimetry [4, 5], mobile land-based systems [6], geophysical monitoring [7], and other applications. Compact quantum gravimeters possess a unique set of advantages and applications and warrant further detailed investigation.

In this context, investigating systematic effects that influence the accuracy of absolute g measurements in small-scale atom interferometers is of high scientific and practical importance. In this work, we present the results of a study on systematic shifts in an atom interferometer gravimeter with a short interrogation baseline (free-evolution time $T \leq 10$ ms). Specifically, we examine in detail Stark shifts [8], the shift induced by additional laser lines in the spectrum of phase-modulated Raman laser [9], and the shift caused by spectroscopic line shape asymmetry, which was first predicted and experimentally observed by our group [10, 11]. Experimental measurements demonstrated that the total magnitude of these shifts can reach several tens of mGal, substantially limiting the absolute accuracy of compact quantum gravimeters. We investigated approaches for their compensation and minimization by optimizing the parameters of the magneto-optical trap and the atom interferometer. As a result, the total magnitude of these shifts was reduced to approx. 1 mGal. Furthermore, we analyzed the impact of these shifts on the sensitivity, stability, and sampling rate of the quantum gravimeter. In particular, by stabilizing the Raman beam power, we demonstrated an improvement in long-term stability down to approx. 50 μGal.

This work was supported by the Russian Science Foundation (Grant No. 23-12-00182-P).

References

[1] M. Kasevich et al., Phys. Rev. Lett. **67**, 181 (1991).
[2] H. J. McGuinness et al., Appl. Phys. Lett. **100**, 011106 (2012).
[3] J. Lee et al., Nat. Commun. **13**, 5131 (2022).
[4] Y. Bidel et al., J. Geod. **94**, 20 (2020).
[5] Y. Bidel et al., Nat. Commun. **9**, 627 (2018).
[6] J. Y. Zhang et al., AIP Adv. **11**, 115223 (2021).
[7] J. Vovrosh et al., Sensors **23**, 7651 (2023).
[8] A. Gauguet et al., Phys. Rev. A **78**, 043615 (2008).
[9] O. Carraz et al., Phys. Rev. A **86**, 033605 (2012).
[10] V. I. Yudin et al., JETP Lett. **122**, 737 (2025).
[11] D. N. Kapusta et al., JETP Lett. **123**, 388 (2026).

Manipulation of the nuclear spin of NV centers

A.V. Akimov[1,2]
[1]*Russian Quantum Center, Moscow, Russia*
[2]*P.N. Lebedev Institute RAS, Moscow, Russia*
E-mail: a.akimov@rqc.ru

Color centers in diamond are popular defects for sensing applications. My group is working on several sensors, including temperature sensors, magnetic field sensors as well as rotation sensors. To this end we use various color center in our research, depending on application. Yet, the main working horse is nitrogen vacancy color center, which allow both vector magnetometry and rotation sensing.

In this work, I will give an overview of our activities on sensing with diamond NV centers, understanding of their interaction with environment and themselves as well as emphasize resent advances on coherent manipulation of NV center nuclear spins using coherent population trapping resonance. Although the forbidden resonances required for coherent control were only partially observed, coherent population trapping was successfully demonstrated at both visible and invisible transitions, with an apparent contrast of up to 98 ± 11% and a true contrast of approximately 35 ± 7%. This finding confirms the feasibility of coherent nuclear spin control even in diamond plates with naturally occurring carbon-13. This achievement may find it application in all types of sensors we are currently developing.

This study was supported by the Ministry of Science and Higher Education of the Russian Federation (agreement/grant No. 075-15-2024-556).

Thulium atom for quantum simulations

A.V. Akimov[1]
[1]*Russian Quantum Center, Moscow, Russia*
E-mail: a.akmov@rqc.ru

Bose-Einstein condensation (BEC) is a powerful tool for a wide range of research activities, a large fraction of which is related to quantum simulations. Various problems may benefit from different atomic species. Thulium atoms possess dipole moment of 4 Bohr magneton in the ground state, allowing long-term interactions. It also has number of non-chaotic low-field Feshbach resonances, allowing fine control of the near-filed interactions. It also has relatively simple level structure compared to the other magnetic lanthanoids and thus is a quite promising subject for applications in quantum simulations. Here we report on our efforts to cool, control collisional properties and internal state of thulium atom as well as use thulium atom for simulations.

In particular aiming into 2-dimensional simulator with rearrangeable array of atoms we found zero polarizability for ground state near wavelength 575 nm, which will allow manipulation of atoms over the loaded with atoms optical lattice. This became possible via careful measurements of the atomic polarizability in the range 575,364 nm – 575,705 nm via both trap oscillations and radiofrequency spectroscopy. Combination of two methods allowed robust separation of tensor and vector polarizability. The presence of zero polarizability was then visually confirmed by direct observation of number of the trapped atoms.

At the same time, at the same trap it is possible to achieve ap to 16 000 atoms in the Bose - Einstein condensate if polarizability is turned to positive enough value, thus proving absence of inelastic channels in the trap. These results thus are paving the way for possibility of atoms sorting in the future simulator.

This work was supported by Rosatom in the framework of the Roadmap for Quantum computing (Contract No. 868/1759-D dated October 3, 2025).

New approaches in high-sensitivity atomic magnetometry for geophysical measurements and medicine

D.V. Brazhnikov[1], A.O. Makarov[1], K.S. Kozlova[1], M.A. Rusina[1], R.A. Tkachenko[1], A.M. Mikhailov[1], V.A. Vasiliev[1], E.V. Tanakov[1], A.N. Goncharov[1], M.A. Bobrov[2], Ya.N. Kovach[2], A.A. Blokhin[2], N.A. Maleev[2], S.A. Blokhin[2]

[1]*Institute of Laser Physics SB RAS, 15B Lavrentyev Avenue, Novosibirsk 630090, Russia*
[2]*Ioffe Institute RAS, 26 Politekhnicheskaya Street, Saint Petersburg 194021, Russia*

E-mail: x-kvant@mail.ru

Optically pumped magnetometers (OPMs) based on laser spectroscopy of alkali-metal atoms are among the most sensitive magnetic sensors [1]. They have a vast range of applications. For example, OPMs are being actively implemented in the field of noninvasive medical diagnostics [2]. The use of compact and energy-efficient OPMs enables compelling opportunities for drone-borne mineral prospecting [3] and other geophysical applications [4]. For medical diagnostics, OPMs are based on the ground-state Hanle effect (GSHE) and operate in the spin-exchange relaxation-free (SERF) regime [5]. The OPM systems offer a high spatial resolution (~ 1 mm) and are well suited for diagnosing deep brain structures. These sensors are capable of detecting various brain disorders at the earliest stages. However, SERF magnetometer requires an extremely high degree of magnetic shielding against the Earth's field and its housing heats up noticeably (≈ 50°C).

At the Institute of Laser Physics, a few novel atomic magnetometry techniques have been developed for operation under both magnetically shielded environments and in the geomagnetic field. The proposed techniques do not require the SERF regime. The first approach enables vector measurements of the magnetic field and is based on the GSHE [6]. The second approach provides scalar measurements and relies on the Bell-Bloom technique [7]. Both approaches depart from their classical implementations through a set of modifications. In particular, instead of employing linear or circular light polarization as in conventional schemes, elliptical polarization is utilized in conjunction with detection of magnetic resonance via polarimetric technique. In the GSHE-based scheme, cw emission from an external-cavity diode laser is employed, whereas in the Bell-Bloom scheme, frequency-modulated emission from a vertical-cavity surface-emitting laser (VCSEL) is used. The sensitivity of the modified Hanle technique is ≈ 180 fT/√Hz, with a bandwidth of ≈ 190 Hz. This sensor is suitable for magnetocardiography and magnetomyography. The scalar Bell-Bloom-like technique exhibits a sensitivity of ≈ 75 fT/√Hz with a bandwidth of ≈ 1 kHz. This measurement technique can provide the foundation for both a scalar sensor and a vector sensor. The latter being of particular interest for medical diagnostic applications in unshielded environments.

The work on the development of total-field measurement technique is supported by the Russian Science Foundation (Grant # 26-12-00132). The development of VCSEL (Project Code FFUG-2025-0006) and the GSHE-based technique (Project Code FWGU-2026-0012) is supported by the Ministry of Science and Higher Education of the Russian Federation under state-funded research assignments of Ioffe Institute RAS and Institute of Laser Physics SB RAS, respectively.

References

[1] J. Kitching et al., J. Phys. Conf. Ser. **723**, 012056 (2016).
[2] V. Maurice et al., Book of Abstracts of the 32nd EFTF Forum, Torino, Italy, Page 243 (2018).
[3] V. S. Letokhov, V. P. Chebotaev. Springer, Berlin (1977).
[4] M.T. Hummon et al., Optica **5**, 443 (2018).
[5] V. Shah et al., Nat. Photonics **1**, 649 (2007).
[6] D. Brazhnikov et al., Eur. Phys. J. D **80**, 52 (2026).
[7] A. Makarov et al., Opt. Commun. **577**, 131369 (2025).

Quantum spectroscopy using correlated photon pairs

A.S. Sabanin[1], S.P. Kulik[1,2], A.V. Paterova[1]
[1]*Laboratory of Quantum Engineering of Light, South Ural State University, Chelyabinsk, Russia*
[2]*Center for Quantum Technologies, Faculty of Physics, Lomonosov Moscow State University, Moscow, Russia*

The infrared (IR) wavelength range is of significant interest because many molecules exhibit characteristic absorption lines in this spectral region. Consequently, IR spectroscopy and IR microscopy are valuable tools for analyzing the chemical composition of a sample. Traditional IR micro-spectroscopy methods suffer from high background noise of detectors. An alternative to direct IR detection is nonlinear interferometry [1], which enables determination of IR characteristics of a sample by detecting visible light. This work proposes an IR metrology scheme based on nonlinear interferometry that allows broadband IR spectroscopy using only optical components and detectors operating in the visible range [2-4]. The method is based on the interference of photon pairs generated via spontaneous parametric down-conversion (SPDC) in a crystal. The nonlinear crystal is integrated into an interferometer setup containing a flat and a parabolic mirror, for the compensation of the transverse phase shifts acquired in the interferometer [3,4]. We demonstrate broadband IR spectroscopy and gas analysis using an SPDC based interferometric scheme that senses IR-absorbing gases via visible-light detection. The system simultaneously identifies multiple gas species (specifically CO_2 and N_2O) through their characteristic mid-IR absorption bands.

References

[1] D. N. Klyshko, J. Exp. Theor. Phys. **77**(2), 222–226 (1993).
[2] D. A. Kalashnikov et al, Nat. Photonics **10**, 98–101 (2016).
[3] A.V. Paterova et al, ACS Photonics **9**, 2151−2159 (2022).
[4] A. Sabanin et al, Laser Physics Letters **22**(1), 015203 (2024).

Planar elements for cold-atom quantum sensors

A.E. Afanasiev[1], D.V. Bykova[1,2], A.A. Idrisova[1,2], A.S. Kalmykov[1,3], V.I. Balykin[1]
[1]*Institute of spectroscopy RAS, Moscow, Troitsk, Russia*
[2]*National Research University Higher School of Economics, Moscow, Russia*
[3]*Moscow Institute of Physics and Technology, Dolgoprudny, Moscow region, Russia*
E-mail: afanasiev@isan.troitsk.ru

Cold atom ensembles are one of platforms for constructing quantum sensors. Extensive experience has been accumulated in the branch of developing and using of such sensors [1]. A key step is the transition to use of transportable systems. Stationary laboratory systems are large in size, weight and power consumption (SWaP parameter). Further development of quantum sensorics requires the development of approaches to reducing the SWaP parameter. Solving this problem requires integrated approaches to optimizing both the sensor head and the control systems.

In case of sensor head SWaP parameter optimization, the mechanisms of laser cooling and trapping of atoms should be considered. Two subsystems determine the size and weight of the sensor head: (1) a system for generating the required spatial distribution of the magnetic field; (2) a system for generating the required spatial configuration of laser radiation. These elements are necessary for efficient cooling and localization of atoms. The most common approach is the use of quadrupole magnetic coils and three pairs of laser beams to form a magneto-optical trap. This approach is effective for creating laboratory systems and is susceptible to significant disturbances when used outdoors.

One of the trends is to change such subsystems with planar structures to increase the control for parameters and SWaP parameter optimization. For magnetic subsystem atom chip approach is widely used. To form required spatial configuration of laser radiation in the trapping region grating chip approach is used. Atomic clocks [2] and gravimeters [3] based on cold atoms are developed using such planar technologies. The use of planar technology makes it possible to combine these two approaches to create compact systems [4].

Figure 1 shows the photography of atom and grating chip developed in Institute of spectroscopy RAS [5]. The temperature of atomic ensemble near the structures being studied is below 10 μK. The experiments shown that near such structures the coherent control of atoms make it possible to form interferometric sequence. Such compact platforms can be used for compact quantum sensors development.

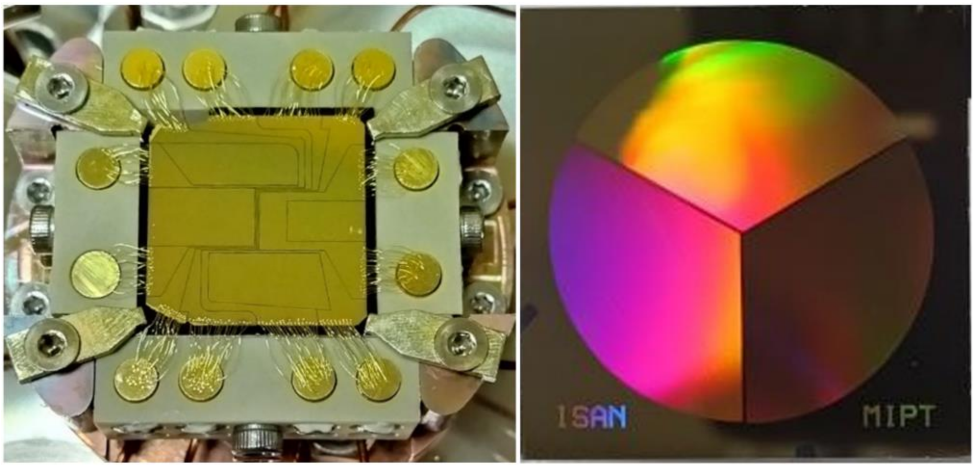

Fig. 1 Atom chip (left) and grating chip (right) developed in ISAN.

Author thanks Russian Science Foundation for their supports (project №26-12-00102).

References

[1] R. Geiger et al., AVS Quantum Sci. **2**, 024702 (2020).
[2] A. Bregazzi et al., Scientific Reports **14**, 931 (2024).
[3] J. Lee et al., Nature communications **13**, 5131 (2022).
[4] H. Heine et al., New J. Phys., **27**, 033019 (2025).
[5] P. Skakunenko et al., Chinese Optics Letters **22**, 060201 (2024).

Silicon Photonics for Gas Sensing

Zhenzhou Cheng[1,2,3]
[1]State Key Laboratory of Precision Measuring Technology and Instruments, Tianjin, 300072, China
[2]School of Precision Instrument and Opto-electronics Engineering, Tianjin University, Tianjin, 300072, China
[3] Key Laboratory of Opto-electronic Information Technology, Ministry of Education, Tianjin 300072, China
E-mail: zhenzhoucheng@tju.edu.cn

Silicon photonics has been widely explored for on-chip gas sensors [1]. However, conventional silicon photonic integrated circuits usually suffer from moderate performance and a trade-off between low optical losses and the presence of significant evanescent fields. In this talk, I presented our efforts to develop novel suspended nanomembrane silicon (SNS) photonic integrated circuits to overcome these limitations.

Specifically, we first studied a subwavelength grating (SWG) coupler [2, 3] that achieved an experimental coupling efficiency of -5.5 dB at 2.27 μm, a 1-dB bandwidth of ~160 nm, and a back-reflection of -21.2 dB for coupling between optical fibers and SNS waveguides. Also, we achieved an SWG-cladding SNS waveguide microring resonator with an intrinsic quality factor of 6×105 and an extraordinarily large confinement factor of ~80% in air [4]. Based on the proposed SNS waveguide devices, we demonstrated chip-integrated refractive index sensors for CO_2 sensing [5-7] and tunable diode-laser absorption spectroscopy sensors for CH_4, NH_3, and CO sensing at the hundreds-of-ppm level [8]. Moreover, to enable effective light detection at mid-infrared wavelengths for gas-absorption sensing, we explored waveguide-integrated detectors based on $PtSe_2$, a low-dimensional material with a tunable band gap and high carrier mobility. Experimental results show that the deep-subwavelength-thickness waveguide configuration can lead to strong optical absorption of in-plane-propagating light [9-11], enabling effective detection of light at 2.2 μm. Furthermore, we discuss some sensing applications based on the proposed devices. Our results open the door to the development of unprecedented nanophotonic integrated circuits for a broad range of sensing applications.

The author thanks the National Natural Science Foundation of China for its support.

References

[1] C. Du et al., Adv. Mater. Technol. **11**, e01609 (2026).
[2] S. Zhang et al., J. Lightwave Technol. **42**, 5279-5285 (2024).
[3] X. Liu et al., Appl. Phys. Lett. **125**, 111102 (2024).
[4] R. Guo et al., Chip **3**, 100104 (2024).
[5] R. Guo et al., Appl. Phys. Rev. **11**, 021417 (2024).
[6] J. Wang et al., ACS Sens. **10**, 4938-4944 (2025).
[7] Q. Lang et al., Sensors and Actuators, B: Chemical **443**, 138260 (2025).
[8] C. Du et al. Laser & Optoelectron. P. **62**, 1906015 (2025).
[9] T. Xu et al. Nanoscale **16**, 3448-3453 (2024).
[10] T. Xu et al. Nanophotonics **14**, 327-333 (2025).
[11] T. Xu et al. ACS Appl. Mater. Interfaces **14**, 24071-24078 (2025).

Calibrating the radiation intensity of a microwave generator using a quantum sensor based on ^{87}Rb Rydberg atoms in a vapor cell

V.M. Entin[1], D.B. Tretyakov[1], E.A. Yakshina[1,2,3] and I.I. Ryabtsev[1,2]

[1]*Rzhanov Institute of Semiconductor Physics, Siberian Branch of the Russian Academy of Sciences, Lavrentiev avenue 3, 630090, Novosibirsk, Russia*

[2]*Novosibirsk State University, Pirogova Str. 2, 630090, Novosibirsk, Russia*

[3]*Institute of Laser Physics, Siberian Branch of the Russian Academy of Sciences, Lavrentiev avenue 15B, 630090, Novosibirsk, Russia*

E-mail: ventin@isp.nsc.ru

Atoms in highly excited Rydberg states have large dipole moments due to the large orbit radius of the excited electron [1]. This allows for the creation of highly sensitive quantum sensors of electric fields based on laser excitation of Rydberg states of alkali-metal atoms in small optical cells. Their main advantages include high sensitivity and accuracy, small size, narrow detection bandwidth, and wide frequency tuning range.

This talk presents experimental results on the detection of a microwave field using the Rydberg resonance of electromagnetically induced transparency (EIT) and the Autler-Townes effect in an optical cell with ^{87}Rb Rydberg atoms. The dependence of the EIT resonance parameters on the powers of the excitation laser radiation has been studied. The possibility of calibrating the intensity of a microwave generator radiation at a frequency of 58.17 GHz, corresponding to the $41S_{1/2}\rightarrow 41P_{3/2}$ transition between the Rydberg states, has been demonstrated (Fig.1).

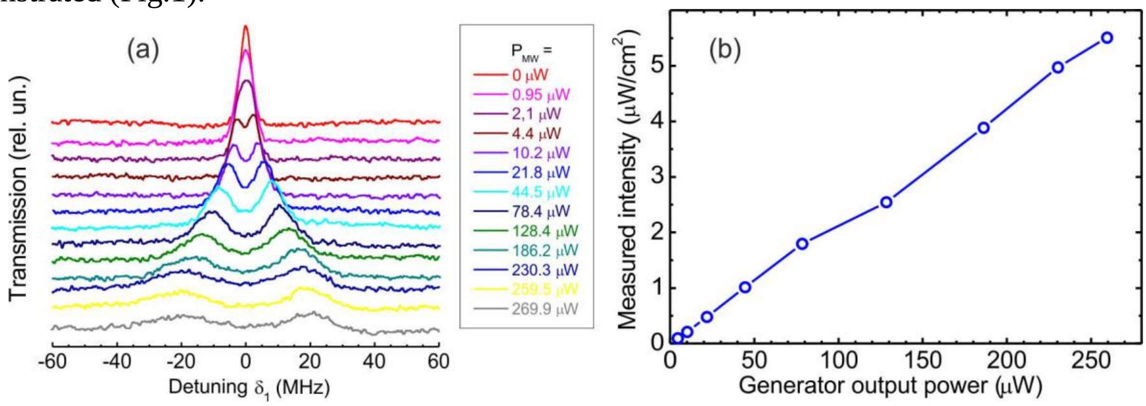

Fig. 1. (a) Experimental traces of Autler-Townes splitting of the first step excitation EIT resonances at various calibrated microwave powers at the frequency 58.17 GHz. (b) True microwave field intensity calculated from splitting data (at the Fig1. (a)) as function of calibrated MW-generator set power.

The obtained results indicate the possibility of reliable measurement of the local microwave field strength and intensity by the Rydberg sensors with high accuracy. The achieved sensitivity value of about 0.1 mW/cm^2 (0.85 V/m) at the frequency of 58.17 GHz corresponds to the values obtained in the experiments of other groups by direct measurement of the Autler-Townes splitting at other frequencies. These strengths also correspond to our theoretical calculations.

The work was supported by the Russian Science Foundation (project 23-12-00067-П, https://rscf.ru/project/23-12-00067-П/).

References

[1] T. F. Gallagher, *Rydberg atoms* (Cambridge: Cambridge University Press, 1994).

[2] D. B. Tretyakov, et al., Pho tonics **10**, 1201 (2023).

[3] V.M. Entin, et al., Calibration of the microwave generator's radiation intensity using a quantum sensor based on Rb Rydberg atoms in a gas cell, (in Russian language), JETP 2026, (accepted for publication).

Comparative analysis of magneto-optical resonances in ^{87}Rb using modulated bichromatic light

M.D. Radchenko[1,2,3], **V.I. Yudin**[1,2,3], **M.Yu. Basalsev**[1,2,3], **A.V. Taichenachev**[1,2], **and O.N. Prudnikov**[1,2]

[1]*Institute of Laser Physics, Siberian Branch, Russian Academy of Sciences, Novosibirsk, 630090 Russia*
[2]*Novosibirsk State University, Novosibirsk, 630090 Russia*
[3]*Novosibirsk State Technical University, Novosibirsk, 630073 Russia*

E-mail: sciencefloppa@gmail.com

The magnetic field measurement is an integral part of many scientific studies and technical applications [1, 2]. There is a variety of quantum magnetometer types, that allow for an unprecedented accuracy and sensitivity of magnetic field measurements to date [3]. However, unlike other quantum magnetometers, atomic magnetometers based on the magneto-optical resonance (MOR) in alkali metal atoms can provide high accuracy and sensitivity in the form of chip-scale, room-temperature operating devices, which do not require background magnetic field shielding [4, 5].

This theoretical study's main focus is to assess the influence of the modulated light parameters and optical transition's angular momentum values on atomic magnetometer metrological characteristics. The developed theoretical model of an atomic magnetometer describes the MOR formed in an alkali atom optical transition $5^2S_{1/2} \rightarrow 5^2P_{1/2}$ (D_1 line) using bichromatic modulated laser light. One component of the bichromatic field is modulated near the Larmour frequency to directly form the MOR signal. The second field component is used to repump atoms from the nonresonant hyperfine level back into the excited state to increase the number of atoms that form the MOR.

The quantum system dynamic is described with density matrix formalism, considering ^{87}Rb real hyperfine structure and Zeeman splitting of each hyperfine level. In the present study, the following light parameters were modulated to form the MOR error signal: amplitude, phase, ellipticity, and polarization ellipse incline. Error signal characteristics reflect metrological characteristics of an optical magnetometer: its sensitivity is proportional to the error signal slope, and accuracy is inversely proportional to the error signal zero shift.

Error signal's shift and slope, as a function of modulation coefficient and intensity of laser light, were obtained with a numerical simulation of the developed theoretical model. The numerical simulation was performed for a typical experimental case of overlapping absorption lines of excited hyperfine states $F_e = 1$ and $F_e = 2$. Analysis of said dependencies indicates that usage of optical transition $5^2S_{1/2}$ ($F_g = 2$) $\rightarrow$ $5^2P_{1/2}$ ($F_e = 1{,}2$) to form MOR leads to an improvement in sensitivity and accuracy of an all-optical atomic magnetometer by one or two orders in comparison with optical transition $5^2S_{1/2}$($F_g = 1$) $\rightarrow$ $5^2P_{1/2}$ ($F_e = 1{,}2$) in a wide light intensity range, regardless of modulation type choice. This result can be used to optimize quantum magnetometers based on magneto-optical resonances in alkali vapor cells, which will further expand their field of applications.

This research was supported by the Russian Science Foundation (project no. 25-42-00093).

References

[1] D. Budker et al., Nat. Phys. **3**, 227 (2007).
[2] K. Jensen et al, Sci. Rep. **6**, 29638 (2016).
[3] A. Fabricant, et al.,, New J. Phys. **25**, 025001 (2023).
[4] Y. Sebbag et al, Light Sci. Appl. **10**, 54 (2021).
[5] M. V. Petrenko et al., Quantum Electron. **52**, 119 (2022).

Physical mechanism and applications on laser cleaning

Feng Song, Dehui Lin, Fei Liang, Yuting Dong, Ming Feng, Lisa Liu
School of Physics & The Key Laboratory of Weak Light Nonlinear Photonics, Ministry of Education, Nankai University, Tianjin 300071, China

E-mail: fsong@nankai.edu.cn

Laser cleaning technology is a green, environmentally friendly, precise, and highly efficient surface treatment method, widely applied in industrial applications such as paint and rust removal, as well as cultural heritage restoration. This paper presents recent research advancements in laser cleaning conducted by our laboratory, covering the physical mechanisms of laser cleaning, the influence of various laser parameters on applications like rust removal and paint removal, and machine vision-based evaluation of laser cleaning effectiveness.

In terms of physical mechanisms, a finite element model of a heterogeneous fiber-resin lattice was established for carbon fiber-reinforced polymer composites. This study revealed the unique heat conduction behavior characterized by two high-temperature zones—one in the resin layer and one in the heterogeneous material—as well as the pattern whereby the superposition of adjacent pulse energies significantly increases the temperature rise of the substrate [1]. For aluminum alloy substrates, a numerical model of multi-pulse cleaning was developed, revealing the heat accumulation effects during laser cleaning [2]. To address the requirement of preserving the anodic oxide film during aircraft skin paint removal, the mechanism of oxide film was elucidated, and a thermal stress-induced peeling (TSIP) strategy was proposed [3].

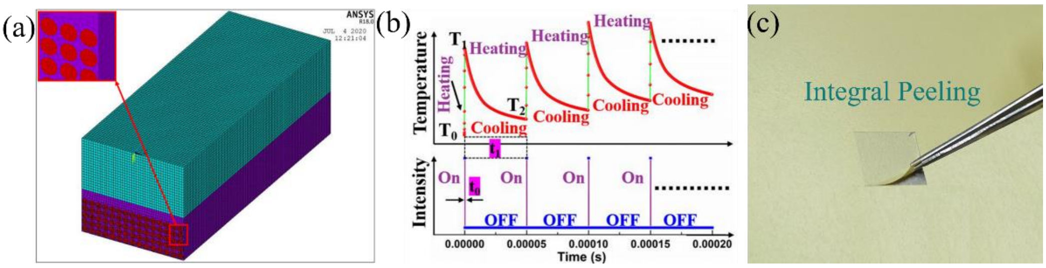

Fig. 1. Laser cleaning: simulation and experimental results. (a) FE mesh of heterogeneous fiber-resin structure [1]; (b) temperature evolution under multi-pulse laser irradiation [2]; (c) integral peeling of paint layer from substrate surface [3].

Regarding the influence of laser parameters on applications, we systematically investigated the effects of key parameters such as laser energy density, spot overlap ratio, and scanning speed on paint removal performance. The scanning speed and spot overlap ratio together determine the number of pulses received per unit area. An excessively low overlap ratio results in incomplete cleaning, whereas an excessively high overlap ratio intensifies heat accumulation and increases the risk of substrate damage [4]. For aluminum alloy substrates, by matching appropriate laser parameters, the thermal stress at the bottom of the paint layer can be made to exceed its adhesion force while remaining below its fracture stress, thereby achieving complete peeling of the paint layer and avoiding damage to the oxide film [3]. When the energy density is too high, micro/nano structures appear on the aluminum alloy surface [5].

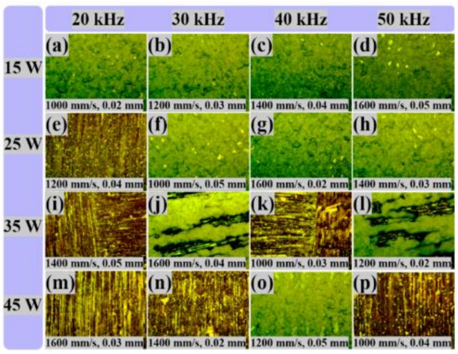

Fig. 2. The macroscopic morphology of samples under different laser process parameters [4].

Regarding the evaluation of laser cleaning effectiveness, we developed a monitoring system based on a convolutional neural network. Three network models, namely VGGNet16, ResNet18, and MobileNet V3-Small, were compared, from which a model suitable for practical working conditions was selected and corresponding evaluation methods were proposed. Based on the monitoring platform, a visual interface software was developed, integrating functions such as image acquisition during the cleaning process, cleaning level determination, and result display. The integration of this system with laser cleaning equipment offers an effective technical solution for objective, real-time, and intelligent assessment of laser cleaning quality.

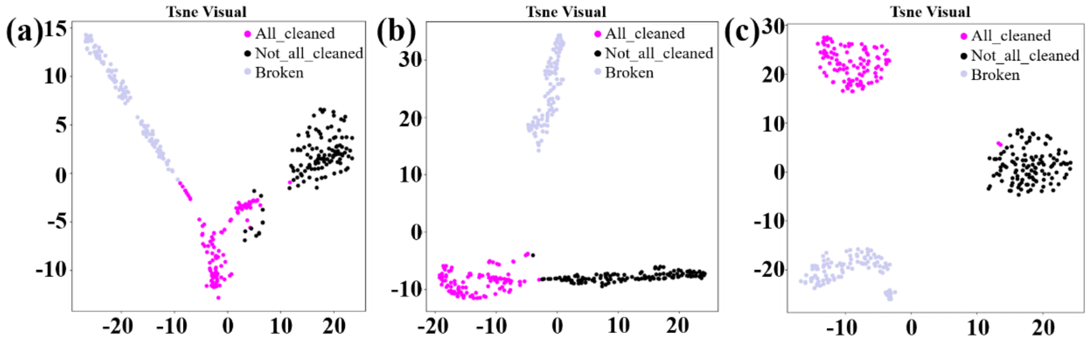

Fig. 3. t-SNE visualization results for the VGG16, ResNet18, and MobileNet V3-Small models.

The authors acknowledge the support from the National Key Research and Development Program of China (Grant Nos. 2022YFB4601500 and 2021YFB3502701) and the National Natural Science Foundation of China (Grant No. 12174206).

References

[1] H. Yang et al., Opt. Laser Technol. **145**, 107450 (2022).
[2] Z. J. Zhao et al., Opt. Quantum Electron. **56**, 179 (2024).
[3] D. H. Lin et al., Opt. Laser Technol. **179**, 112023 (2025).
[4] Z. J. Zhao et al., Vacuum **217**, 112572 (2023).
[5] Z. J. Zhao et al., Int. J. Adv. Manuf. Technol. **126**, 3193 (2023).

Terahertz Spectroscopy of Nonlinear Crystals: In Search of New Radiation Sources

N.A Nikolaev[1]
[1]Institute of Automation and Electrometry, Siberian Branch of the Russian Academy of Sciences, 1 Academician Koptyug Ave., 630090 Novosibirsk, Russia
E-mail: nazar@iae.nsk.su

The terahertz range (0.1–10 THz) remains in demand for a number of fundamental research and practical applications. These include molecular spectroscopy for astrophysics, ecological monitoring, and medical diagnostics; testing of the semiconductors and low-dimensional structures based on them; and study and characterization of new two-dimensional and topological materials. To make progress in these areas and develop new technologies, tunable laser sources with wavelengths longer than 20 μm (<15 THz) are required, but available options are limited today.

One of the solutions is based on the nonlinear optical generators that convert the frequencies of well-developed intense but compact near-infrared laser sources. Although all nonlinear crystalline media have phonons in the region under consideration, we still consider the possibility of their application due to the enhancement of quadratic susceptibility in their vicinity and the predominance of gain over loss in local transparency windows between phonon modes.

The report describes the features of the study of the optical properties of nonlinear crystals in the terahertz region of the spectrum and examines several crystals that can be potentially efficient THz generators.

The proposed approach can be demonstrated using the example of a nonlinear crystal of $KTiOPO_4$ (KTP) in various configurations, demonstrating its potential as a generator of terahertz radiation. We showed that KTP possesses a lower absorption coefficient compared to lithium niobate while simultaneously satisfying the phase-matching conditions for the difference frequency generation process when pumped by intense near-infrared laser sources [1, 2]. Subsequent studies have demonstrated that KTP satisfies the conditions for collinear phase matching in the process of second-harmonic generation within the sub-terahertz frequency range [3]. KTP is known to exhibit high radiation generation efficiency based on the stimulated polariton scattering effect at a frequency of 5.7 THz located in the phonon absorption region [4]. We have demonstrated the possibility of subsequent down-conversion of frequencies from the vicinity of 5.7 THz into the sub-terahertz range [5].

Thus, the series of aforementioned studies suggests that only by employing different cuts and methods of nonlinear optical frequency conversion within a single nonlinear optical crystal is it possible to achieve efficient terahertz radiation generation over a broad frequency range in the far-infrared region. We believe that isomorphs of KTP crystal can be used analogously as well.

References

[1] A. Rybak et al., Crystals 11(2), 125 (2021)
[2] J.-G. Huang et al., Laser Phys. Lett., 15(7) 075401 (2018)
[3] A. Mamrashev et al., Crystals 8(8) 310 (2018)
[4] M.-H. Wu, et al., Optica 6(6) 723 (2019)
[5] N. A. Nikolaev, G. V. Lansky, Atmos. Ocean. Opt. 38(S1) S73 (2025)

Sub-ppm, fast optical humidity sensor

A.S.Kuchyanov, P.A.Chubakov, V.A.Sorokin and A.A. Apolonskiy*
Institute of Automation and Electrometry SB RAS, Novosibirsk, Russia
*E-mail: apolonsky@iae.nsk.su

We describe a cheap sensor for measuring low humidity at a level of 500 ppb (~500 μg/м^3) as well as low humidity generator at a level of 50 ppb for its verification.

Humidity sensors with a sensitivity of less than ppm are needed in a number of applications where water-free gas is a demand [1]. A few examples: the semiconductor industry, uranium enrichment, human health analysis via exhaled air [2].

The most sensitive humidity sensor registered in the Russian Federation is an external cavity-based laser spectrometer from the American company Tiger Optics, capable of measuring as low as 200 ppt. The sensitivity of compact sensors based on semiconductor structures does not exceed 10 ppm. A humidity generator is usually based on the controlled mixing of dry nitrogen, produced by evaporation from a liquid state, with air/nitrogen of known humidity. The Sever-4 generator, developed in Russia, produces a minimum humidity value of 5 ppm.

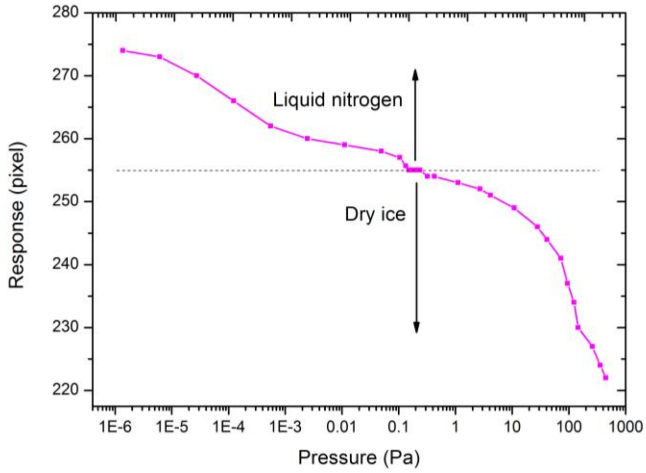

Fig. Sensor response (in pixel) vs gas temperature and pressure

The sensor we developed is based on an opal-like silica structure. Its response to humidity changes is based on the interferometric measurement using a laser. The experiment demonstrated that its limit of detection (LOD) reached 500 ppb, together with the response time 200 μs and the dynamic range 7 orders of magnitude of water pressure (Figure). The combination of these parameters makes the developed sensor unique.

The level of humidity produced by our generator was determined by measuring the rate of water evaporation through a narrow long needle in the container lid. The reduction in the container mass resulting from water diffusion through various needles confirmed the known dependence of the flux on their diameter and length [3].

Since an air sample containing water to be analyzed is difficult to transport and store without undergoing uncontrolled changes, it is desirable to position a humidity sensor close to the volume being measured. This factor favors the development of a cheap, compact sensor like presented here as an alternative to an infrared spectrometer that, while more sensitive, is costly, bulky and requires highly qualified maintenance.

References

[1] Zh. Ma, T. Fei, T. Zhang. Sensors and Actuators B: Chemical **376,** 133039 (2023).
[2] K. Maiti et al. J. Breath Research **12,** 046003 (2018).
[3] R.B. Bird, W.E. Stewart, E.N. Lightfoot, Transport Phenomena, 2nd ed., John Wiley & Sons Inc., New York, 2002, pp. 543–581.

Biomedical applications of terahertz technology

O. Cherkasova[1,2,3]
[1]*Institute of Automation and Electrometry, Siberian Branch of the Russian Academy of Sciences, 1 Academician Koptyug Ave., 630090 Novosibirsk, Russia*
[2]*Institute of Laser Physics, Siberian Branch, Russian Academy of Sciences, 15B Lavrentiev Ave., Novosibirsk, 630090, Russia*
[3]*Novosibirsk Technical University, 20 Karl Marx Ave., Novosibirsk, 630073, Russia*
E-mail: o.p.cherkasova@gmail.com

Biomedical applications of THz technology are an actively developing field of knowledge. Terahertz spectroscopy has shown great potential in biomedical research due to its unique features, such as the non-invasive and label-free identification of biological samples and medical imaging [1]. Application of THz spectroscopy for non-invasive or minimally invasive diagnostics has already been demonstrated for diabetes [2], liver cancer [3], glioma [4] and thyroid cancer [5] diagnosis. Implementing plasmonic metamaterials or metasurfaces can improve the THz spectroscopy's sensitivity to biomarkers [6, 7]. We will discuss applications of machine learning techniques to THz spectroscopy data, which will help to differentiate of glioblastoma and traumatic brain injury [8]. We will demonstrate the unique capabilities of THz radiation in the diagnosis of benign and malignant neoplasms of different nosology and localization [1, 9], diabetic foot [10] and in ophthalmology [11]. We also highlight the biological effects of THz radiation [12] and establishment of safe doses using THz-sensitive fluorescent biosensors [13].

Progress in using THz radiation for biomedical purposes depends on creating simpler and more affordable THz devices, developing systems to deliver THz radiation to tissues, and advancing optical clearing techniques. This work outlines the most viable pathways for the future integration of THz technology in medicine.

The work was carried out within the framework of the state assignment of the IA&E and ILP SB RAS.

References

[1] O.A. Smolyanskaya et al, Progress in Quantum Electronics **62**, 1 (2018).
[2] O.P. Cherkasova et al., Optics and Spectroscopy **120** (1), 50 (2016).
[3] M.M. Nazarov, et al, Optics and Spectroscopy **126** (6), 721 (2019).
[4] O. Cherkasova et al., Appl. Sci. **13**, 5434 (2023).
[5] M.R. Konnikova et al, Biomedical Optics Express **12** (2), 1020 (2021).
[6] O.P. Cherkasova et al., Opt. Quantum Electron. **57**, 340 (2025).
[7] O. Cherkasova et al., Photonics **8**(1), 22 (2021).
[8] D. Vrazhnov et al, Appl. Sci. **14**, 2872 (2024).
[9] N.V. Chernomyrdin et al, Opto-Electronic Advances **6**, 220071 (2023).
[10] G.G. Hernandez-Cardoso et al, Sci. Rep. **7**, 42124 (2017).
[11] I. Ozheredov et al, Laser Phys. Lett. **15** (5), 055601 (2018).
[12] O.P. Cherkasova et al, Journal of Biomedical Optics **26** (9), 090902 (2021).
[13] D. Serdyukov et al., Biomed. Opt. Express **11**, 5258 (2020).

High-resolution laser calorimetry of transparent optical materials

S.M. Vatnik[1]
[1]*VPG LaserONE LLC, Fryazino city, Russian Federation*
E-mail: sVatnik@vpglaserone.ru

With a custom-designed laser calorimeter, whose prototype is described in [1], we measured the absorption performance, front-surface absorption, and estimated the volume scattering in high-quality fused silica samples manufactured by Heraeus and LBO crystals produced by Siberian Crystals LLC. The results of calorimetric measurements of absorption coefficients are in good agreement with data from photothermal common-path interferometry (PCI). For samples shaped as 3×3×20 mm prisms, laser calorimetry yields the accuracy and reproducibility as high as 0.1 ppm/cm. As an example, Fig. 1 presents a series of 10 consecutive measurements of the absorption coefficient α for LBO crystal #o/83.

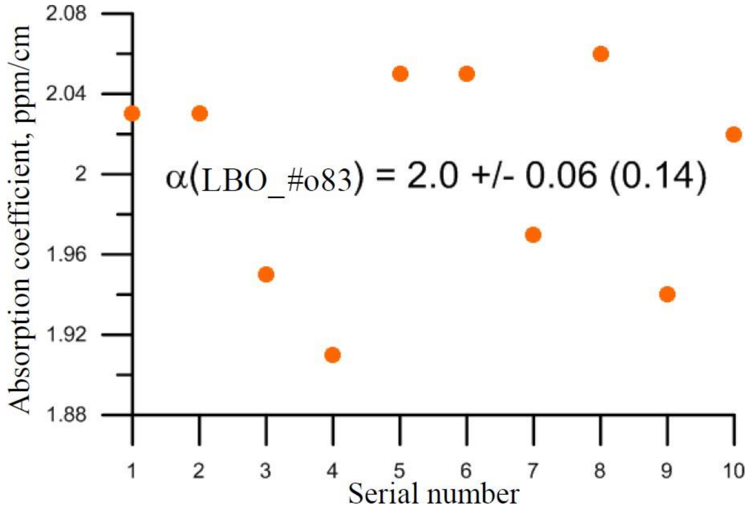

Fig. 1 A series of 10 consecutive measurements of the absorption coefficient α for LBO crystal

The main results of the calorimetric measurements for LBO crystals are given in Table.

## LBO	α, ppm/cm	α(F), ppm	α(B), ppm	S1, ppm	S2, ppm
9A576	1.09±0.16	21.0±0.15	92.8±5.3	3.4±0.034	2.28±0.056
o/83	1.96±0.14	30.8±0.09	68.2±2.6	4.28±0.04	1.72±0.03
321003	5.09±0.09	39.0±0.13	83.0±2.4	4.74±0.07	2.85±0.07
322005	6.0±0.1	55.3±0.38	97.5±4.0	9.10±0.11	3.10±0.05

Statistical analysis of the measurement errors was performed in accordance with the GOST R 8.736-2011 standard. The reproducibility and statistical error are at the level of ~ 0.1 ppm/cm and are practically independent of the duration of the heating-cooling cycles ranged within 8 to 32 seconds. The measurement time for one sample — which includes the absorption coefficient α, the absorption at the front surface α(F), and scattering at the front surface S1 and the balk of the sample S2 — is about 3 minutes. This makes the laser calorimeter suitable for mass quality control of optical elements.

References

[1] S. Vatnik et al., Quantum Electronics **49** (4) 362-364 (2019).

Pulsed inductive discharge as an alternative method for pumping gas active media under low pressure

D.S. Churkin[1], **E.S. Kargapol'tsev**[1], **and R.A. Tkachenko**[1]
[1] *Institute of Laser Physics SB RAS*
E-mail: churkin@laser.nsc.ru

Pulsed inductive discharge is an alternative electrodeless method for pumping low-pressure laser gas media, employing various mechanisms for population inversion formation on electronic and vibrational-rotational transitions of atoms and molecules. The main difference and characteristic of inductive discharge from classical longitudinal or volume transverse electrical discharges is that it is formed by electromagnetic induction, in the absence of metal electrodes in the active medium. Consequently, it is free from the disadvantages associated with sputtering of the electrode material. At the same time, differences in electronic parameters of the inductively coupled plasma occur, which in turn determines difference in the characteristics of spontaneous and laser emission from active media in the inductive discharge compared to the aforementioned classical pumping methods using a high-current electrical discharge between metal electrodes of the discharge gap.

Over the past 20 years, a number of inductive lasers in UV, visible, and IR spectral regions have been created using this method. These include a nitrogen laser with wavelengths of 337.1 nm, 357.7 nm, and 405.9 nm, pulsed inductive IR laser on vibrational-rotational transitions of CO_2 molecules with wavelength of 10.6 μm, and lasers on 3p → 3s transitions of neon atoms with wavelengths in the range of 540 – 693 nm. To date, output energy of the UV inductive nitrogen laser has been achieved 11 mJ with pulse duration 10±1 ns (FWHM). Thus, the pulse power of the laser exceeded 1 MW. The pulsed inductive CO_2 laser had output energy 1.3 J, and its maximum efficiency exceeded 27%. The neon laser radiation in the yellow region of the spectrum had a unique combination of characteristics, namely, pulsed output power and variability of laser operating modes with simplicity and reliability performance.

Authors thank Ministry of Science and Higher Education of the Russian Federation for their supports (Theme No. FWGU-2026-0006).

Adaptive Algorithm for Laser Sensorless Wavefront Correction Using Multi-Criteria Beam Focusing Analysis

V.V. Gromyko[1,2,3], **I.V. Khorsova**[1,3] **and I.I. Beterov**[1,2,3,4]
[1]*Institute of Semiconductor Physics SB RAS, Novosibirsk, Russia*
[2]*Institute of Laser Physics SB RAS, Novosibirsk, Russia*
[3]*Novosibirsk State Technical University, Novosibirsk, Russia*
[4] *Novosibirsk State University, Novosibirsk, Russia*
e-mail: vgromyko0@yandex.ru

Adaptive optical and laser systems offer exceptional capabilities across a wide range of applications. The primary goal of adaptive optics is to fine-tune multiple parameters of an optical system in order to achieve the desired performance characteristics. This approach is widely used in fundamental research, including the generation of arrays of ultracold neutral atoms. Similarly, many modern optical systems with long atmospheric paths, such as telescopes, require dynamic correction of wavefront distortions. Wavefront aberrations can severely degrade the performance of laser systems in numerous applications; therefore, a universal and effective method for compensating aberrations and optical imperfections is highly desirable.

In practice, phase-modulating devices such as spatial light modulators (SLMs) displaying digital holograms and deformable micromirror arrays are commonly used to control the shape of a laser wavefront. The distorted wavefront is corrected by applying an appropriate phase distribution to the correcting element. The required phase shift at each pixel of a hologram or the tilt angle of a micromirror is controlled by the voltage applied to the liquid crystal or the micromirror actuator, respectively. Consequently, the optimization task reduces to determining the optimal voltage distribution across the active elements.

A common limitation of conventional wavefront optimization methods is that they often rely on metrics that do not directly characterize the quality of beam formation when seeking to achieve tight focusing.

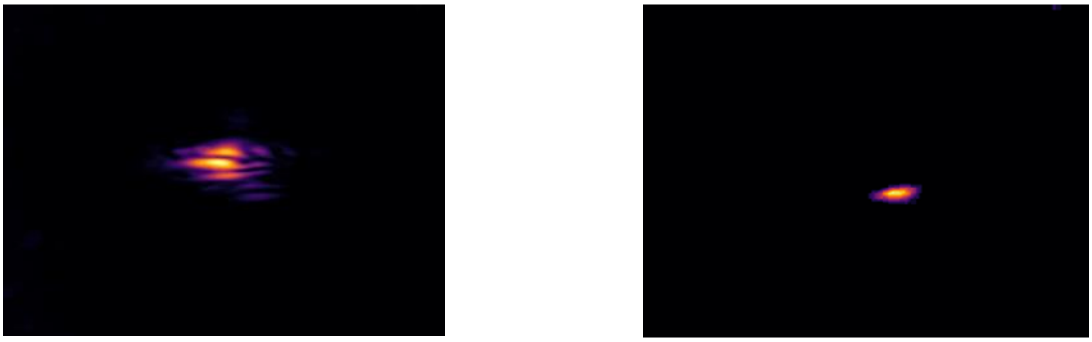

Fig. 1. Experimental optimization of the laser radiation wavefront: intensity distribution before and after optimization

In this work, we implemented an optimization algorithm in a laser system that uses a liquid crystal spatial light modulator as the wavefront-correcting element. The objective function is formulated as an additive scalarization of multiple metrics that characterize the integral intensity, beam size, and beam shape. We validated the proposed multi-criteria optimization algorithm both experimentally and through numerical simulations for the task of morphological laser beam focusing. Figure 1 shows the laser beam correction achieved on the experimental setup. Morphological spot analysis shows promise as a new optimization metric for adaptive optical systems.

This work was supported by Russian Science Foundation grant 23-12-00067П.

Chip-scale SIL laser stabilized to a miniature Fabry-Pérot cavity

O.V. Khronusova[1,2], **A.K. Vorobyev**[2,3], **D.V. Morozov**[2,3], **K.S. Kudeyarov**[1], **N.O. Zhadnov**[1], **D.A. Chermoshentsev**[2,3], **I.A. Bilenko**[3], **N.N. Kolachevsky**[1,3]

[1]*Lebedev Physical Institute, Russian Academy of Sciences, Moscow, Russia*
[2]*Moscow Institute of Physics and Technology, Dolgoprudny, Russia*
[3]*Russian Quantum Center, Skolkovo, Moscow, Russia*

E-mail: olya.hronusova@gmail.com

Ultrastable lasers stabilized to Fabry-Perot (FP) cavities are an essential component of optical atomic clock, precision spectroscopy, low-phase-noise microwave generation [1], coherent optical communication, radar systems, and distributed fiber sensing. At the same time, many emerging applications – transportable optical clocks, navigation and ranging systems, especially airborne and space instruments – require compact laser sources with similarly high coherence. Integrated photonics provides a promising approach to meeting this demand. Recently, a chip-scale self-injection locked (SIL) laser stabilized to a FP cavity with a volume of only 8 ml demonstrated a fractional frequency instability at the 10^{-14} level [2].

In this work, we develop a compact narrow-linewidth laser with improved long-term stability and a reduced cavity volume. The laser source is based on the hybrid integration of a commercially available distributed-feedback laser diode with a high-Q integrated Si_3N_4 microring resonator. The resonator operates in the linear SIL regime [3], although it is also suitable for nonlinear operation accompanied by comb generation. The laser frequency is further stabilized to a miniature vacuum-gap ULE FP cavity ($V < 3$ ml) using the Pound-Drever-Hall locking technique [4].

Following a systematic investigation of the noise sources in the stabilization system and careful optimization of the experimental setup, we achieved stable laser operation close to the thermal-noise limit of the cavity. The resulting fractional frequency instability reaches $5 \cdot 10^{-15}$ for averaging times between 0.5 and 10 s (Fig. 1).

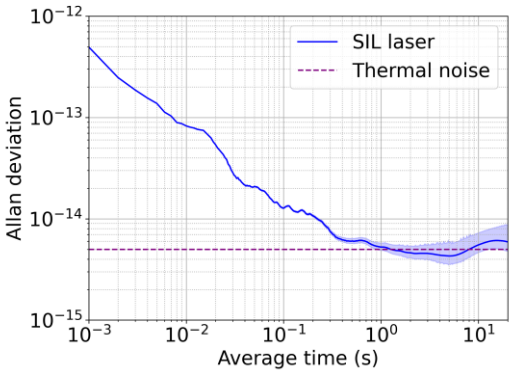

Fig. 1 Fractional frequency instability of the SIL laser locked to FP cavity (blue) and FP thermal noise level (red)

The combination of a narrow-linewidth microresonator-based laser with long-term stability provided by a miniature FP cavity, together with its capability to generate frequency comb, paves the way toward fully integrated photonic frequency references for transportable optical clocks and low-noise microwave photonic systems.

References

[1] I. Kudelin et al., Nature **627**, 534 (2024).
[2] J. Guo et al., Science advances **8**, eabp9006 (2022).
[3] N. Kondratiev et al., Optics Express **25**, 28167 (2017).
[4] R. W. P. Drever et al., Appl. Phys. B **31**, 97–105 (1983).

Laser generation on NV-centers in diamond

D. Genin[1], E. Lipatov[1,2], P. Komarova[2] and V. Vins[3]
[1]Insitute of High Current Electronics SB RAS, Tomsk, Russia
[2]National Research Tomsk State University, Tomsk, Russia
[3]"Velman" LTD, Novosibirsk, Russia
E-mail: de.genin@hcei.ru

Diamond is receiving increasing attention as a material for electronics and photonics devices. This is due to its unique properties: extreme hardness, high thermal conductivity, high charge carrier mobility and high radiation resistance. It also has a low coefficient of thermal expansion, which, combined with the above properties, makes it a promising material for creating active laser elements.

Pure diamond is an indirect-gap material. That's why it is impossible to create light-emitting devices based on pure diamond. On the other hand, it can contain over one hundred different impurity-defect centers, a significant portion of which are color centers, so it is possible to create light-emitting devices based on diamonds with colour centers. One such center is the nitrogen-vacancy center (NV-center). The technology for producing diamonds with NV-centers is currently well established: nitrogen-containing diamond is irradiated by electron beam and then annealed at about 800-100 K. In the negative charge state NV-center typically exhibits a zero-phonon line (ZPL) in the luminescence spectrum at 637 nm and a so-called phonon wing extending to 850 nm.

Laser generation at NV centers was first achieved in 2021 [1]. To date, the parameters of NV lasers have been significantly improved: pulse energies of 400 μJ and generation efficiency exceeding 6% have been achieved. This report presents the latest results obtained in the development of NV-lasers in diamond and discusses future development directions for this class of lasers, existing challenges, and possible solutions.

A study was conducted on the spectral composition of the generated laser radiation. It was shown that the spectrum consists of two components, which are unresolvable at room temperature due to thermal broadening. These components begin to resolve at a temperature of approximately 220 K and have maxima near 706 and 715 nm.

It was shown that the laser pulse duration is always significantly shorter than the pumping pulse duration, with lasing ending when the pumping power level is still quite high. It has been hypothesized that induced absorption of an unknown nature occurs in the active element, which could be induced by the pump radiation. The lifetime of this absorption is presumably less than 100 μs.

This research was supported by Russian Science Foundation, project № 25-29-00702.

References

[1] A. D. Savvin et al., Nat. Com. **12**, 7118, (2021).

Inhomogeneous vs homogeneous spectral line broadening in different superradiant lasing modes

E. R. Kocharovskaya[1], Vl. V. Kocharovsky[1]
[1]*Federal research center A.V. Gaponov-Grekhov Institute of Applied Physics of the Russian Academy of Sciences (IAP RAS), 46 Ul'yanov Street, Nizhny Novgorod, Russia.*
E-mail: katya@ipfran.ru

According to our recent works, there are a variety of superradiant lasing modes under a continuous-wave pumping of an active medium with a homogeneous broadening of spectral line in the case of a symmetric combined Fabry-Perot cavity with distributed feedback of waves (class D combined lasers): 1) single-mode steady-state symmetric lasing with a self-consistent half-wavelength population-inversion grating, 2) symmetric and asymmetric self-modulation lasing with a time-dependent population-inversion grating, 3) spontaneous switching of asymmetric self-modulation lasing with a complete reformation of the population-inversion grating, pressed first to one, then to the other cavity mirror, 4) emission of a periodic or quasiperiodic sequence of pulses of coherent spontaneous radiation with a partially collapsed population-inversion grating; 5) quasi-chaotic lasing of the superradiant pulses with a continuous spectrum and a weakly expressed population-inversion grating, etc. [1-3].

Now, based on numerical modeling of the nonlinear one-dimensional Maxwell-Bloch equations, we examine the influence of a weak inhomogeneous broadening of the spectral line of an active medium on the main features and parameters of the superradiant lasing modes in the class D combined laser [1].

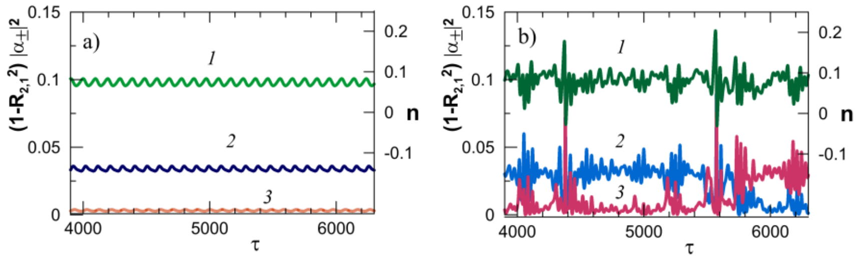

Fig. 1 The dynamics of the sample-averaged population inversion of active centers (curves 1) and oscillograms of the radiation intensity from the left (curves 2) and right (curves 3) ends of a symmetric laser with a pumping level $n_p = 1$, a reflection factor of mirrors R = 0.37, and a length L = 2; see notation in [1,2]. a) Asymmetric self-modulation of a polariton mode in the case of a narrow spectral line with inhomogeneous broadening Δ_0=0.01 that is less than a width of homogeneous broadening Γ_2=0.02. b) Switching of lasing in the case when the widths of inhomogeneous and homogeneous broadening are comparable, $\Gamma_2 = \Delta_0 = 0.02$.

In the case of a Fabry-Perot cavity without distributed feedback, an inhomogeneous broadening with the spectral width smaller than or on the order of a homogeneous broadening can significantly alter the aforementioned modes due to an increase in the number of generated discrete modes and a broadening of the continuous spectrum radiation; see an example in Fig. 1. In particular, switching between quasi-chaotic lasing of superradiant pulses and asymmetric quasi-periodic multimode lasing can take place; spontaneous switching of the predominant emission between the left and right laser ends can also occur.

An addition of an external distributed feedback can lead to constructive or destructive interference between scattering of the counter-propagating waves of the electromagnetic field and polarization of the active medium on two resonant half-wavelength gratings, namely, the intrinsic self-consistent grating of the population inversion of the active medium and the modulation of the external waveguide layers or dielectric permittivity of an active-medium matrix [2,3]. This phenomenon results in other modifications of the superradiant lasing modes, which are described in the present paper as well.

The work was supported by the contract No. FFUF-2024-0038 of the Federal Research Center A.V. Gaponov-Grekhov Institute of Applied Physics of the Russian Academy of Sciences.

References

[1] Vl.V. Kocharovsky et al., Physics Uspekhi **60**, 345 (2017).
[2] E.R. Kocharovskaya et al., FTP **58**(4), 202 (2024).
[3] E.R. Kocharovskaya et al., Opticheskii Zhurnal **93**(8), (2026) in press.

Poster Session A

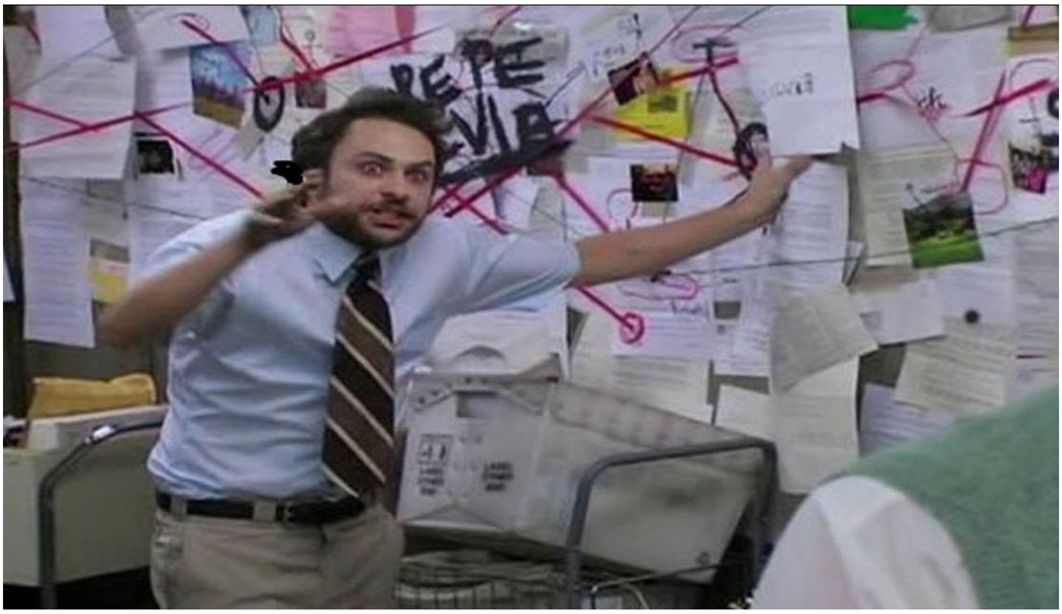

Detection of N_2O and NO_2 Absorption in the Atmosphere Using a Laser Gas Analyzer

Ya.V. Antonenko[1,2], **I.V. Sherstov**[1,2]
[1]*Institute of Laser Physics, Siberian Branch, Russian Academy of Sciences, Novosibirsk, 630090 Russia*
[2]*Novosibirsk State Technical University, Novosibirsk, 630073 Russia*
E-mail: antonen-ko.y@yandex.ru

The present work is dedicated to the development and experimental study of a highly sensitive photoacoustic laser gas analyzer for nitrogen oxides (NO_2 and N_2O). The increased content of nitrogen dioxide (NO_2) significantly worsens the air quality, which negatively affects human health [1]. Nitrous oxide (N_2O) has a strong greenhouse effect in the atmosphere [2]. This explains the importance of monitoring these gases in the environment.

To control low concentrations of nitrogen oxides, it is proposed to use a two-channel photoacoustic gas analyzer based on two resonant differential photoacoustic detectors (PAD) [3] and two lasers: a quantum cascade laser (λ = 4.472 μm) and a laser diode (λ = 447 nm) for N_2O and NO_2, respectively. Nitrogen oxides absorptions is detected in the absorption bands of N_2O and NO_2 which are free from the absorption bands of water vapor (H_2O) and other atmospheric gases (CO, $^{12}CO_2$, $^{13}CO_2$, O_3, O_2) [4].

Experiments have been carried out to determine the threshold sensitivity of two optical channels of a gas analyzer. Lasers operate in a pulse-periodic mode with repetition rate equal to the lowest resonant frequency of the differential PAD (~1750…1780 Hz). The noise level was measured in a buffer gas, nitrogen (N_2), and to measure the concentration, the detector was filled with calibration gas mixtures based on N_2 with an admixture of N_2O or NO_2. Due to absorption in the gas (photoacoustic effect), pulses of laser radiation excite acoustic vibrations in the PAD, which are recorded by a microphone. Calibrated readings of the N_2O and NO_2 sensors are shown on the Fig. 1.

Laboratory measurements of the concentration with an integration time of τ = 0.1 s showed threshold sensitivity (with a *signal/noise* = 1) n_{min} = (36.85 ± 6.01) ppb N_2O and n_{min} = (52.04 ± 4.27) ppb NO_2. Calibration of the responses was performed using calibration gas mixtures (N_2 + 10 ppm N_2O) and (N_2 + 48.3 ppm NO_2). We suppose that with an increase in the integration time to τ = 10 s, the threshold sensitivity will reach ~1 ppb.

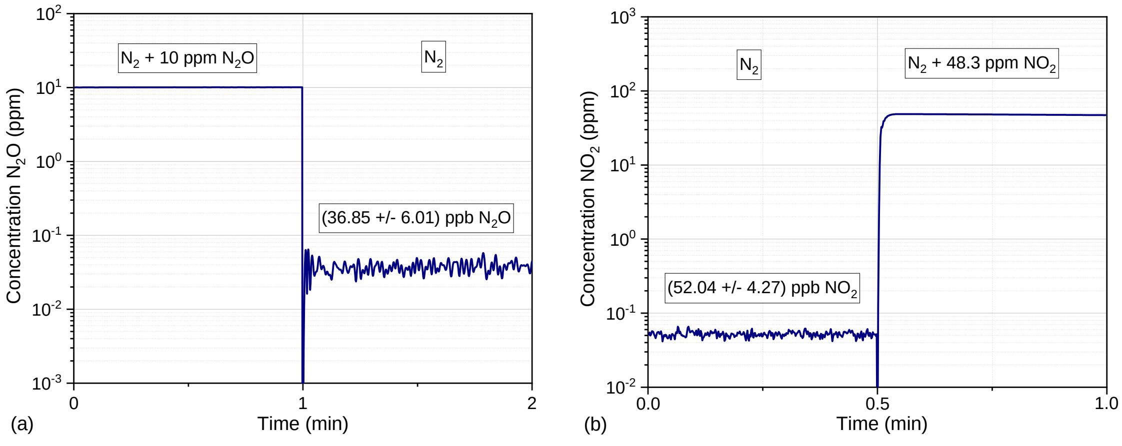

Fig. 1 Calibrated readings of the N_2O sensor (a); calibrated readings of the NO_2 sensor (b)

The experimental setup of the laser photoacoustic gas analyzer developed in this study enables high-sensitivity measurements of nitrogen oxides (NO_2 and N_2O) concentrations in real time and under field conditions.

References

[1] World Health Organization, WHO global air quality guidelines. Particulate matter ($PM_{2.5}$ and PM_{10}), ozone, nitrogen dioxide, sulfur dioxide and carbon monoxide. WHO, Geneva (2021).
[2] World Meteorological Organization, WMO Greenhouse Gas Bulletin No. 21. WMO, Geneva (2025).
[3] I.V. Sherstov et al., Infrared Phys. Technol. **133**, 104868 (2023).
[4] HITRAN database [Электронный ресурс]. URL: https://hitran.iao.ru

Modeling of Pump Distribution and Thermal Lensing in a Flashlamp-Pumped Nd:YAG Laser

H. Diab[1,2], P. A. Statsenko[1], S. I. Trashkeev[1], S. G. Strutz[1], M. N. Khomyakov[1], N. V. Shakhaov[1], A.P. Mayorov[1]

[1]*Institute of Laser Physics SB RAS, Russia, Novosibirsk, 630090*

[2]*Novosibirsk State University, Russia, Novosibirsk, 630090*

E-mail: haladyab7@gmail.com

A self-consistent numerical model of thermal-lens formation in a pulsed flashlamp-pumped Nd:YAG laser is presented. The model combines spectrally resolved ray tracing of pump radiation in an elliptical cavity, transient heat-transfer calculations, and thermo-optical analysis [1,2] within a unified computational framework. The absorbed pump-energy distribution is calculated using the xenon flashlamp emission spectrum [3], wavelength-dependent Nd:YAG absorption [4], Fresnel reflection and refraction, and diffuse scattering [5]at the laser-rod surface.

The calculated absorbed-energy distribution is used as the heat source in a transient thermal model based on the heat-conduction equation. Thermal-lens formation is subsequently analyzed through optical-path-length variations induced by the temperature field. The model predicts both the mean thermal-lens focal length and its temporal evolution under repetitive pulsed pumping.

Calculations were performed for a side-pumped Nd:YAG laser consisting of a 6-mm-diameter, 100-mm-long Nd:YAG rod and an INP-6/90 xenon flashlamp installed in a K-301D elliptical pump chamber. Thermal-lens measurements were carried out using a 660-nm probe beam at repetition rates of 10, 20, and 50 Hz. Independent validation of the thermal model was performed using infrared thermal imaging of the laser-rod end face.

The simulations show that thermal-lens pulsations are governed by the ratio between the interpulse period and the characteristic thermal-diffusion time of the laser rod. Increasing the repetition rate leads to a significant reduction in focal-length oscillations, indicating improved thermo-optical stability. The calculated temperature distribution is in good agreement with thermal-imaging measurements, supporting the validity of the proposed model.

Comparison of calculated and experimental focal-length dependences yielded a pump-to-absorbed-energy conversion efficiency of $\eta = (5.0 \pm 0.1)$ %, while an independent estimate obtained from the ray-tracing model gave $\eta \approx 4.9\%$. The discrepancy between calculated and measured focal lengths did not exceed 10% over the investigated pulse-energy range.

The results demonstrate that thermal-lens measurements can provide a reliable indirect method for determining absorbed pump energy and validating thermal models of flashlamp-pumped solid-state lasers. The developed approach may be useful for the design, optimization, and diagnostics of high-energy Nd:YAG laser systems.

References

[1] W. Koechner, Appl. Opt. **9**, 2548–2553 (1970).

[2] J. D. Foster et al., J. Appl. Phys. **41**, 3656–3663 (1970).

[3] PerkinElmer Optoelectronics, "High Performance Flash and Arc Lamps," technical catalog, Available: perkinelmer.com www.perkinelmer.com/opto

[4] P. Cross, "Nd:YAG — Nd:Y3Al5O12," S. Prahl, Ed., Oregon Medical Laser Center Spectra Database, Available: omlc.org https://omlc.org/spectra/lasermedia/html/052.html

[5] B. T. Phong. (1975). Illumination for computer generated pictures. Seminal graphics: pioneering efforts that shaped the field.

Erbium-doped NALM fiber laser with dispersion wedges

A.A. Filonov[1], V.S. Pivtsov[1,2], and N.A. Koliada[1,3]

[1]*Institute of Laser Physics SB RAS, Novosibirsk, Russia*

[2]*Novosibirsk State Technical University, Novosibirsk, Russia*

[3]*Institute of Automation and Electrometry, SB RAS, Novosibirsk, Russia*

E-mail: aa.filonov@mail.ru

In this work, we demonstrate and experimentally investigate a new configuration of a figure-nine passively mode-locked erbium fiber laser based on a nonlinear amplifying loop mirror (NALM). For the first time, we explore mode locking in this architecture using optical wedges to adjust the net cavity dispersion (Fig. 1.a). Quartz wedges with a group velocity dispersion of 11550 fs^2/cm were employed. Typically, the net cavity dispersion (NCD) is adjusted by varying the resonator fiber length. However, this is very difficult to achieve with high precision due to the fiber splicing process. Using optical dispersion wedges circumvents this problem. First, the intracavity dispersion is roughly adjusted using optical fibers, and then fine adjustment is performed using the dispersion wedges. Precise tuning of the NCD is necessary to achieve the minimum pulse duration. This is critical for applications where the laser serves as an integral part of a system for metrology and navigation, such as a femtosecond frequency comb [1, 2].

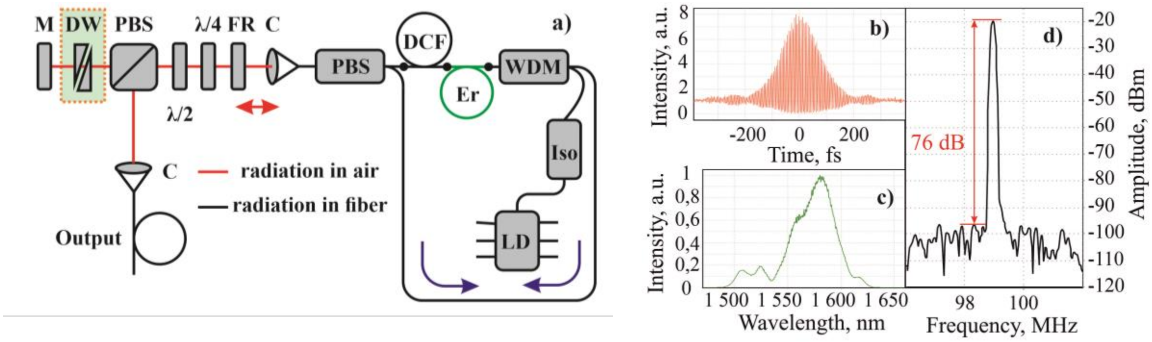

Fig. 1. a) Schematic diagram of the Er-doped NALM laser with dispersion wedges. M: mirror, DW: dispersion wedges, PBS: polarizing beam splitter, λ/2 and λ/4: waveplates, FR: Faraday rotator, C: collimator, DCF: dispersion compensating fiber, Er: erbium-doped fiber, WDM: wavelength division multiplexer, Iso: isolator, LD: laser diode; b) radio spectrum, the resolution is 100 kHz; c) optical spectrum, the resolution is 1 nm; d) interferometric autocorrelation trace, the resolution is 1 fs.

During the first stage of this work, we experimentally investigated the output parameters of the erbium-doped NALM laser at NCD values of 1.9 ps^2, 0.18 ps^2 and -0.001 ps^2. The dispersion was varied using a highly normal-dispersion fiber (Force Photonics HNLF DS). The use of dispersion wedges in the next step of this work significantly improved the optical properties of the laser radiation. The pulse duration was reduced from 200 fs to 110 fs (Fig. 1.b). At the same time, the optical spectrum width increased from 20 nm to 40 nm at the full-width at half-maximum (Fig. 1.c). A record signal-to-noise ratio (SNR) of 76 dB for the fundamental repetition rate of a NALM erbium fiber laser operating without frequency stabilization was achieved (Fig. 1.d). Such an SNR value was enabled by the optimization of nonlinear-dispersion effects and the use of a low-noise pump laser diode.

In conclusion, an erbium-doped fiber laser based on a NALM with dispersion wedges exhibiting a pulse duration of 110 fs and a record SNR of 76 dB for the fundamental repetition rate was demonstrated and characterized.

The study was carried out within the framework of the state assignment (Project No. 075-00468-26-00) using the equipment of the "Femtosecond Laser Complex" Center for Shared Use at the Institute of Laser Physics SB RAS.

References

[1] P.G. Kryukov, Quantum Electron. **31**, 2 (2001).

[2] A.A. Filonov et al., Laser Phys. Lett. **20**, 095101 (2023).

Local surroundings of Nd^{3+} ions in CeO_2 nano- and microparticles

A.K. Ginkel[1], O.A. Morozov[1,2], S.L. Korableva[1], M.S. Pudovkin[1], R.M. Rakhmatullin[1*], A.A. Rodionov[1], V.V. Semashko[1,2]

[1]*Kazan Federal University, Institute of Physics, Kazan, Russia*

[2]*Zavoisky Physical-Technical Institute, FRC Kazan Scientific Center of RAS, Kazan, Russian Federation*

E-mail: fyz0561999@gmail.com

This work presents an EPR and luminescence investigation of CeO_2 nano- and microparticles doped with Nd^{3+} ions (0.1, 0.5, and 1 at.%) and prepared via different synthesis routes. CeO_2:Nd^{3+} nanoparticles were obtained using two main methods: direct coprecipitation from an aqueous solution, and a conversion approach that involves first synthesizing CeF_3:Nd^{3+} nanoparticles followed by air annealing to transform them into CeO_2:Nd^{3+} structures. The results show that Nd^{3+} ions in nanoparticles prepared by direct coprecipitation reside predominantly in low-symmetry crystal fields and are EPR-silent. This suggests that in this type of nanoparticle, the doped Nd^{3+} ions lack an eightfold oxygen coordination in their nearest-neighbor shell.

Microparticles were produced by grinding CeF_3:Nd^{3+} crystals, followed by annealing in air. XRD analysis of all samples annealed at 600 °C confirmed a pure fluorite-type CeO_2 structure with no secondary phases. Unlike in the nanoparticles, EPR and luminescence measurements revealed that a portion of Nd^{3+} ions in the microparticles occupy distorted cubic symmetry sites.

It is proposed that in all studied samples, the majority of Nd^{3+} ions reside in trigonal crystal field sites, with charge compensators oriented along the local [111] axis (fig.1 (a)). This interpretation is consistent with theoretical predictions that the lowest energy level of Nd^{3+} in a trigonal field is a "non-resonant" doublet ($\Gamma_{4,5}$) [1], which exhibits zero transition probability regardless of the magnetic field orientation.

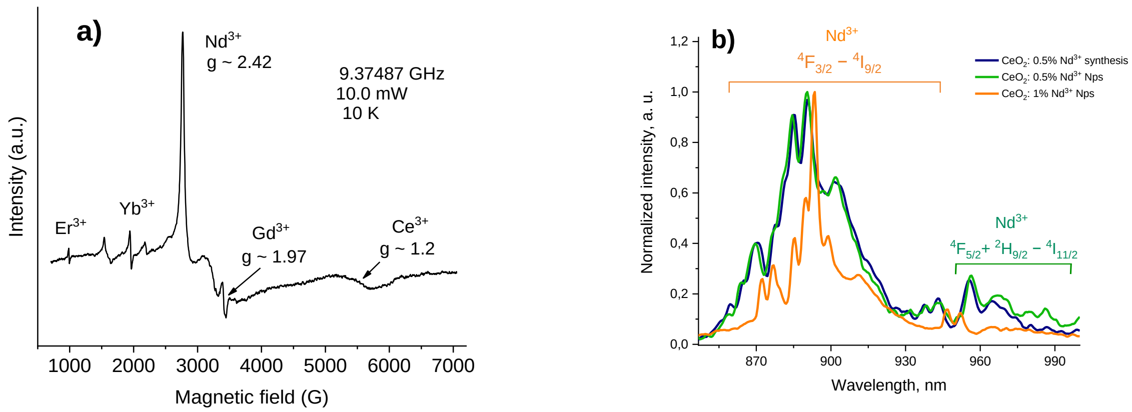

Fig. 1 a) EPR spectra of microparticles with CeO_2 structure, measured at 10 K $CeF_3 \rightarrow CeO_2$: 1%Nd^{3+}, 9.37487 GHz, b) The luminescence spectra of the sample #4 ($CeF_3 \rightarrow CeO_2$:0.5%Nd^{3+} NPs), sample #5 ($CeF_3 \rightarrow CeO_2$:1%Nd^{3+} NPs), and sample #6 (CeO_2:0.5%Nd^{3+} NPs), at 300 K and excited at λ_{ex} = 780 nm (corresponding to $^4I_{9/2}$ - $^4F_{5/2}$, $^2H_{9/2}$ transitions of the Nd^{3+} ions).

A significant alteration in the shape of the luminescence spectra was observed upon annealing at 600 °C relative to the non-annealed state (fig.1 (b)). All detected luminescence peaks were attributed to either transitions between the Stark components of the $^4F_{3/2}$ and $^4I_{9/2}$ manifolds (856–960 nm) or the $^4F_{5/2}$ + $^2H_{9/2} \rightarrow {}^4I_{11/2}$ transitions (960–1000 nm) [2]. Moreover, the spectra reveal that axial symmetry sites (trigonal and tetragonal) constitute the dominant environment for Nd^{3+} ions.

This work was supported by a subsidy granted to Kazan Federal University for the implementation of a state task in the field of scientific research. Project FZSM-2025-0004.

References

[1] L.Y. Shekun, Fiz. Tverd. Tela **9**, 948 (1967) [(Sov. Phys. Sol. State **9**, 742 (1967)).

[2] M. Michalska et al., Heliyon, **7**, e06958 (2021).

The effect of Coronal Mass Ejections on exoplanet Lyα line absorption

M. P. Golubovsky[1,2], **A.G. Zhilkin**[2], **D.V. Bisikalo**[2,3] **and G.N. Tsurikov**[2]
[1]*Institute of Laser Physics, Siberian Branch Russian Academy of Sciences, Novosibirsk, 630090 Russia*
[2]*Institute of Astronomy, Russian Academy of Sciences, Moscow, 119017 Russia*
[3]*National Center for Physics and Mathematics, Sarov, Nizhny Novgorod oblast, 607182 Russia*
E-mail: maxym9121@gmail.com

Modern and next-generation observational instruments enable the detection of absorption in exoplanetary atmospheres across multiple spectral lines. In particular, the hydrogen Lyα line plays a key role in probing atmospheric escape and extended exospheres of exoplanets [1]. Variations in Lyα absorption observed during planetary transits are often associated with stellar high-energy irradiation and activity.

Coronal Mass Ejections (CMEs) are explosive stellar events involving the ejection of large amounts of plasma with energies up to ~10^{34} erg. Although direct observations of stellar CMEs remain limited, their presence can be inferred indirectly through their impact on planetary atmospheres and observed spectral signatures.

In this work, we investigate the influence of CMEs on Lyα absorption using a hybrid 3D aeronomical model of an exoplanetary atmosphere. The simulation begins under steady-state stellar wind conditions. At a specified moment, the stellar mass-loss rate and XUV/X-ray flux are increased to mimic flare and CME conditions. Enhanced irradiation affects both the ionization state and the dynamics of escaping hydrogen, modifying the observed Lyα transit signal.

The Lyα absorption signature is particularly sensitive to high-velocity neutral hydrogen populations. It has been shown that the interaction between the stellar wind and planetary outflow leads to charge-exchange reactions producing energetic neutral atoms (ENAs), which generate blue-shifted absorption in the Lyα line [2, 3]. These ENAs can contribute to absorption at velocities up to ~100 km s^{-1}.

Our model predicts that CME events enhance this effect, leading to stronger and more extended absorption in the blue wing of the Lyα line. The velocity distribution of ENAs is calculated using a kinetic approach, allowing us to resolve their contribution to the line profile. Since ENAs originate from stellar wind protons, their velocities differ significantly from those of the bulk atmospheric hydrogen.

Observationally, Lyα transit measurements are challenging due to interstellar absorption and limited UV capabilities of current instruments. Nevertheless, Lyα absorption has been robustly detected for several systems, including HD 209458b and GJ 436b [4, 5].

This work was supported by the Russian Science Foundation (project no. 22-12-00364-p).

References

[1] J. E. Owen et al., MNRAS **518**, 4357 (2022).
[2] Holmström, M. et al., Nature **451**, 970 (2008).
[3] Kislyakova, K. G. et al., Science **346**, 981 (2014).
[4] Vidal-Madjar, A. et al., Nature **422**, 143 (2003).
[5] Ehrenreich, D. et al., Nature **522**, 459 (2015).

Laboratory simulation of plasma jet expansion in a transverse magnetic field

<u>A.E. Ivanov[1]</u>, I.F. Shaikhislamov[1], V.G. Posukh[1], A.G. Berezutsky[1], A.A. Chibranov[1], M.V. Loginov[1], M.S. Rumenskikh[1], I.B. Miroshnichenko[1], Yu.P. Zakharov[1]

[1]*Institute of Laser Physics SB RAS*

E-mail: arteemiyy.iv@gmail.com

A jet is defined as a narrowly directed, collimated plasma flow [1]. On the KI-1[2] facility, extended jets with lengths of up to 1 meter were successfully generated. Such a scale of the plasma flow enabled comprehensive probe-based diagnostics, which provided a detailed spatial structure of the jet.

The magnitude of the external magnetic field was B_0 = 340 G. The plasma front velocity was 150 km/s with an energy of $E_0 \approx 30$ J. Initially, a magnetic cavity was formed with a transverse dimension consistent with the theoretical estimate for magnetic-field inhibition R_b. Beyond this cavity, the flow compresses into a thin current sheet. The thickness of the sheet was ~ 4 cm. Within the sheet, the magnetic field gradually penetrates back as the jet propagates, while the plasma density decreases. Concurrently, the plasma expands freely along the magnetic field lines.

For the first time in a laboratory experiment, the magnetic field component along the jet propagation direction was measured, which can be interpreted as an Alfven wing [3]. Two distinct phases were observed. The first phase corresponds to the propagation of the Alfvenic component at the characteristic high velocity through the low-density background plasma. The second phase is associated with the denser plasma of the jet itself. In both phases, the B_x field component exhibits opposite polarities on either side of the sheet (±Z). In the first phase, the B_x component reverses sign upon reversal of the external field, a hallmark of an MHD process. In the second phase, no such reversal occurs, indicating a Hall-dominated process.

Overall, the obtained data demonstrate the frozen-in condition of the external magnetic field into the propagating jet. The magnetic Reynolds number, $R_{eM} \approx 115$, along with the observed Alfven wing signatures, are consistent with the frozen-in flux constraint for the plasma electrons.

The work was carried out within the framework of the scientific program of the National Center for Physics and Mathematics (NCPM) "Experimental Laboratory Astrophysics and Geophysics"

References

[1] R.E. Pudritz et al., Space Sci. Rev. **169**, 27–72 (2012).
[2] I. F. Shaikhislamov, et al., Astronomy Reports **69**, S91–S102 (2025).
[3] Neubauer F. M., Journal of Geophysical Research: Space Physics. **85**, 1171-1178 (1980).

Investigation of the temperature dependence of the luminescent intensity ratio in CeF_3-YF_3-TbF_3 nanoparticles

S.I. Kalinichenko, M.S. Pudovkin
Kazan (Volga) Federal University, Institute of Physics, 18 Kremlevskaya Street, building 1, Kazan, 420008
E-mail: kalinichenko_sveta12@mail.ru

Rare-earth-doped fluoride nanoparticles are promising candidates for luminescent thermometry, as they combine stability with low cytotoxicity [1]. Particularly attractive are co-doped systems like Ce^{3+}/Tb^{3+}, in which the donor ion is excited via an allowed 4f-5d transition, leading to high temperature sensitivity thanks to the strong electron–phonon coupling at the Ce^{3+} 5d levels [2, 3]. However, the processes of thermal quenching and energy transfer in these materials, especially at cryogenic temperatures (below 300 K), have not yet been thoroughly investigated.

The studied $Ce_{0.5}Y_{0.5-X}Tb_XF_3$ (X = 0, 0.001, 0.002, 0.005, 0.01, and 0.05) nanoparticles were synthesized via the water-based co-precipitation method. All the samples demonstrated diameters in the 17–20 nm range and a hexagonal phase corresponding to the phase of CeF_3. Under 266 nm excitation (4f–5d absorption band of Ce^{3+}), the luminescence spectrum shape was notably dependent on temperature. The integrated luminescence intensity ratio (LIR) of Ce^{3+} and Tb^{3+} ($^5D_4 - {}^7F_3$) peaks was chosen as a temperature-dependent parameter. It is shown that the LIR function for these transitions monotonically decreases with temperature; however, the slope of the curve depends significantly on the sample composition. This is explained by the fact that at low Tb^{3+} concentrations, the temperature dependence of the spectra is mainly governed by the effective thermal quenching of Ce^{3+} luminescence. With increasing Tb^{3+} concentration (X = 0.01-0.05), the probability of energy transfer from Ce^{3+} to Tb^{3+} increases. The temperature sensitivity of this process is lower, so the rate of decrease of LIR is also reduced. The revealed role of Tb^{3+} concentration in shaping the temperature response underscores the importance of further investigations into energy transfer processes, since a deeper understanding of these processes will enable targeted control over the thermometric characteristics of the material.

In addition, the spectral characteristics of $Ce_{0.5}Y_{0.5-X}Tb_XF_3$ (X = 0) nanoparticles were investigated. The shape of the temperature dependence of the LIR for this sample is attributed to the predominance of thermal quenching of cerium ion luminescence due to strong electron–phonon coupling. The activation energy for this process was also calculated. The calculated activation energy for thermal quenching of Ce^{3+} luminescence was found to be 0.16 eV. This value is comparable with literature data for Ce^{3+}/Tb^{3+} systems in various crystalline matrices, where the activation energy ranges from 0.1 to 0.3 eV depending on the composition and structure of the material. [4].

This research was funded by the subsidy allocated to Kazan Federal University for the state assignment in the sphere of scientific activities (project number FZSM-2025-0004).

References

[1] C.D. Brites et al., Advanced Materials **35**(36), 2302749 (2023).
[2] M. S. Pudovkin et al., Optical Materials **148**, 114831 (2024).
[3] X. Zhang et al., Dyes and Pigments **145**, 476-485 (2017).
[4] W. R. Liu et al., Optics express **17**(20), 18103-18109 (2009).

Symmetric quantum gates for entanglement generation in arrays of ultracold neutral atoms

K. V. Kozenko[1,2], V.V. Gromyko[2,4] and I.I. Beterov[1,2,3,4]
[1]*Novosibirsk State University, Novosibirsk, Russia*
[2]*Institute of Semiconductor Physics SB RAS, Novosibirsk, Russia*
[3]*Novosibirsk State Technical University, Novosibirsk, Russia*
[4]*Institute of Laser Physics SB Ras. Novosibirsk, Russia*
E-mail: k.kozenko@g.nsu.ru

Scaling quantum processors remains one of the central challenges in modern quantum information science. One of the most promising platforms for this task is arrays of ultracold neutral atoms serving as qubits. Realizing the full computational power of these systems requires high-fidelity two-qubit gates that can reliably generate entanglement. While recent experiments have demonstrated excellent gate performance under global illumination of the entire array, the implementation of universal quantum algorithms demands the ability to address individual qubits. The main experimental obstacle to individual addressing is the spatial inhomogeneity of focused laser beams, which leads to position-dependent Rabi frequencies and degraded gate fidelity. A promising approach to overcome this limitation is three-photon laser excitation, for which the effective Rabi frequency is significantly less sensitive to atomic displacements in the optical dipole trap [1]. The goal of this work is to develop and numerically optimize high-fidelity two-qubit gates that are robust against laser intensity variations, a key requirement for scalable individual qubit control.

In this work, we perform numerical optimization of controlled-Z (CZ) gates with smooth control profiles using a modified version of the RydOpt library. We show that, under experimentally realistic parameters, the optimized gates achieve a maximum fidelity of 99.95%, thereby validating the proposed approach [2]. To ensure robustness against spatial intensity inhomogeneities, we develop a multi-stage cascade optimization algorithm for the laser pulse phase profile. This approach enables the synthesis of amplitude-robust protocols across various classes of amplitude ansatzes. We find that constant-amplitude protocols exhibit excellent robustness, keeping the infidelity below 10^{-5} for amplitude deviations up to ±5% [3].

Furthermore, we show that the amplitude-robust gates developed in this work provide a significant advantage for individual addressing. This advantage becomes especially important under spatial intensity inhomogeneities that closely simulate realistic experimental conditions. The infidelity due to imbalance of laser intensities for two atoms does not exceed 10^{-4}, making the gate schemes suitable for use in scalable quantum computing devices. The analytically defined phase profiles can be directly implemented in the experiments. This work was supported by the Foundation for the Advancement of Theoretical Physics and Mathematics ”BASIS” Grant No. 25-1-1-57-1.

References

[1] Bezuglov N.N. et al., Phys. Rev. A. **112**, 063103 (2025).
[2] Beterov I.I. et al., arXiv:2510.04766.
[3] Kozenko K. V. et al., arXiv preprint arXiv:2604.12279 (2026).

Magnetooptical Hanle resonances in the cesium vapor for quantum magnetometry application

<u>**K.S. Kozlova[1]**</u>**, A.O. Makarov[1], D.V. Brazhnikov[1] and A.N. Goncharov[1]**

[1]*Institute of Laser Physics SB RAS*

<u>E-mail:</u> katyak065@gmail.com

Nowadays, optically pumped magnetometers (OPM) are developing rapidly and have applications in different areas: medicine (MEG, MCG, etc.), navigation, mineral exploration, geophysics and space exploration. OPM are highly sensitive, have small sizes and power consumption, can work in near-room temperatures, and, because of this, have lower cost in comparison to superconducting quantum interference devices (SQUID), which were considered the most sensitive magnetic field sensors.

In the current work magnetometer scheme based on registration of magnetooptical resonances arising due to ground state Hanle effect [1.2] were considered. In the experimental setup a miniature cell ($V \approx 0.1$ cm^3) filled with ^{133}Cs vapor and 200 Torr $Ar+N_2$ buffer gas are used. In the classical Hanle scheme circularly polarized light and modulation of the transverse component of the magnetic field were used. Resonances were registered in changing the transmission of light through the cell.

In this work a modification of setup with using an elliptically polarized light and polarimetric registration method was suggested [3]. In such a configuration, the circular components of elliptical polarization can be represented as a probe wave and a pump wave. By directing two components to different channels of a balanced photodetector, it is possible to subtract the same noise present in them and improve signal-to-noise ratio in resulting resonance (Fig. 1).

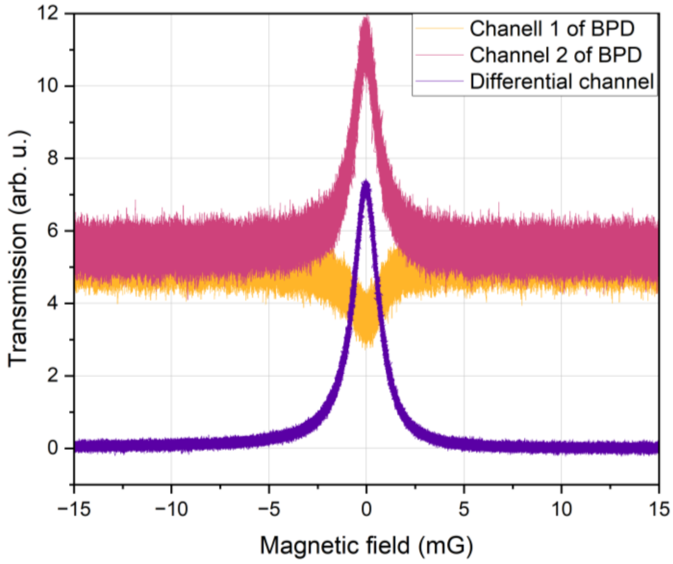

Fig. 1 Example of the magnetooptical resonance in modified Hanle scheme with cell temperature ≈85°C, optical power ≈600 mkW and polarization ellipticity ≈10°

Resonance registration was carried out for both schemes depending on the experimental setup parameters: cell temperature, optical power of light beam and polarization ellipticity. Improving the signal-to-noise ratio in the modified circuit results in improved sensitivity of the modified circuit compared to the classical one. The results presented in this work can be used to develop a highly sensitive magnetic field sensor for biomedical application.

The work was supported by the Ministry of Science and Higher Education of the Russian Federation under state-funded research assignment of the Institute of Laser Physics SB RAS (Project Code: FWGU-2024-0001).

References

[1] W.Hanle, Zeitschrift fur Physik. **30**, 93–105. (1924).

[2] Новиков Л. Н. и др. Успехи физических наук **4**, (113) 597–625 (1974).

[3] Makarov A. et al. Opt. Commun. **577**, 131369 (2025).

Temperature and wavelength dependent absorption in Yb:YAG and its application for high-power laser systems

A.O. Kuptsova[1,2], **G.V. Kuptsov**[1], **V.A. Petrov**[1], **and V.V. Petrov**[1,2]
[1]*Institute of Laser Physics SB RAS, 15 B Lavrentyev Ave., 630090, Novosibirsk, Russia*
[2]*Novosibirsk State University, 1 Pirogova Str., 630090, Novosibirsk, Russia*
E-mail: aokupts@gmail.com

Experimental determination of the temperature distribution in the active element is especially important for systems with high average power, since in such systems, temperature gradients in the active element can reach significant values. Laser thermometry method can be used to experimentally measure temperature fields in the pumping region of the ytterbium-doped active elements of laser amplifiers [1]. The method is based on the dependence of the absorption coefficient of media on temperature near the gain wavelength of 1030 nm [2,3]. For Yb:YAG crystals, the absorption value depends on the wavelength and thus affects the sensitivity range of laser thermometry: the larger the slope of absorption cross-section on the element temperature, the smaller the temperature measurement error.

Absorption measurements were conducted in an Yb:YAG crystal with an active ion concentration of 9.8 at.% at different wavelengths. Measurements were conducted simultaneously in the temperature range of 40-300 K with a resolution of 0.5 K and in the range of 300-360 K with a resolution of 5 K. A continuous-wave Yb:YAG laser with wavelength tuning in the range of 1025.9 to 1034.5 nm was used for the measurements. The radiation spectral width is less than 0.3 nm (FWHM). The error in determining the central wavelength is less than 0.2 nm.

An analysis of the obtained results was carried out. The absorption cross-section slope reaches its maximum of $8.9 \cdot 10^{-24}$ cm^2/K at the wavelength of 1030 nm in the temperature range of 170-235 K, that corresponds to temperature measurement error of ~0.6 K. It was shown that wavelength tuning can be used to expand temperature measurement range. The largest temperature measurement range of 100-350 K is achieved at a wavelength of 1029.2 nm, with an absorption cross-section slope from 2 to $8 \cdot 10^{-24}$ cm^2/K.

The study was supported by the Ministry of Science and Higher Education of the Russian Federation (project no. FWGU-2026-0002).

References

[1] G.V. Kuptsov et al., Photonics **805**, (2022).
[2] A.O. Kuptsova et al., Photonics **748,** (2024).
[3] V.A. Petrov et al., Technical Physics Letters **50**, 85 **(**2024).

Dynamics of a superradiant laser with a four-level inhomogeneously broadened active medium

I. Kuzmin[1], E. Kocharovskaya[1]
[1]*Federal Research Center A.V. Gaponov-Grekhov Institute of Applied Physics of the Russian Academy of Sciences*
46 Ul'yanov Street, Nizhny Novgorod, 603951, Russia
E-mail: kuzminiv@ipfran.ru

The dynamics of systems close to class-D lasers [1] operating in the superradiance mode remain a relevant topic [2]. This work presents an analytical and numerical study of infrared superradiant pulse-train generation in a solid-state four-level medium with spatial effects included. The medium is characterized by an inhomogeneously broadened laser transition, a plane-parallel cavity with a low Q-factor, and a high cooperative frequency. In the present work, we use the semi-classical Maxwell–Bloch equations [3,4] in a two-dimensional (2D+t) geometry for linearly polarized pump and signal radiation. The spatial part is presented in two coordinate systems: Cartesian (z,x) and cylindrically symmetric (z,r). The key parameters of the medium, including longitudinal and transverse relaxation times, cavity Q-factor, concentration of active centers, and transition dipole moments, are selected to satisfy the necessary conditions for pulse-train superradiance in the picosecond range. The dynamics of the system are studied under continuous transverse pumping and the medium is initially not inverted on the laser transition. The longitudinal population-inversion grating on the laser transition is also taken into account.

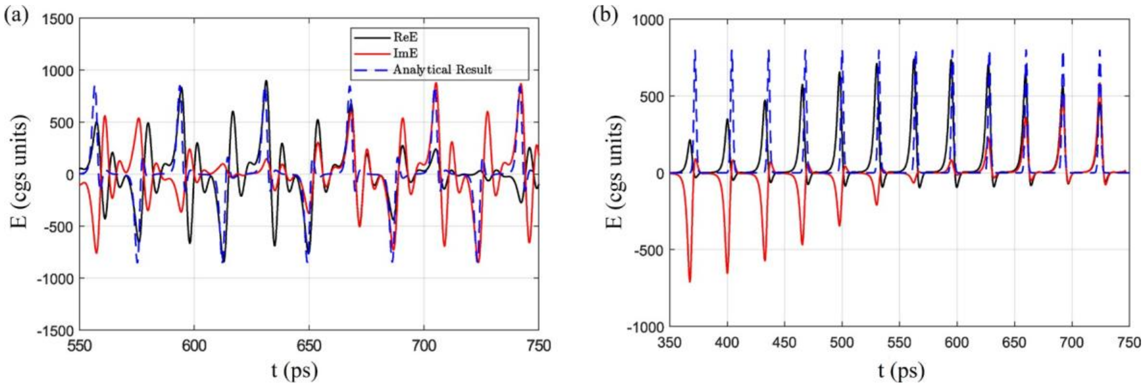

Fig. 1 The field amplitude dependencies are obtained analytically and numerically for $T_2>\Delta t$ case (a) and $T_2\approx\Delta t$ case (b) at z=0,x=0

Figure 1 demonstrates the comparison between the numerical simulation results and the analytical theory for the two cases. Let T_2 be the transverse relaxation time on the laser transition, Δt the pulse duration, and ΔT the pulse-train period. The first case is $T_2>\Delta t\sim\Delta T$ (Figure 1a) and the second case is $T_2\approx\Delta t\ll\Delta T$ ((Figure 1b). The laser field amplitude is taken at the point (z=0, x=0) on the boundary of the active medium. In both cases, the laser field dynamics are well approximated by Hill-type equations. For the chosen parameters, these equations admit limit-cycle solutions. Note that for $T_2<\Delta t$, the laser field dynamics are described as the dynamics of the classical free-running mode.

This work is supported by the Ministry of Science and Higher Education of the Russian Federation (Project No. FFUF-2024-0038).

References

[1] Y. Khanin, Principles of Laser Dynamics, Elsevier (1995).
[2] V. Kocharovsky et al., Phys. Usp. **60** (2017).
[3] S-H. Chang and A.Taflove, Optics Express **12**(16) (2004).
[4] E. Roldan et al., Revista Mexicana de Física E **52**(2) (2006).

Numerical simulation of the tight focusing of the ultrashort laser pulses taking into account spatio-temporal nonidealities

I. Kuzmin[1]

[1]*Federal Research Center A.V. Gaponov-Grekhov Institute of Applied Physics of the Russian Academy of Sciences*
46 Ul'yanov Street, Nizhny Novgorod, 603951, Russia

E-mail: kuzminiv@ipfran.ru

Modern multi-petawatt laser facilities are equipped with high-numerical-aperture focusing systems with significant off-axis angles. For example, the CoReLS system (10 PW peak power) described in [1] employs an F/1.1 focusing geometry and an off-axis angle of approximately 60 degrees. The XCELS laser facility architecture [2] involves tight off-axis focusing at F/1 with coherent beam combining of radiation from its individual channels. Thus, the correct calculation of the spatio-temporal structure of fields near the focal plane goes beyond the paraxial approximation typically employed near the beam waist. Accurate field calculations for an ultrashort (3-25 fs) infrared laser pulses over several Rayleigh lengths are significantly hindered by strongly non-paraxial focusing and a clearly non-Gaussian beam structure. For instance, in the planned XCELS and SEL-100PW [3] facilities, the spatial-spectral distribution of the laser pulses is expected to be super-Gaussian. Furthermore, modeling complex spatio-temporal and polarization field structures in the focal region – for example, a flying-focus pulse [4] generated by non-paraxial focusing – requires high-precision calculations.

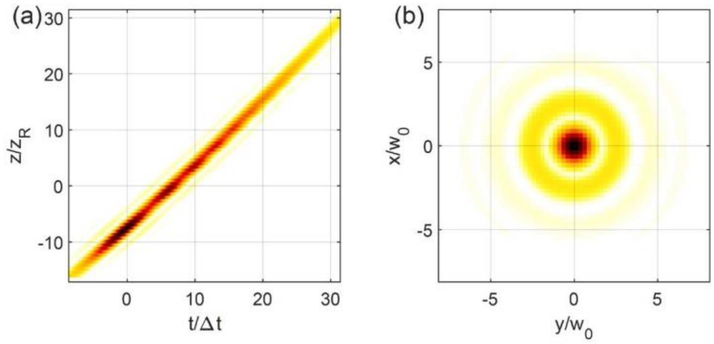

Fig. 1 Spatio-temporal distribution of $|E_x(z,t)|^2$ at x=0,y=0 (a), spatial distribution of $|E_x(x,y)|^2$ at $t=t_{max}, z/z_R=0$ (b)

Thus, the present work considers the features of tight focusing of ultrashort infrared laser pulses. The simulations involve aberrations in the spatio-temporal phase distribution of the laser beam, as well as aberrations introduced by the focusing system. The numerical simulation in this work is based on the Stratton–Chu vector diffraction theory [5]. This method enables the calculation of all electric and magnetic field components in the focal region for each spectral component of the broadband laser pulse. Figure 1 presents numerical simulation results for the tight (F/1) focusing of a femtosecond laser pulse (10 fs duration, central wavelength 910 nm) with non-zero Z^{2} and Z^{4} Zernike aberration coefficients for the parabolic mirror. A "flying-focus"-like intensity distribution is produced by these conditions (Figure 1a). The spatial intensity distribution at the focal point z=0 is shown in Figure 1b.

This work is supported by the Ministry of Science and Higher Education of the Russian Federation (Project No. FFUF-2024-0038).

References

[1] J.W. Yoon et al., Optica **8**, 5 (2021).
[2] E. Khazanov et al., High Power Laser Science and Engineering **11** 78 (2023).
[3] E. Khazanov et al, Matter Radiat. Extremes **11**, 3 (2026).
[4] K. Oubrerie et al., Journal of Optics **24**, 4 (2022).
[5] S. Bahk et al. Appl. Phys. B **80** (2005).

UV laser induced surface modification of TiNi alloy

<u>I.K. Lopatkin</u>[1,2], M.Yu. Kandaurova[2], T.Yu. Sablina[2], I.A. Zyatikov[2] and Yu.N. Panchenko[2]

[1]*Tomsk Polytechnic University, Russia, Tomsk, Lenin str., 30, 634050*

[2]*Institute of High-Current Electronics, Russia, Tomsk, Academic Avenue, 2/3, 634055*

<u>E-mail:</u> ikl5@tpu.ru

The surface properties of TiNi shape memory alloys are critical for biomedical applications, yet conventional methods offer limited control and can damage the subsurface layer [1,2]. Nanosecond UV laser treatment offers an alternative for controllable surface modification with negligible thermal effects on the bulk [3]. In this work, the effect of 266 nm laser irradiation on the surface properties and microstructure of TiNi alloy is studied at fluences of 0.14, 0.28, and 0.42 J/cm^2. TiNi specimens (50.5%–Ni, 49.5%–Ti, at.%) were irradiated in air using the fourth harmonic of a Nd:YAG laser (λ = 266 nm, pulse duration 7 ns, repetition rate 10 Hz, spot diameter 3 mm). A common scanning strategy for specimens was employed, involving overlapped pulses along linear tracks with a defined hatch distance. The scanning speed was constant in all regimes at V = 500 µm/s. Wettability was evaluated by the sessile drop method (deionized water, glycerol); the surface free energy was calculated using the Owens–Wendt–Rabel–Kaelble method. Fig. 1 shows the change in the contact angle (CA) and free surface energy of TiNi specimens after UV laser treatment at different fluences. The initial CA was 75.1±3.8°. Irrespective of the laser treatment regime, a considerable decrease in CA was observed, with the minimum value of 10.2±2.1° obtained at a fluence of 0.42 J/cm^2.

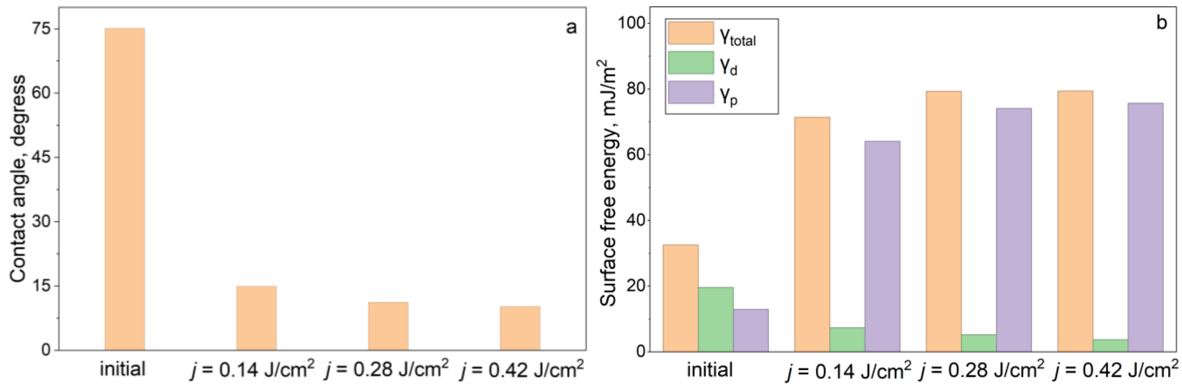

Fig. 1 Contact angle as a function of laser fluence (a) and surface free energy γ_{total} and its components (polar γ_p and dispersion γ_d) (b) of TiNi specimens at laser fluences of 0.14, 0.28, and 0.42 J/cm^2

UV laser treatment of the TiNi surface leads to an increase in the surface free energy of the TiNi alloy, driven by a significant rise in the polar component (fig. 1). This effect is attributed to the formation of a laser-induced oxide layer, as confirmed by electron microscopy and X-ray diffraction (XRD). Energy-dispersive X-ray spectroscopy revealed a substantial rise in oxygen content in the laser-treated specimens across all regimes. At higher fluences (0.28 and 0.42 J/cm^2), the XRD patterns exhibited peaks corresponding to TiO_2 and $Ni_2Ti_4O_x$ oxide phases, in addition to those of the initial austenitic B2 phase. Corrosion tests were carried out on untreated and laser-treated specimens in a 0.9% NaCl solution. The results demonstrate that UV laser treatment enhanced the corrosion resistance of the TiNi alloy relative to the untreated state for all treatment regimes, reducing the corrosion rate from approximately 80×10^{-5} mm/year for the untreated specimens to 6–8×10^{-5}mm/year for the laser-treated TiNi specimens.

This research was carried out with support from the Russian Science Foundation grant No. 25-79-31008, https://rscf.ru/en/project/25-29-01116.

References

[1] Otsuka K., Ren X. Intermetallics. **7**, 511 (1999).
[2] Pelton A.R. et al. JOM. **55**, 33 (2003).
[3] Slobodyan M.S. et al., Russ. Phys. J. **67**, 565 (2024).

Energy transfer and dynamics of the $^3F_4 \rightarrow ^3H_6$ and $^5I_7 \rightarrow ^5I_8$ states of Tm^{3+} and Ho^{3+} ions in mixed $LiY_{0.3}Lu_{0.7}F_4$ crystals

T.M. Minnebaev[1], A.S. Nizamutdinov[1], A.A. Shavelev[1], V.V. Semashko[2]
[1]*Institute of Physics, Kazan Federal University, Kazan, Russia*
[2]*Kazan Research Center of RAS, Kazan, Russia*
E-mail: timurminnebaev271@mail.ru

Interest in thulium and holmium ions is based on the possibility of achieving lasing in the infrared spectral range—in the 1.8 and 2 μm range—with single or dual activation of crystals. Such lasers have a wide range of applications, the most important of which are laser surgery and atmospheric sensing using LIDAR technology, due to the strong absorption of water in this wavelength range [1].

Achieving lasing in crystals with single activation by Tm^{3+} or Ho^{3+} ions is difficult due to strong cross-relaxation processes. Therefore, to achieve laser emission at a wavelength of 2 μm, a sensitized energy transfer scheme is often used, in which Tm^{3+} ions act as donors and Ho^{3+} ions act as acceptors. Laser generation occurs at the $^3F_4 \rightarrow ^3H_6$ and $^5I_7 \rightarrow ^5I_8$ transitions, respectively; these levels can be efficiently pumped around 790 nm using readily available laser diodes. At the same time, mixed crystals can provide broadening of spectral lines, which may lead to increased energy transfer efficiency.

In this study, we investigated the polarized spectral characteristics and luminescence decay characteristics of a concentration series of mixed $LiY_{0.3}Lu_{0.7}F_4$ crystals doped with Tm^{3+} and Ho^{3+} ions. The crystals exhibited intense sensitized luminescence, with some broadening of the spectral lines observed. The measured data allowed us to estimate the energy transfer parameters and the Förster radius in the $Tm^{3+} \rightarrow Ho^{3+}$ ion system. The value of the reverse energy transfer turned out to be lower than the previously presented literature data ($C_{Ho\text{-}Tm}$=1.2, 2.7 cm^6/s) [2], and amounted to $C_{Ho\text{-}Tm}$= 0.83 cm^6/s, which may indicate a more efficient energy transfer in the $LiY_{0.3}Lu_{0.7}F_4$ crystal. The paper also discusses the results of modeling and experiments on achieving lasing in this active medium and its prospects in comparison with other matrices.

The work was carried out within the framework of a subsidy allocated to Kazan (Volga Region) Federal University for the implementation of a state assignment in the field of scientific activity, project No. FZSM-2024-0004.

References

[1] Zhu X. et al., Chinese Optics Letters **10**(1) 012801 (2012).
[2] Toncelli, Alessandra et al., Journal of luminescence **92**(3) 237-244 (2001).

Experimental Approach to Detection of Photoinduced Residual Absorption in Direct Diode-Pumped Ti:Sapphire

K.E Reznikov[1,2], A.V. Naumov[2,3]
[1]Avesta Ltd., 108840 Moscow, Russia
[2]P.N. Lebedev Physical Institute of the Russian Academy of Sciences, 119991 Moscow, Russia
E-mail: k.reznikov@avesta.ru

Direct blue diode pumping has improved the efficiency and compactness of Ti:sapphire laser systems. However, photoinduced processes in Ti:sapphire crystals under continuous blue excitation remain poorly understood and may introduce additional optical losses.

One possible mechanism is photoinduced residual absorption associated with intervalence charge transfer (IVCT) involving Ti^{3+}/Ti^{4+} centers and crystal defects [1]. Although IVCT has been discussed for titanium-containing oxide crystals, its role in directly diode-pumped Ti:sapphire lasers is still unclear. Experimental observation of this effect is difficult because weak induced absorption is masked by optical gain during pumping.

A pump-probe technique was developed to study this problem. A CW probe beam passed through the pumped region of a Brewster-cut Ti:sapphire crystal. The transmitted probe power was recorded with a silicon photodetector and a digital oscilloscope. Careful alignment of the pump and probe beams was required because the measured signal strongly depended on their spatial overlap.

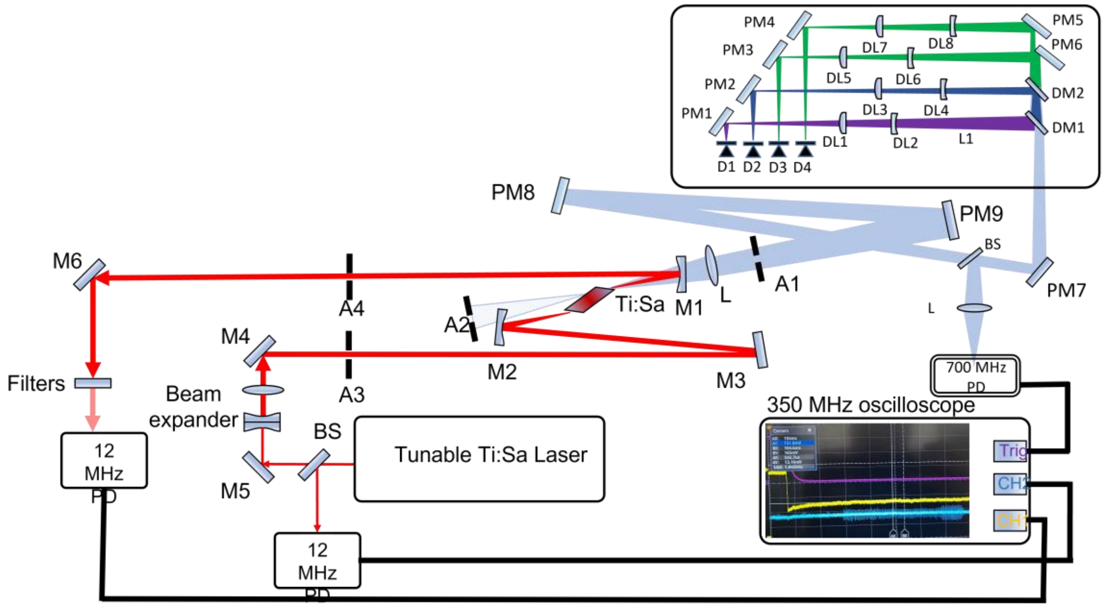

Fig. 1 Experimental setup used for detection of photoinduced residual absorption in a directly diode-pumped Ti:sapphire crystal. The probe beam propagates through the pumped region of the crystal, while its transmitted power is monitored by a high-speed photodetector connected to a digital oscilloscope.

After the pump was switched off, transient changes in the probe transmission were observed. Under certain alignment conditions, the probe intensity dropped below its initial level and then gradually recovered. The effect disappeared after changing the beam overlap, suggesting that it originates in the optically excited region of the crystal. Although its physical origin is still under investigation, the results show that the proposed technique is sensitive to weak transient absorption in diode-pumped Ti:sapphire.

Future work will focus on improving pump-probe overlap and replacing mechanical pump interruption with fast electronic modulation to investigate shorter time scales and identify the origin of the observed absorption.

References
[1] R. Sawada et al., Appl. Opt. **56**, 6 (2017).

Surface ion traps at room and cryogenic temperatures

R. Safonov[1, 2], I. Gerasin[1, 3], A. Russkikh[1, 2], N. Zhadnov[1], K. Kudeyarov[1], P. Sidorov[1], V. Erin[1, 2], I. Semerikov[1, 3], N. Kolachevsky[1, 3]

[1]*Lebedev Physical Institute of the Russian Academy of Sciences*

[2]*Moscow Institute of Physics and Technology (National Research University)*

[3]*Russian Quantum Center*

E-mail: r.safonov@lebedev.ru

Surface ion traps are considered as a promising platform for the development of scalable quantum processors based on the QCCD architecture [1], which relies on the transport of ion chains between different functional zones of a chip. One of the factors limiting the fidelity of quantum operations in ion traps is electric-field noise, which causes heating of the ions' motional degrees of freedom [2]. Cooling the trap to cryogenic temperatures is an effective approach to suppressing this noise [3].

This work presents the current results of research on surface ion traps carried out at the Lebedev Physical Institute of the Russian Academy of Sciences. Experiments performed on two setups are considered: one operating at room temperature and the other inside a cryogenic system with an operating temperature of approximately 6 K.

To date, ion trapping has been demonstrated in the room-temperature setup (fig. 1) using traps of two different designs developed in the laboratory. Spectroscopy of a narrow optical transition at a wavelength of 435 nm has been performed, coherent Rabi oscillations have been observed, and the heating rate of the ions' motion has been determined based on their dephasing (fig. 2). A value of $\dot{n} = 880 \pm 100\ s^{-1}$ has been obtained [4]. In June 2026, ions were trapped for the first time in the cryogenic setup at a trap temperature of 6 K. The technical solutions implemented in the cryogenic setup, including a cryogenic RF-resonator, an in-vacuum objective, and a system for isolating the ion trap from cryocooler-induced vibrations, are also discussed.

Further studies will include the implementation of two-qubit quantum operations, measurement of the ion heating rate in the cryogenic trap, and comparison with the result obtained at room temperature; a reduction in the heating rate by 2–3 orders of magnitude is expected [5]. Experimental testing of theoretically calculated ion-shuttling schemes, involving the controlled transport and separation of ion chains, is also planned.

This work was supported by the State Corporation Rosatom within the framework of the Roadmap for Quantum Computing (Agreement No. 868/1653-D).

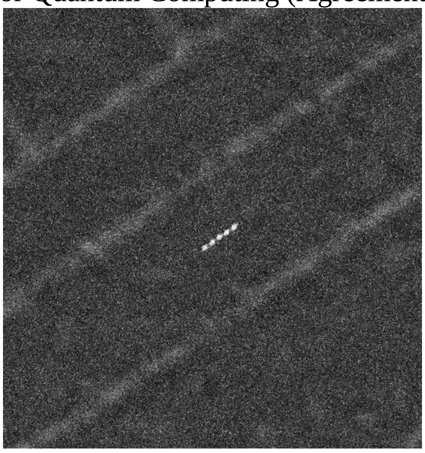

Fig. 1. Chain of 5 ions trapped in a surface trap at room temperature

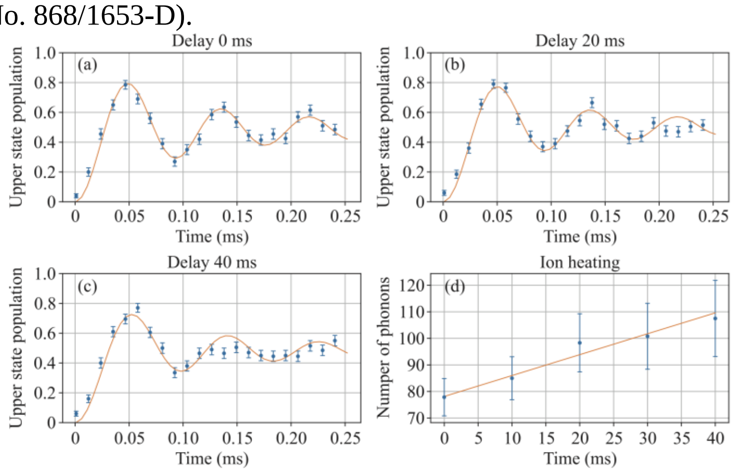

Fig. 2 Heating rate measurement based on dephasing of Rabi oscillations. Rabi oscillations measured after delays of (a) 0 ms, (b) 20 ms, and (c) 40 ms. (d) Mean phonon number as a function of delay time.

References

[1] D. Kielpinski et al., Nature **417**, 709 (2002).
[2] C. J. Balance, Springer Theses (2017).
[3] J. Labaziewicz et al., Phys. Rev. Lett. **101**, 180602 (2008).
[4] I. S. Gerasin et al., JETP Lett. **124**, 31 (2026).
[5] M. Brownnutt et al., Rev. Mod. Phys. **87**, 1419 (2015).

Improving performance of Compton radiation sources by controlling the dynamics of laser beam focus

A. S. Samsonov[1], A. A. Zakharova[1,2], I. Yu. Kostyukov[1]
[1]Federal Research Center A.V. Gaponov-Grekhov Institute of Applied Physics of the Russian Academy of Sciences, Nizhny Novgorod, Russia
[2]Lomonosov Moscow State University, Sarov Branch, Sarov, Russia
E-mail: asams@ipfran.ru

Methods to increase the brightness of Compton gamma-ray sources, which are crucial for scientific and medical applications, are investigated. These sources operate via inverse Compton scattering, where a laser pulse collides with a relativistic electron beam to produce high-energy photons. However, the inherent smallness of the Compton scattering cross-section limits the source brightness. A straightforward method to boost photon yield is to increase laser intensity. This approach, however, quickly becomes problematic due to nonlinear effects, particularly ponderomotive broadening. This effect broadens the energy spectrum of the emitted photons, reducing the source's monochromaticity — a critical property for many applications. We propose using a "flying focus" optical scheme as an alternative [1]. In this technique, the laser focus is not stationary but moves along the optical axis, synchronized with the electron bunch. This allows for an extended interaction length while maintaining a small focal spot and moderate intensity. The key advantage is that it permits a significant increase in laser pulse duration to keep the scattering process linear (parameter $a_0 \ll 1$), thereby suppressing nonlinear spectral broadening, while still achieving a high photon yield [2].

We derive an approximate analytical expression for the total number of Compton photons for the flying focus scheme, assuming the focus moves synchronously with the electron bunch. This expression is compared to the analogous result for a stationary focus. The analysis shows that the maximum possible photon yield is, in principle, the same for both schemes when optimized. However, the conditions for reaching this maximum differ. For a stationary focus, the optimal laser pulse duration is limited to a value comparable to the electron bunch length. To increase photon yield via higher laser energy in this scheme, one must increase the intensity, driving the system into a nonlinear regime ($a_0 > 0.1$) and causing undesirable spectral broadening. In contrast, the flying focus scheme decouples the optimal photon yield from the laser pulse duration. Using parameters for a prototype source (1 GeV electron beam, 10 ps duration, 20 J laser energy), the authors demonstrate that with a flying focus, the optimal laser pulse duration can be increased from a few picoseconds to hundreds of picoseconds. This reduces the nonlinearity parameter a_0 from 0.42 down to 0.05 while maintaining a photon yield of around 10^{11} photons. As a result, the spectral width, dominated by the electron beam's energy spread, is three times narrower (11.2% vs. 3.5%) than in the stationary focus case. The analytical results are validated against numerical simulations.

Thus, is is demonstrated that the flying focus scheme is a powerful method for increasing the spectral brightness of Compton sources, as it allows for the maximum photon yield to be achieved with a long, low-intensity laser pulse, thus minimizing nonlinear spectral broadening and preserving the source's monochromaticity.

This study was conducted within the framework of the scientific program of the National Center for Physics and Mathematics, section 6.

References

[1] A. Sainte-Marie et al., Optica **4**, 1298 (2017).
[2] A.A. Zakharova et al., Izvestiya Vuz. Radiofizika (2026).

Optimizing the Compton radiation source in linear and weakly nonlinear regimes using GPU-accelerated code

A. S. Samsonov[1], **A. A. Zakharova**[1,2], **I. Yu. Kostyukov**[1]
[1]*Federal Research Center A.V. Gaponov-Grekhov Institute of Applied Physics of the Russian Academy of Sciences, Nizhny Novgorod, Russia*
[2]*Lomonosov Moscow State University, Sarov Branch, Sarov, Russia*
E-mail: asams@ipfran.ru

The CRS NCPM project aims to build a Compton radiation source with unprecedented parameters and is expected to bring breakthrough advancements in nuclear photonics, materials science, and other fields of scientific research. The source operates by significantly increasing the frequency of laser radiation scattered by a colliding beam of relativistic electrons, reaching the X-ray and gamma ranges. For many applications, it is important to obtain as many scattered photons as possible on the sample under study with the smallest possible energy spread. Numerical codes are indispensable tools for solving such optimization problems under non-ideal conditions close to experimental ones. The present work discusses application of modern approaches to the development of such codes.

The most basic model of calculating angular-spectral characteristics of a Compton radiation source is based on performing an integration of the differential cross-section of Thomson scattering of a laser pulse on an electron beam [1]. Although simple, such a model allows to take many effects into account, including self-consistent focusing of the electron beam and the laser pulse, the absence of cylindrical symmetry of the electron beam, the energy spread of the electron beam, the spectral width of the laser pulse, weakly nonlinear effects associated with dependence of the scattering cross-section on the laser intensity, etc. A number of both analytical and numerical sophisticated algorithms and techniques, that have recently been suggested in order to efficiently perform the multidimensional integration, are implemented in our newly developed code. Besides that, our code, written in Python programming language, leverages GPU acceleration via CuPy package to achieve performance of computing the full three-dimensinal angular-spectral distribution of the compton photons in a matter of a second even on a consumer-grade hardware. This ultimately allows to perform optimization of the Compton source characteristics in a vast parameter space in a reasonable time.

The developed code was used in order to find the parameters of the laser system, in particular the focusing degree, that would maximize total photon yield and monochromaticity. The optimization has proved that technical capabilities of the CRS NCPM project would allow achieving total photon flux exceeding 10^{11} ph/s in the tens to hundreds MeV range with a relative energy spread not exceeding 1%, placing it among the top performing Compton radiation sources worldwide.

This study was conducted within the framework of the scientific program of the National Center for Physics and Mathematics, section 6.

References

[1] S. G. Rykovanov, et al., Radiophysics and Quantum Electronics **67**, 749-765 (2025).

Laser testbed for inverse Compton scattering experiments at the VEPP-4M collider

I.A. Samsonov[1], I.B. Mukhin[1], K.A. Glushkov[1] and I.I. Kuznetsov[1]
[1]A.V. Gaponov-Grekhov Institute of Applied Physics of the Russian Academy of Sciences, Nizhny Novgorod, Russia
E-mail: i.samsonov@ipfran.ru

Currently in Russia, work is underway to create a source of (quasi)monochromatic γ-quanta based on the effect of inverse Compton scattering of photons on relativistic electrons [1]. For the successful implementation of this project, it is necessary to develop technologies for the interaction of pulsed laser radiation with electron beams in a storage ring. To this end, a laser testbed has been developed at the Institute of Applied Physics (IAP RAS, Nizhny Novgorod), which will be employed using the infrastructure of the VEPP-4M collider (BINP SB RAS, Novosibirsk) to conduct laser-electron interaction experiments.

The laser testbed is designed to operate with pulse durations ranging from hundreds of picoseconds to a few nanoseconds at repetition rates from 100 kHz to 10 MHz. The average radiation power at the fundamental wavelength (1030 nm) exceeds 100 W and is achieved through two-pass amplification in an active element made of a Yb:YAG crystal in the form of a thin rod. The generated radiation is directed to an LBO crystal for second harmonic generation (515 nm). At the current stage, the average power at the second harmonic is 46 W with a conversion efficiency of 50%.

The development of the laser testbed for inverse Compton scattering at the VEPP-4M collider was carried out within the framework of the state assignment No. FFUF-2026-0013.

References

[1] Grigorenko L.V., et al., Fizmat **1**(3-4) 124-264 (2023).

Modeling the Upper Atmosphere of the Ultra-Hot Jupiter KELT-20 b

S.S. Sharipov[1], I.F. Shaikhislamov[1], M.S. Rumenskikh[1], and I.B. Miroshnichenko[1]
[1]*Institute of Laser Physics, Siberian Branch of Russian Academy of Sciences, Novosibirsk, 630090 Russia*
E-mail: stas.sharipov@mail.ru

Ultra-hot Jupiters provide unique laboratories for studying atmospheric physics under intense stellar irradiation, where non-local thermodynamic equilibrium (non-LTE) processes play a decisive role in shaping observable transmission spectra. We present a self-consistent three-dimensional hydrodynamic model of the upper atmosphere of KELT-20 b coupled with detailed photo-plasma chemistry, radiative transfer, and non-LTE kinetics of excited hydrogen and Fe II [1]. Unlike previous studies, our approach simultaneously reproduces transit absorption in the hydrogen Balmer series (Hα–Hδ) and the Fe II 5018 Å line within a unified physical framework [2].

The calculations demonstrate that vacuum ultraviolet (VUV) irradiation dominates the thermal and ionization balance of the atmosphere, whereas stellar XUV radiation has only a minor influence on the observed line formation. VUV-driven photoionization substantially increases the free-electron abundance, promoting recombination cascades that efficiently populate excited hydrogen states responsible for the Balmer absorption. Simultaneous modeling of hydrogen and iron diagnostics significantly reduces the degeneracy between stellar VUV flux and atmospheric composition.

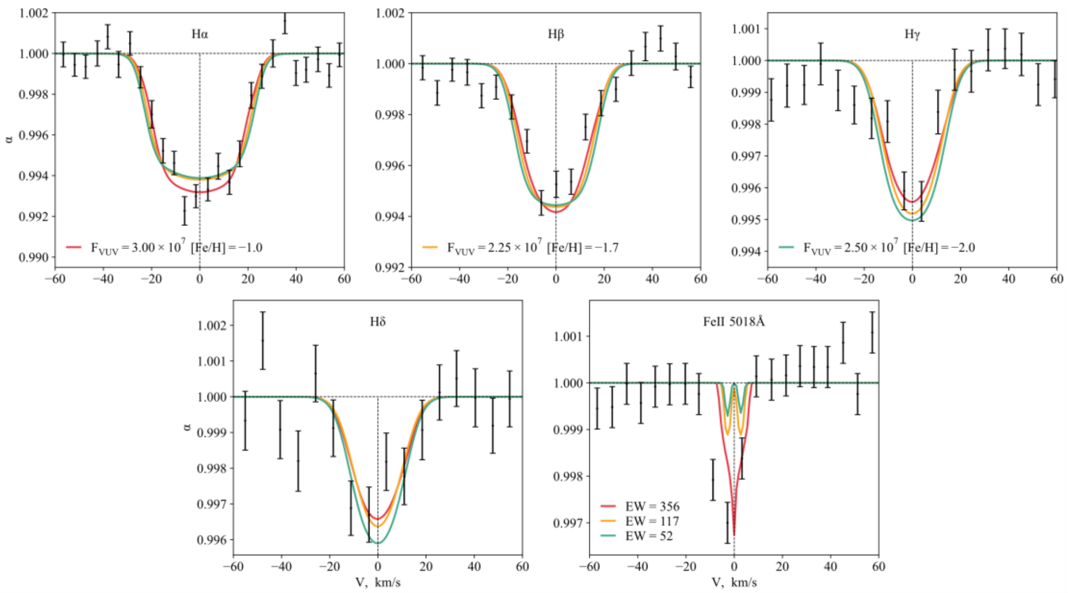

Fig. 1. Absorption profiles for different sets of parameters that give best-fit to observations.

The best agreement with high-resolution transit observations is achieved for a VUV flux of approximately 3×10^7 erg cm^{-2} s^{-1} (scaled to 1 AU) and a subsolar atmospheric metallicity of [Fe/H] ≈ −1. The inferred atmosphere remains compact, nearly hydrostatic, and exhibits an extremely low mass-loss rate compared with typical ultra-hot Jupiters. Our results emphasize that joint non-LTE analysis of hydrogen and metal lines provides a powerful tool for constraining the physical conditions and chemical composition of highly irradiated exoplanetary atmospheres and demonstrates the importance of detailed kinetic modeling for interpreting high-resolution transmission spectroscopy.

This research was supported by the National Center for Physics and Mathematics within the framework of the Experimental Laboratory Astrophysics and Geophysics research program.

References

[1] N. Casasayas-Barris et al., A&A **628**, id. A9 (2019).
[2] I.F. Shaikhislamov et al., A&A **696**, id. A211 (2025).

Control of defect concentration in YF_3: Nd^{3+}, Yb^{3+} nanoparticles and their application in luminescent thermometry

E. Shosheva[1], M. Pudovkin[1], and R. Rakhmatullin[1]

[1]Kazan (Volga Region) Federal University, Institute of Physics, Kazan, 420008 Russian

E-mail: Kate15-05@mail.ru

Recently, in our studies, we have observed defect-related emission (400–700 nm) in the YF_3 matrix under optical excitation at 355 nm [1]. The formation of defects in YF_3 proceeds in two stages: first, fluorine vacancies are generated during synthesis, and subsequently, these sites are occupied by oxygen during annealing in air, resulting in the formation of complex defect centers O_F–V_O [2]. This broadband emission opens up new possibilities. The defect luminescence is highly temperature-dependent. This feature can be exploited to develop a luminescent thermometer operating on the luminescence intensity ratio (LIR) principle, utilizing the narrow emission peaks of the rare-earth ions and the broad defect band. In this work, YF_3: Nd^{3+} (0.1 mol.%), Yb^{3+} (0.5 mol.%) nanoparticles were synthesized using varying amounts of the NH_4F fluorinating agent (10% deficit, stoichiometric amount, and 20% and 40% excess) to control the defect concentration. The nanoparticles were prepared via a hydrothermal method; a portion of the samples was subsequently annealed in air for 4 hours at 400 °C. The phase composition was determined by powder X-ray diffraction (XRD) analysis, revealing an average particle size of approximately 60 nm. Samples with varying concentrations of the fluorinating agent, both before and after post-treatment, exhibit distinct luminescence behaviors (Fig. 1). The as-synthesized 0F and -10F samples (Fig. 1a) exhibit emission from both defects and Nd^{3+} ions. Notably, no energy transfer between the O_F–V_O complex and Nd^{3+} ions was observed. For the 20F and 40F samples, virtually no luminescence is detected. This is attributed to the formation of a KYF_4 phase resulting from the high concentration of the fluorinating agent. The absence of defect luminescence is due to the lack of fluorine vacancies, while the lack of Nd^{3+} emission is caused by the different crystal field environment in this phase compared to the YF_3 matrix. Conversely, the post-treated 20F and 40F samples (Fig. 1b) exhibit both defect and Nd^{3+} luminescence, as the annealing process restores the YF_3 matrix structure. The greater the initial excess of fluorine, the more oxygen can be incorporated into the sample during annealing, resulting in brighter defect emission.

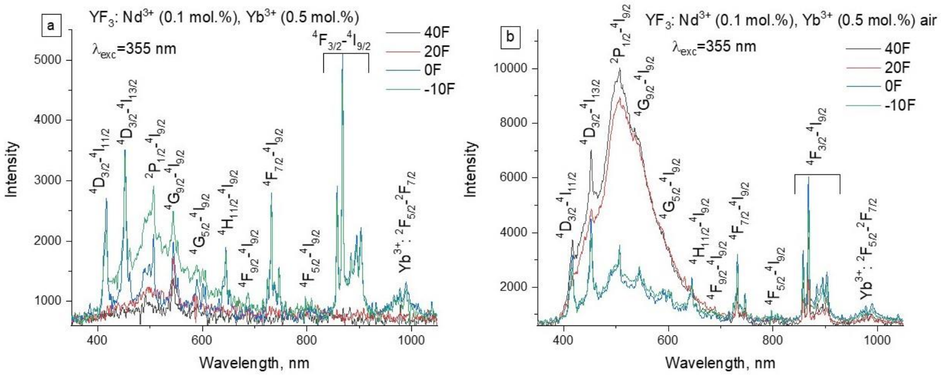

Fig. 1 Luminescence spectrum of the YF_3: Nd^{3+} (0.1 mol.%), Yb^{3+} (0.5 mol.%) samples with a different content of fluorinating agent a) before and b) after post-treatment

The EPR lines in the 40F sample are significantly broader than those in the -10F sample. This indicates greater disorder in the local environment of the Yb^{3+} ions in the 40F sample. In other words, the sample with an excess of NH_4F exhibits a higher concentration of structural defects.

The research was funded by the subsidy allocated to Kazan Federal University for the state assignment in the sphere of scientific activities (FZSM-2025-0004).

References

[1] E. Oleynikova et al., Opt. mat. **177**, 118147 (2026).

[2] H. Santos et al., J. of lum. **201**, 156-162 (2018).

Achieving navigation-grade accuracy in a miniature resonant fiber-optic gyroscope with a broadband source

E. Trefilova[1], **A. Kalinin**[1], **E. Ivashkina**[1], **A. Shevalenko**[1] **and D. Sutyrin**[1]
[1] *OOO «Bazovye Technologii»*
E-mail: e.trefilova@btlabs.ru

The interferometric fiber-optic gyroscope (IFOG) requires kilometer-scale coils that hinder miniaturization, while conventional resonant fiber-optic gyroscopes (RFOGs) suffer from coherence-related noises. Recently, broadband-driven RFOGs with a 100-meter fiber ring resonator have been shown to reach navigation-grade accuracy (bias instability (BI) < 0,01 °/h, angle random walk (ARW) < 0,005 °/$\sqrt{h}$). This coil length represents an optimal middle ground - shorter than IFOG coils yet longer than ultra-short resonators - effectively mitigating thermal errors and complexity while enabling miniaturization, cost savings, and robustness [1, 2]. However, thermal drift remains a critical challenge for practical deployment. To address this, a hybrid LSTM-PINN compensation method has been proposed, embedding physical heat-transfer constraints to suppress low-frequency drift [3].

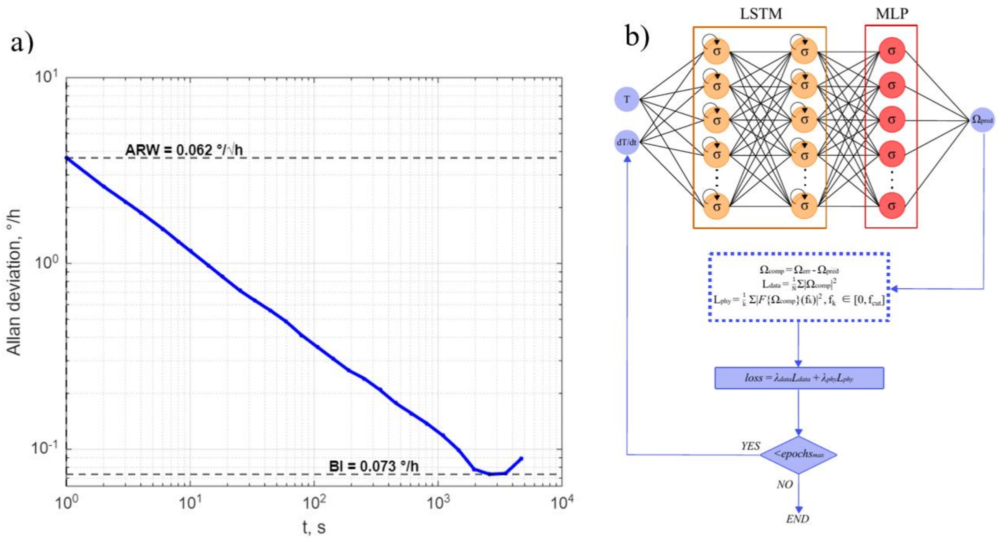

Fig. 1: a) Allan deviation of test results obtained using sinusoidal modulation of optical path length and synchronous quadrature demodulation technique of RFOG output signal for 230 min acquisition time, b) The schematic diagram of LSTM-PINN.

Following the optical configuration reported in [4], we built a prototype RFOG with several modifications. Specifically, we employed a 15-dBm broadband laser source and a low-cost piezoelectric phase modulator. With the current setup, we achieved BI=0.073 °/h and ARW=0.062 °/$\sqrt{h}$ (Fig. 1a). The increased optical power at the photodetector enabled clear observation of the Sagnac effect and allowed us to acquire raw gyroscope data for training the LSTM-PINN drift compensation model (Fig. 1b). We expect that the synergy of the resonant cavity, quadrature demodulation, and neural-network drift compensation will enable navigation-grade performance.

This work is supported by the NTI Project Support Fund (Grant No. 70-2025-002066 dated 12.12.2025).

References

[1] S. Zhao et al., Photonics Res. **10**, 542 (2022).
[2] Y. Wang et al., Opt. **63**, 6434 (2024).
[3] Y. Zhang et al., IEEE Photonics Technol. Lett. **37,** Early Access (2025).
[4] K. A. Ovchinnikov et al., Opt. Continuum **4**, 1688 (2025).

Online Session

Quantum Technologies with Light: From Security to Sensing

A. Kumar
Department of Physics,
Indian Institute of Space Science and Technology, Thiruvananthapuram, Kerala, India 695547
Email: ashokkumar@iist.ac.in

Quantum technologies leveraging light, particularly squeezed light, have emerged as powerful tools for advancing quantum communication, sensing, and computation. In this talk, I will describe how we use bright two-mode squeezed states of light for information encoding and quantum-enhanced sensing. I will first discuss the generation of squeezed light in the laboratory through nonlinear optical interactions between laser fields and hot atoms, followed by a demonstration of the EPR paradox using these beams, providing a clear manifestation of their entanglement [1, 2]. I will then discuss how such entangled beams can be exploited not only to explore fundamental aspects of quantum physics but also for applications such as information encoding through the manipulation of their spatial correlations and temporal quantum noise [3, 4]. Finally, I will highlight our recent work on quantum-enhanced sensing, including the development of quantum-enhanced gyroscopes based on two-mode squeezed states [5].

Figure 1 shows the intensity-difference squeezing obtained with bright two-mode squeezed states. In Fig. 1(a), the intensity-difference noise power is plotted as a function of the noise-analysis frequency. The red trace represents the shot-noise limit, while the blue trace shows the measured intensity-difference noise of the two-mode squeezed state. We observe quantum noise reduction over a bandwidth extending beyond 4 MHz, with a maximum squeezing of approximately 7 dB at around 500 kHz. Figure 1(b) shows the intensity-difference noise power at a fixed analysis frequency of 500 kHz as a function of time. The measurement demonstrates stable and persistent squeezing of approximately 7 dB, corresponding to an ~80% reduction in noise power relative to the shot-noise limit.

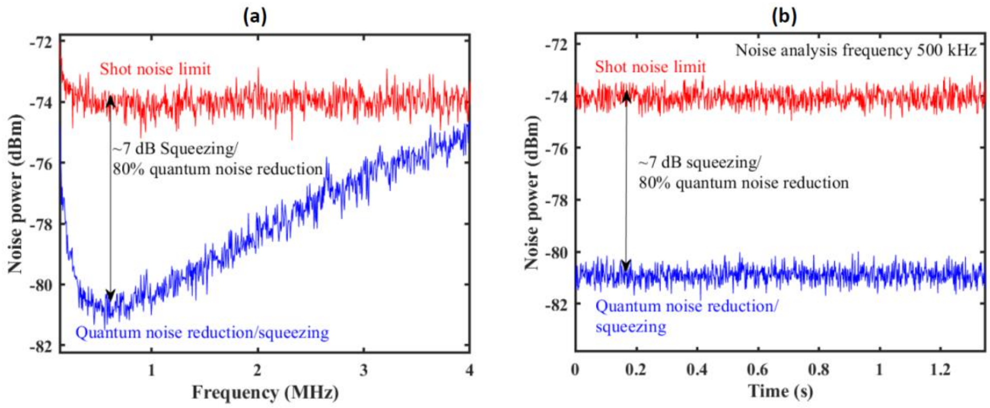

Fig. 1. (a) Intensity difference noise power vs noise analysis frequency. (b) Intensity difference noise power vs time at noise analysis frequency of 700 kHz. Traces are recorded by a spectrum analyzer with a resolution bandwidth 30 kHz and a video bandwidth 300 Hz.

References

[1] J.A. Thachil et al., Phys. Rev. A **112**, 053718 (2025).
[2] A. Kumar et al., Quantum Sci. Technol. **6** (4), 045016 (2021).
[3] A. Shekar et al., Appl. Phys, Lett. **127** (10) (2025).
[4] G. Nirala et al., Science Advances **9** (22), eadf9161 (2023).
[5] P.M. Kannath et al., Phys. Rev. Res. **7** (4), 043269 (2025).

Perspectives to create a gamma laser based on the ^{229}Th embedded into AlF_3 dielectric medium

P.V. Borisyuk[1], **V.A. Shilov**[1], **D.A. Myzin**[1], **Y.Y. Lebedinskiy**[1, 2], **E.V. Chubunova**[1], **Z.M. Nauryzbaev**[1], **E.V. Tkalya**[1, 3, 4], **and R.K. Kurbaniyazov**[5]

[1]*National Research Nuclear University MEPhI, Moscow, Russia*
[2]*Moscow Institute of Physics and Technology, Dolgoprudny, Russia*
[3]*Russian Federal Nuclear Center – All-Russian Research Institute of Experimental Physics, Sarov, Russia*
[4]*Nuclear Safety Institute of the Russian Academy of Sciences, Moscow, Russia*
[5]*Karakalpak State University named after Berdakh, Nukus, Uzbekistan*

E-mail: pvborisyuk@mephi.ru

The anomalously low-lying isomeric state of the ^{229}Th nucleus ($E = 8.356\,eV, \lambda = 148.38\,nm$ [1]) makes it the only known candidate for a nuclear gamma laser operating in the optical range [2]. A population inversion maintained in a wide-bandgap dielectric host, where the internal conversion channel is energetically forbidden, could provide stimulated emission of VUV photons directly on a nuclear transition. This work analyzes quantitatively the prospects of such a laser based on thin-film AlF_3:^{229}Th structures produced by pulsed laser deposition (PLD) of metallic targets in a CF_4 atmosphere, and formulates the requirements to the excitonic pumping scheme.

The multilayer AlF_3/$^{229}ThF_4$/AlF_3 heterostructures were synthesized by PLD and characterized in situ by XPS and REELS [3]. Thorium is stabilized exclusively in the Th^{4+}–F chemical state. The surface density of implanted nuclei reaches $N_s = (4.6 \pm 1.3) \cdot 10^{14}\,cm^{-2}$ confined within a sub-nanometer layer ($\sigma < 3\,nm$) buried at a depth of 5 nm, as follows from the two-line (Th 4f / Th 5d) attenuation analysis. The band gap of the AlF_3 matrix measured by REELS, $E_g = 10.4 \pm 0.5\,eV$, exceeds the isomer energy by 2 eV, keeping the radiative decay channel open. The layer is chemically (diffusion $D(Th) < 5 \cdot 10^{-20}\,cm^2/s$ at 300 K) and radiation stable (He^+ irradiation).

The inhomogeneous broadening of the nuclear transition in the amorphous fluoride environment was evaluated by Monte-Carlo modeling of electric field gradients (point-charge lattice with Sternheimer antishielding, quadrupole moments $Q(5/2^+) = 3.11\,b$, $Q(3/2^+) = 1.74\,b$ [4]), giving $\Delta\nu_{inh} = 1.6\text{–}2.8\,GHz$. The corresponding stimulated emission cross section $\sigma \approx (1.2\text{–}2.0) \cdot 10^{-24}\,cm^2$ yields a single-pass gain $gL \sim 10^{-4}$ for the present sub-monolayer geometry – five orders of magnitude below the mirrorless threshold (Fig. 1). The gain deficit splits into two well-defined factors: the amorphous-matrix linewidth ($\times\, 10^5\text{–}10^6$ against single-crystal hosts) and the areal nuclear density ($\times\, 10^3$). A realistic road map therefore requires: (i) an epitaxial or single-crystal fluoride host reducing $\Delta\nu_{inh}$ to the kHz–MHz range, (ii) volume doping $n(Th) \geq 10^{18}\,cm^{-3}$ over $L \geq 1\,cm$, (iii) a VUV cavity (MgF_2/CaF_2/LaF_3 mirrors), and (iv) cryogenic operation. Under these conditions the same formalism predicts $gL \sim 10^3\text{–}10^4$, well above the threshold.

For the excitonic pumping of the isomer we rely on the temperature-tunable m-STE luminescence of solid Kr [5]: the emission line shifts from 8.44 eV (10 K) across the ^{229m}Th resonance at $T \approx 55\text{–}57\,K$, with the maximum spectral density at 148.38 nm reached at $T = 45\text{–}50\,K$. With the parameters of the fs-laser two-photon excitation setup ($207\,nm, 220\,fs, 15\,kHz, 2.5\,\mu J, J_0 \approx 10^{11}\,W/cm^2$) [6] the exciton flux to the Kr/target interface is $2 \cdot 10^{16}\,cm^{-2}s^{-1}$, which corresponds to a steady-state population of 10^2 excited nuclei in the present target via the photon channel. Narrowing of the source line in the cavity-assisted ASE regime and the contact (Förster-type) energy transfer through an ultrathin ($\leq 2\,nm$) AlF_3 cap are identified as the key levers, promising several orders of magnitude enhancement of the pumping rate.

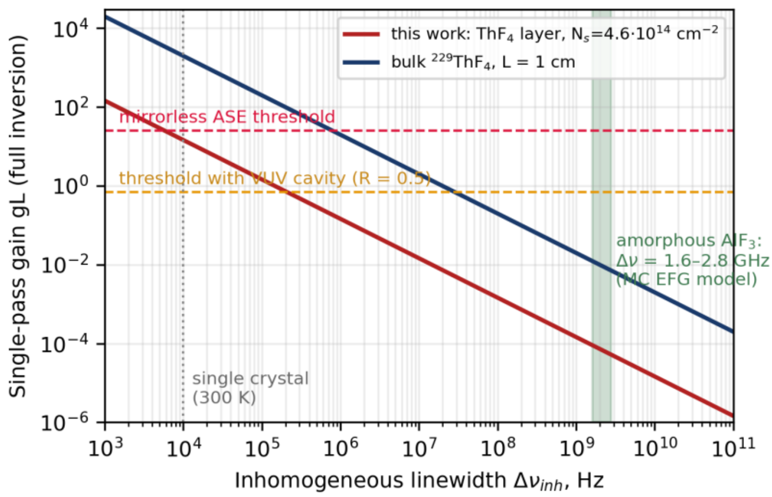

Fig. 1 Single-pass gain of the ^{229}Th VUV transition vs inhomogeneous linewidth for the present sub-monolayer AlF_3:^{229}Th structure and for a hypothetical bulk-doped single crystal; the green band marks the MC estimate for the amorphous matrix

This work was supported by the Russian Science Foundation, grant No. 24-12-00053, and within the framework of the scientific program of the National Center for Physics and Mathematics (project “Nuclear and Radiation Physics. Stage 2026-2027”).

References

[1] J. Tiedau et al., Phys. Rev. Lett. **132**, 182501 (2024).
[2] E.V. Tkalya, Phys. Rev. Lett. **106**, 162501 (2011).
[3] D.A. Myzin et al., Phys. Atom. Nuclei, accepted.
[4] J. Thielking et al., Nature **556**, 321 (2018).
[5] P.V. Borisyuk et al., JETP Lett. **122**, 455 (2025).
[6] P.V. Borisyuk et al., Phys. Usp., accepted.

Wednesday
August 26

Monday	Tuesday	Wednesday	Thursday	Friday	Saturday	Sunday
27	28	29	30	31	1	2
3	4	5	6	7	8	9
10	11	12	13	14	15	16
17	18	19	20	21	22	23
24	25	26	27	28	29	30
31	1	2	3	4	5	6

Observation of topological vortex solitons in aperiodic waveguide arrays

V.O. Kompanets[1], A.V. Kireev[1,2], K. Sabour[2], S.Y. Alyatkin[3], N.S. Kostyuchenko1[1,4], S.A. Zhuravitskii[1,4], N.N. Skryabin[4], I.V. Dyakonov[4], A.A. Kalinkin[4], K.A. Sitnik[3], S.K. Ivanov[5], S.P. Kulik[1,4], S.V. Chekalin[1], P.G. Lagoudakis[3], Y. Zhang[6], Y. Li[6], V.N. Zadkov[1,7], Y.V. Kartashov[1]

[1]*Institute of Spectroscopy, Russian Academy of Sciences, Troitsk, Moscow, 108840, Russia*
[2]*Moscow Institute of Physics and Technology, Dolgoprudny, 141701, Russia*
[3]*Skolkovo Institute of Science and Technology, Skolkovo, Moscow, 121205, Russia*
[4]*Quantum Technology Centre, Lomonosov Moscow State University, Moscow, 119991, Russia*
[5]*Instituto de Ciencia de los Materiales, Universidad de Valencia, Paterna, 46980, Spain*
[6]*Key Laboratory for Physical Electronics and Devices, Xi'an Jiaotong University, Xi'an 710049, China*
[7]*Faculty of Physics, Higher School of Economics, Moscow, 105066, Russia*

Corresponding author: kompanetsvo@isan.troitsk.ru

Localized vortex-carrying beams propagating in nonlinear optical media may form self-sustained excited states – vortex solitons – which are however usually prone to azimuthal instabilities in uniform medium and require high powers for their stabilization even in non-topological periodic structures. Here, using the method of fs-laser writing, we create aperiodic waveguide arrays representing topologically nontrivial structures that are capable of supporting stable and thresholdless topological vortex solitons. The first topological system is realized by removing a sector from honeycomb array to obtain a structure with disclination core and C5 discrete rotational symmetry. We demonstrate experimentally that it supports stable, thresholdless vortex solitons bifurcating from the protected in-gap vortex disclination states and remaining localized at the disclination core across the entire topological bandgap. The second topological system that we consider is realized as a third-generation (G3) Sierpiński-gasket fractal array, where we also demonstrate stable topological vortex solitons residing in the corner of the structure and exhibiting exceptional robustness across a broad power range and, unlike vortex solitons in topologically trivial lattices, forming without a power threshold. To experimentally excite vortex solitons, we used pulsed radiation from a Ti:Sa laser system, structured using a spatial light modulator into several coherent excitation spots with a controlled phase increment. Measurements of the intensity at the output of the arrays and holographic reconstruction of the phase structure directly show the formation of a stable vortex soliton. These findings demonstrate topologically protected nonlinear states with non-trivial phase structure, establishing a platform for robust optical information transport, vortex-based switching, and structured-light generation in topological photonics. Our results open new prospects for applications of vortex-carrying beams in topological photonics.

This work was supported by the Russian Science Foundation (Grant No. 24-12-00167)

Laser synthesis of linear carbon chains: prospective applications in photonics and sensing

V. Samyshkin[1], A. Abramov[1],
A. Lelekova[1], A. Povolotskiy[2], A. Osipov[1], and A.O. Kucherik[1]
[1]*Department of Physics and Applied Mathematics, Stoletov Vladimir State University, 600000 Gorkii street, Vladimir, Russia*
[2]*Institute of Chemistry, St. Petersburg State University,198504, Ulianovskaya str. 5, St. Petersburg, Russia*
E-mail: kucherik@vlsu.ru

Carbon-based structures represent a highly adaptable foundation for discovering novel frontiers in materials science, offering significant potential in diverse areas such as organic electronics, chemical and optical detection systems, high-speed optoelectronic devices, and green energy generation [1].

Lately, carbyne - a strictly one-dimensional carbon allotrope featuring sp-hybridized bonds—has attracted substantial attention due to its single-atom thickness, rendering it a promising candidate for molecular-scale electronics [2]. This unique structural geometry endows the material with remarkable heat tolerance, outstanding electrical transport properties, and superior mechanical robustness [3]. In contrast to graphene or carbon nanotubes, carbyne possesses unique structural merits that make it particularly compelling for functional applications, notably in the field of sensing.

Sensors utilizing carbyne matrices exhibit distinctive features, such as an expansive active surface area coupled with enhanced charge carrier mobility, which ensures high responsiveness to environmental changes [4]. This enables gas detection systems to operate with exceptional precision and target selectivity. Thanks to its specific molecular structure and high chemical resilience, carbyne serves as an optimal substrate for sensor manufacturing, maintaining operational stability across diverse conditions [5].

Consequently, this creates opportunities for developing highly sensitive and precise analytical tools for healthcare, industrial monitoring, and ecology. Given these prospects, gaining insight into diverse synthesis pathways for carbon nanomaterials, especially carbyne, is essential for precisely tailoring their morphology, dimension, and physical properties [6]. Access to varied fabrication techniques expands the methodologies for engineering carbon nanostructures with custom characteristics, unlocking innovative applications across multiple technological domains.

The work was supported within the framework of the state assignment in the field of RNF-grant #26-12-20015 (https://rscf.ru/project/26-12-20015/).

References

[1] J. Zhang et al., Carbon **218**, 118700 (2024).
[2] A. Kucherik et al., Phys. Rev. Lett. **132**, 056902 (2024).
[3] Q. Zheng et al., Cryst. Growth Des. **26**, 4442 (2026).
[4] A. Kucherik et al., Nanotechnology **36**, 072002 (2025).
[5] M.-A. Hejazi et al., Diam. Relat. Mater. **159**, 112854 (2025).
[6] Y. Jin et al., Nano Research **17**, 6571 (2024).

Nonlinear photographic media with fluorescence imaging, their research and applications

E.F. Martynovich[1,2], **V.P. Dresvianskiy**[1,2]
[1]*Irkutsk Branch of the Institute of Laser Physics SB RAS*
[2]*Irkutsk State University*
E-mail: femto@bk.ru

Black-and-white photography emerged and gained widespread popularity thanks to the development and refinement of photosensitive storage materials based on silver halides in the 18th and 19th centuries. Photographic images in these materials were formed through the precipitation of colloidal silver during photographic exposure and subsequent processing. Research conducted at the turn of the 1920s and 1930s at the University of Göttingen under the direction of Robert Pohl, as well as at the Physics Institute of the USSR Academy of Sciences and the State Optical Institute in Leningrad by S.I. Vavilov's colleagues, demonstrated that similar processes also occur in alkali halides when they interact with optical or X-ray radiation.[1-3] This analogy is determined by the identical symmetry of the crystal lattices and the electronic structure of the atoms that form these compounds. However, alkali halide compounds were significantly different in that colloidal metal particles formed in them only at very high irradiation doses, following a series of complex aggregation processes and the transformation of simple primary radiation defects formed during photoexposure. Therefore, it became clear that using photographic materials based on colloidal metal particles in alkali halide compounds was practically impractical.

Nevertheless, this problem can be solved by forming a latent image in alkali halide or other crystals during photoexposure using primary radiation defects capable of effectively luminescing at room temperature and being thermally stable rather than colloidal metal particles. Under these conditions, fluorescent visualization of the formed latent image can be achieved. Crystalline media with an exciton defect formation mechanism can serve as such photographic materials. The spectral region of photosensitivity of such materials is determined by the position of their intrinsic electron absorption spectra, including the spectra of exciton and electron-hole pair formation. For many crystals, these spectra lie in the ultraviolet region, and their optical absorption coefficients are large. Therefore, an image in a linear interaction regime can only be formed in a thin layer on the surface of the photographic material.

However, the use of a nonlinear regime at the initial stage of interaction between optical radiation and the photographic medium allows these media to be transformed into three-dimensional ones.[4] As a result of these studies, a new class of functional materials has been developed – three-dimensional nonlinear photographic media with luminescent visualization of latent images formed during photographic exposure. They are intended for use in scientific photography to identify and decipher the mechanisms of complex, interconnected, non-stationary, and spatially inhomogeneous processes of highly nonlinear interaction between light and matter.[5-9] These materials enable the experimental visualization, recording, digitization, study, and storage of a three-dimensional spatial image of such interaction. In addition, they can be used to produce optical media for direct laser recording of information in the form of images, including color ones, or in digital formats.

References

[1] R. Hilsch et al., Gott. Nachr. Math. Phys. Klasse, **334** (1930).
[2] J. H. Webb, Journal of the Optical Society of America **26**, 367-383 (1936).
[3] S.A. Artsybyshev, Trudy FIAN im. Lebedeva, **1**(3), 5-70 (1938).
[4] E.F. Martynovich et al., Appl. Phys. Lett. **114**, 121901 (2019).
[5] E.F. Martynovich. Patent RU 2758567 C1, 10.29.2021.
[6] E.F. Martynovich. Patent RU 2781512 C1, 10.12.2022.
[7] E.F. Martynovich et al., Laser & Photonics Reviews **19**, 2401252 (2025).
[8] A.V. Kuznetsov et al., Computer Optics **49**, 560-565 (2025).
[9] N.D. Krivosheev et al., Optics Commun. **617**, 133426 (2026.)

Nonlinear Optics and DUV/VUV generation in strontium tetraborate

A.S. Aleksandrovsky[1,2]
[1]*Kirensky Institute of Physics, Krasnoyarsk*
[2]*Siberian Federal University, Krasnoyarsk*
E-mail: aleksandrovsky@kirensky.ru

Orthorhombic strontium tetraborate (α-SBO) is a unique physical object featured by 1) shortest-wavelength position of fundamental absorption edge in the VUV 2) ability to form spontaneous alternating oppositely poled domain structure unprecedented for non-ferroelectric crystals. These features make α-SBO crystals an attractive medium for nonlinear optical generation in the VUV. From the point of view of optics, domains structures in α-SBO must be classified as 1D random nonlinear photonic crystals (NPC). In the present talk we review the studies on the investigation of the peculiarities of NPC α-SBO structure and different nonlinear optical processes in these structures. In the particular, both collinear and non-collinear nonlinear optical processes were considered in two geometries 1) random QPM 2) nonlinear diffraction. Nonlinear optical properties of random NPC SBO are described in terms of reciprocal superlattice vector spectra (RSV) arising from the NPC structure. RSV spectra are shown to be extremely wide. As the sequence, NPC α-SBO are shown to support enhancement of nonlinear optical processes in the wide spectral range from near infrared to deep UV including generation of VUV radiation. The processes investigated for NPC α-SBO are frequency doubling of Nd:YAG laser, of tunable Ti:S laser, of the second harmonic of Ti:S laser, autocorrelation measurements in geometries of QPM and nonlinear diffraction, conversion of visible supercontinuum to the DUV, and, finally, continuously tunable VUV generation in the 172 – 121 nm range.

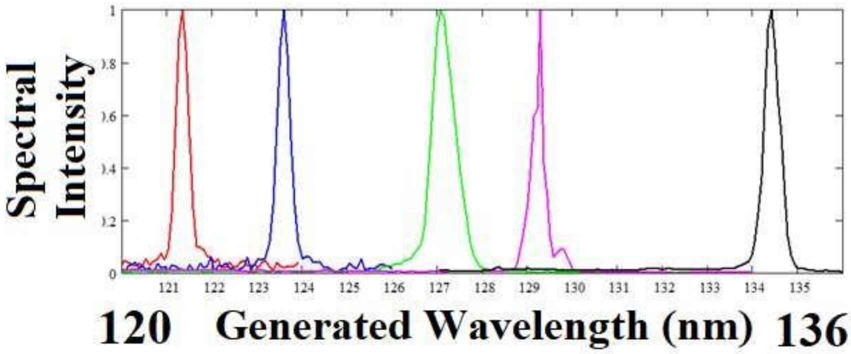

Fig. 1 Normalized spectra of VUV from NPC α-SBO [1]

Presently, the interest in VUV generation below 150 nm has grown in connection with metrology [2]. Our recent results on NPC α-SBO include 1) new closer-to-experiment DFT simulation of linear and nonlinear properties of α-SBO revealing the origin of these properties [3] 2) Experimental verification of the concept of spatially selective RQPM [4] 3) VUV generation in NPC α-SBO with improved structure [5]. In the latter study, VUV radiation from 200 nm to 162.5 nm was generated, and preservation of the RSV amplitude at shorter wavelengths was admitted [5]. DFT simulations predict that indirect interband transitions in in α-SBO can be expected at wavelength below 140 nm, and for larger wavelengths only impurities may produce unwanted absorption [3]. On the whole, at present moment random NPC α-SBO have certain potential for competing against nominally regular NPC α-SBO that are suspected to be used in IPG experiment [6].

References

[1] P. Trabs et al., Opt. Lett., **41**, 618 (2016).
[2] L. Toscani De Col et al, https://arxiv.org/pdf/2606.04997.
[3] S. N. Krylova et al., Comput. Mater. Sci. **261**, 114306 (2026).
[4] R. G. Bikbaev et al. Opt. Commun. **603,** 132836 (2026).
[5] R.G. Bikbaev et al., JETP Lett. **123**, 409 (2026).
[6] S. Vasilyev et al, https://arxiv.org/abs/2606.19484.

Dynamic processes in low-lying states of the Er^{3+} ion in the $BaY_{1.8}Lu_{0.2}F_8$ crystal

A.V. Astrakhantseva[1], T.M. Minnebaev[1], A.A. Shavelev[1], A.G. Nikolaev[2], K.N. Boldyrev[3], A.S. Nizamutdinov[1]

[1] *Institute of Physics, Kazan (Volga Region) Federal University, Kazan, Russia*
[2] *Institute of Geology and Oil and Gas Technologies, Kazan (Volga Region) Federal University, Kazan, Russia*
[3] *Institute of Spectroscopy of the Russian Academy of Science, Troitsk, Moscow, Russia*

E-mail: av.astrakhantseva@mail.ru

Modern gas analyzers based on lasers emitting in the infrared (IR) range of the spectrum are used to detect and control the concentration of greenhouse gases in the atmosphere [1]. The Er^{3+} ion provides the infrared laser oscillation at wavelengths of about 1.5 and 2.7 μm, which correspond to the groups of lines of the absorption of water, carbon dioxide and methane [2]. Infrared laser oscillation at a wavelength of about 2.7 μm in matrices doped with Er^{3+} ions is realized between two excited states $^4I_{11/2}$ and $^4I_{13/2}$. This transition is self-limited for most solid-state laser media, what imposes limitations on achieving laser oscillation in continuous mode to the low depopulation rate of the lower laser level. The phenomena of cross-relaxation and up-conversion at high concentrations of the active impurity help to depopulate the lower state of the Er^{3+} ion $^4I_{13/2}$ and provide the population of the upper laser level $^4I_{11/2}$ [3,4].

The main processes providing the population inversion between the $^4I_{11/2}$ and $^4I_{13/2}$ levels in heavily doped active media are so-called W_{22} and W_{11} up-conversion processes [5]. Using the Förster-Dexter theory can help to estimate the values of these parameters for further optimization of the active medium characteristics and achieving efficient laser generation at a wavelength of 2.7 μm.

In this work, the spectral-kinetic characteristics in the IR region of the spectrum of the concentration series of $BaY_{1.8}Lu_{0.2}F_8{:}Er^{3+}$ crystals were investigated. The lifetime of the excited states $^4I_{11/2}$ and $^4I_{13/2}$ was determined and it was shown that at high concentrations of Er^{3+} ions the lifetime of the upper laser level $^4I_{11/2}$ becomes longer than the lifetime of the lower laser level $^4I_{13/2}$.

Based on experimental values of energy levels lifetimes and spectral overlap integral the energy transfer parameters W_{11} and W_{22} were determined within the Förster-Dexter theory. It was shown that at a high doping concentration (30 at.% Er^{3+}), the lower laser level $^4I_{13/2}$ depopulates faster than the upper laser level $^4I_{11/2}$ due to the enhanced energy transfer ($W_{11}=326\cdot10^{-20}$ cm^3s^{-1} and $W_{22}=222\cdot10^{-20}$ cm^3s^{-1}). The energy transfer constant C_{DA} and the critical radius R_0 were also determined. For the scheme including the up-conversion processes from the upper and lower laser levels, a system of rate equations was constructed to estimate the population distribution of excited states and the gain for pulsed pumping of different powers. With a pulse duration of 10 ms, a pulse repetition rate of 10 Hz and a pump power of 4 W, the gain was 0.05 cm^{-1} for a sample with an Er^{3+} ion concentration of 30 at.%.

The work was funded by the subsidy allocated to Kazan Federal University for the state assignment in the sphere of scientific activities, project No. FZSM-2024-0004.

References

[1] P. Siozos et al., Remote Sensing **14**, 460 (2022).
[2] K.N. Gorbachenya et al., Crystals **12**, 519 (2022).
[3] F. Auzel, Springer Series in Materials Science **83**, 266 (2005).
[4] A.M. Tkachuk et al., Laser Optics 2000: Solid State Lasers **4350**, 81 (2001).
[5] S. Georgescu et al., J. of Lum. **114**, 43 (2005).

Thursday
August 27

Monday	Tuesday	Wednesday	Thursday	Friday	Saturday	Sunday
27	28	29	30	31	1	2
3	4	5	6	7	8	9
10	11	12	13	14	15	16
17	18	19	20	21	22	23
24	25	26	27	28	29	30
31	1	2	3	4	5	6

Optical clocks based on neutral thulium atoms

A.A. Golovizin
P.N. Lebedev Physical Institute, Leninsky prospekt 53, 119991 Moscow, Russia
E-mail: golovizinaa@lebedev.ru

Optical clocks are among the most precise physical instruments, with the measurement accuracy reaching 10^{-18} and below. In the next 5-10 years, the BIPM plans to redefine the SI second using optical clocks. Transportable optical clocks are an essential part of this roadmap, as they are crucial for building an international-scale network and verifying the consistency of geographically separated primary standards.

Optical clocks based on thulium atoms are particularly attractive for high-performance transportable systems. This is due to insensitivity of the $1.14\ \mu m$ clock transition frequency to external perturbations [1-3], including blackbody radiation and magnetic field, as well as the simplicity of the setup [4,5]. In this talk, we will discuss these advantages of thulium optical clocks in detail and present recent results [5,6].

Author thanks Russian Science Foundation grant #24-72-10102 for their supports.

References

[1] Golovizin, A., et al., Nat. Comm. **10**(1), 1724 (2019).
[2] Golovizin, A. A., et al., Nat. Comm. **12**(1), 5171 (2021).
[3] Golovizin, A., et al., JETP Letters **119**(9), 659-664 (2024).
[4] Golovizin, A., et al., Optics Express **29**(22), 36734-36744 (2021).
[5] Provorchenko, D. I., et al., JETP Letters **123**(11), 783-791 (2026).
[6] Mishin, D., et al., PRX Quantum **6**(4), 040329 (2025).

Quantum transport with cold atoms in optical lattices

Andrey R. Kolovsky
[1]*L.V. Kirensky Institute of Physics, Siberian Branch of the Russian Academy of Sciences*
[2]*Siberian Federal University, Krasnoyarsk, Russia*
E-mail: andrey.r.kolovsky@gmail.com

This contribution gives an overview of transport problems that have been studied or can be studied by using cold atoms in optical lattices. Special attention is paid to the dynamics of cold atoms in a two-dimensional optical lattice in the presence of artificial electric and magnetic fields [1,2,3,4] and to the problem of atomic current between two reservoirs of Bose atoms connected by a lattice [5,6].

Fig. 1 Time evolution of a localized wave packet in the square lattice of the width $L=40$ sites induced by an electric field which is alined with the y-axis. Snapshots at $t=0$ (left), $t=0.75T$ (middle), and $t=1.5T$ (right) where $T=L/v$ with v being the drift velocity proportional to magnetic field magnitude.

Author thanks Russian Science Foundation for their supports under Grant No. 25-12-00268.

References

[1] A.R.Kolovsky, Europhys. Lett. **93**, 20003 (2011).
[2] M. Aidelsburger, et al., Phys. Rev. Lett. **107**, 255301(2011).
[3] A.R.Kolovsky et al., Phys. Rev. E **83**, 041123 (2011).
[4] I.Yu.Chesnokov et al., Europhys. Lett. **106**, 50001 (2014).
[5] A.R.Kolovsky, arXiv: 2601.22553 (2026).
[6] A.R.Kolovsky, arXiv: 2604.12409 (2026).

Extremal unravelling for control of a double-well atomic Bose-Einstein condensate

V.A. Tomilin, A.V. Shepelin, A.M. Rostom, and L.V. Il'ichov
Institute of Automation and Electrometry SB RAS, 630090 Novosibirsk, Russia, Ac. Koptyuga ave. 1
E-mail: tomilin@iae.nsk.su

Quantum control theory provides a detailed framework for designing efficient strategies for manipulating quantum states [1]. It has become an indispensable element of the tasks of quantum state engineering [2] and control of evolution of quantum systems [3]. In this work we develop a novel approach to control of an open quantum system by manipulating the unravelling [4] of quantum operation that governs its interaction with environment. The control action is initiated by time-local spontaneous events detected during the course of system's evolution and effectively changes the informational content of these events. Such an intervention affects the evolution of conditional quantum states of the system. Proper post-selection procedures allow creation of highly non-classical states without directly affecting the parameters of the system.

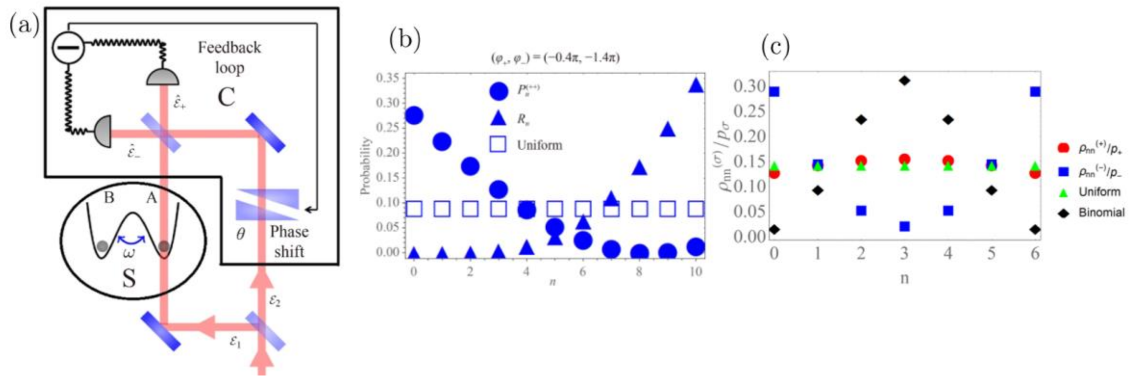

Fig. 1 (a) Principle of the control scheme. The system labelled (S) (two-mode atomic BEC in a symmetric double-well trap, with well A being interferometrically probed; ω is the tunnelling rate) generates detection events (+) and (-) recorded in the classical part of the scheme labelled (C). These events initiate the change of unravelling via feedback loop controlling the phase shift θ. (b) Steady-state conditional population of well A for post-selected two-event histories $P_n^{(++)}$ (n is the number of atoms in well A) for unravelling choice demonstrating maximal population imbalance. R_n is the conditional distribution for no-feedback case. (c) Steady-state conditional populations in well A normalized to unity for feedback with extremal unravelling, versus uniform and binomial distributions. Probability of detecting one of the event types (the (+) one) is close to unity.

We apply the proposed scheme to control of the two-mode atomic Bose-Einstein condensate (BEC) subject to non-resonant interferometric probing (Fig. 1(a)). Atoms in one of the modes interact with the probing radiation field in a dispersive regime. The photons are then detected by a pair of photodetectors in the exit channels of Mach-Zehnder interferometer (MZI). The unravelling of this detection is controlled in real-time by switching the phase-shift in the free arm of the MZI. We study two cases – pre-determined choice of unravelling based on a fixed-length event history [5], or extremal unravelling minimizing the information contained in each detected event at any time. In the first case we demonstrate that highly non-uniform population distributions of atoms over the modes can be achieved, with arbitrary high population imbalance (Fig. 1(b)). In the second case we show that the feedback almost suppresses the probabilities of all but one type of the events (Fig. 1(c)). We also investigate the time performance of the scheme and its robustness against the tunneling between the modes.

This work was supported by the State Order (project 124041700105-5) at the Institute of Automation and Electrometry SB RAS.

References

[1] H.M. Wiseman, G.J. Milburn, *Quantum Measurement and Control* (Cambridge, Cambridge University Press, 2010).
[2] C. Sayrin et al., Nature (London) **477**, 73 (2011).
[3] D. Vitali et al., Journal of Modern Optics **51**, 799 (2015).
[4] C.M. Caves, Phys. Rev. Lett. **47**, 4010 (1993).
[5] V.A. Tomilin et al., Front. Phys. **19**, 41201 (2024).

Efficient loading of the magneto-optical trap from a Zeeman-slowed atomic beam and detection of Tm atoms using the 530-nm transition with a natural linewidth of 350 kHz

A. A. Dvurechenskiy[1], D.I. Provorchenko[1], B.A. Bessmertnykh[1], D. A. Mishin[1], D. O. Tregubov[1], N. N. Kolachevsky[1], and A. A. Golovizin[1]

[1]*Lebedev Physical Institute, Russian Academy of Sciences, Moscow, 119991 Russia*

E-mail: a.dvurechenskiy@lebedev.ru

Optical clocks now surpass microwave frequency standards in both accuracy and stability [1], and this advantage has opened a wide range of uses: relativistic geodesy and mapping of the Earth's gravitational potential, stringent tests of fundamental physics from general relativity to possible drifts of the fundamental constants and searches for dark matter, and the synchronization of distributed networks for navigation and timekeeping. Many of these applications, however, must be performed beyond the laboratory, which has motivated a sustained effort to make optical clocks compact and transportable without sacrificing their metrological performance. For neutral-atom standards the principal difficulty lies in the laser systems needed for cooling, trapping, state preparation, and interrogation, several of which rely on frequency doubling or wave mixing and are awkward to miniaturize.

The neutral thulium atom is a promising platform in this respect. Its clock transition lies within an inner electronic shell near 1.14 μm and is correspondingly insensitive to the surrounding thermal field — by two to three orders of magnitude less than in the species more commonly used [2] — so that the clock can run at room temperature without cryogenic shielding. The hyperfine structure of the two interrogated transitions permits a synthetic frequency in which the linear Zeeman shift vanishes and the quadratic part is strongly suppressed, removing the sensitivity to stray magnetic fields. In addition, all of the required wavelengths — 1.14 μm, 1063.7 nm, 530 nm, and 506 nm — are accessible from robust ytterbium and erbium fiber lasers, directly or after second-harmonic generation, and a compact vacuum design that dispenses with a long separate Zeeman slower has already been demonstrated.

Despite all the advantages outlined above, the 410-nm laser system remains the most demanding component. In the conventional arrangement its radiation performs three duties at once — Zeeman slowing, the first cooling stage in the magneto-optical trap (MOT), and readout of the atom number by fluorescence — and must therefore deliver more than 50 mW of blue light with sub-MHz frequency stability. Such a source can be built only by resonant doubling of an amplified diode laser or by summing and doubling fiber lasers, making it either technically intricate or bulky and power-hungry. Easing the demands on the 410-nm system is thus a direct route to a more compact clock.

In the present work we show that these demands can be relaxed substantially. Atoms are loaded directly from a Zeeman-slowed beam into a MOT operating on the narrow 530-nm line (natural width γ = 350 kHz), so that the broad-line 410-nm MOT of earlier experiments is no longer needed, and the atom number is afterwards read out on the same 530-nm transition. The 410-nm source is consequently reduced to two undemanding roles — Zeeman slowing and hyperfine repumping — which require only about 10 mW and a frequency stability of a few MHz, comfortably maintained with a wavelength meter instead of a reference cavity or an optical frequency comb [3].

Loading directly into a narrow-line trap is delicate, because the small linewidth restricts the velocity class that can be captured. A Monte Carlo model nonetheless indicated that it should succeed at a large red detuning (about twenty linewidths) and a comparatively high total cooling power near 30 mW; an initial attempt at these settings, however, retained only about a tenth of the atoms available in the standard scheme. Since the yield depends on six interdependent quantities — the detunings and powers of the cooling and Zeeman beams together with the MOT and Zeeman coil currents — the optimization was entrusted to an evolutionary algorithm (CMA-ES, implemented through Optuna) that controlled the apparatus automatically and used the measured atom number as feedback. Convergence was rapid and reproducible: from different starting points the algorithm reached essentially the same optimum within roughly a hundred cycles, about fifteen minutes of run time, recovering more than three-quarters of the atom number of the original 410-nm trap — close to 2.5×10^5 atoms, well above the needs of a clock cycle. As shown in Fig. 1, the dependence on the two most sensitive controls saturates near 30 mW of 530-nm power and near 2.5 A of Zeeman coil current, which sets the modest power the green source must provide.

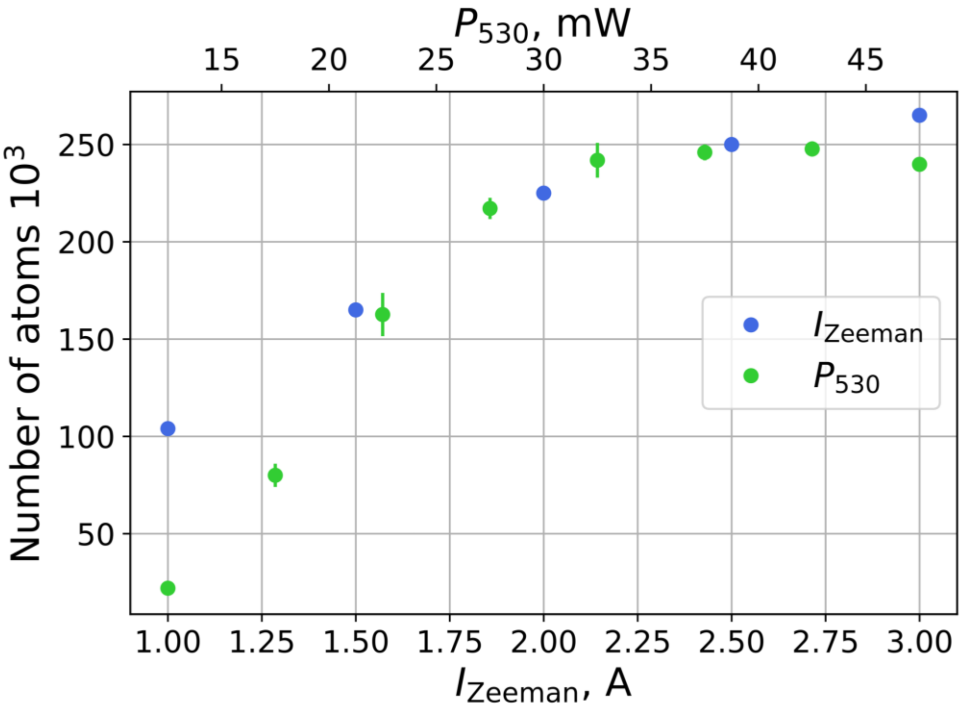

Fig. 1. Number of atoms in the 3D MOT as a function of the total 530-nm cooling power (green points) and the Zeeman coil current (blue points). Both dependences saturate — near 30 mW of cooling power and near 2.5 A of coil current.

Detection on the 530-nm line needs no additional optics — the trapping beams themselves serve as the probe — and only a modified pulse sequence with somewhat higher power. The lower scattering rate of the narrow line is offset by lengthening the probe pulse about tenfold (from roughly 0.2 to 2 ms) and by the higher quantum efficiency of the camera in the green (about 1.4 times), raising the signal-to-noise ratio to the value previously obtained on the strong blue transition; for longer pulses the signal saturates as heating ejects atoms and distorts the cloud. The readout is likewise forgiving of systematic shifts: because the ground- and excited-state g-factors are nearly equal (0.998 and 1.017), a field change of about 200 mG — far larger than ordinary laboratory fluctuations — is required to move the line by its own width, while the deepest 1063.7-nm lattice in use shifts the components by only about 1.5γ (≈ 500 kHz).

Taken together, these measurements allow the blue laser system to be scaled back from above 50 mW to roughly 10 mW, low enough to be generated directly by a laser diode, while the additional green power (up to ~50 mW) is readily supplied by a single-pass frequency-doubled 1060-nm fiber laser [4]. Every source required for the clock can thus be realized in a rugged, fiber-based form, bringing a transportable thulium optical clock appreciably closer.

This work was supported by the Russian Science Foundation, project no. 24-72-10102.

References

1. T. M. Fortier, et al., Optica **13**, 143 (2026).
2. A. Golovizin et al., Nat. Commun **10**, 1724 (2019).
3. D. I. Provorchenko, et al., JETP Letters 123.11-12: 811-820 (2026).

Ramsey spectroscopy of the octupole transition of ytterbium-171 ion in small magnetic fields

D.S. Krysenko[1,2], O.N.Prudnikov[1], V.I. Yudin[1,2,3], A.V. Taichenachev[1,3], S.V. Chepurov[1]
[1]*Institute of Laser Physics, Siberian Branch, Russian Academy of Sciences, ILP SB RAS, Novosibirsk, Russia*
[2]*Novosibirsk State Technical University, NSTU, Novosibirsk, Russia*
[3]*Novosibirsk State University, NSU, Novosibirsk, Russia*
E-mail: denizkrysenko@yandex.ru

Optical frequency standards are currently among the most accurate physical instruments. The high level of accuracy 10^{-18} opens up new opportunities for the development of fundamental and applied research, such as tests of the constancy of fundamental constants, tests of general relativity, Lorentz invariance of space, and the search for dark matter and so on.

To achieve record levels of measurement accuracy in modern frequency standards, it is necessary to suppress systematic shifts in atomic levels of various natures. For the frequency standard based on a single $^{171}Yb^+$ ion, further progress in improving characteristics may be associated with the control and suppression of shifts caused by the action of equilibrium thermal radiation, systematic shifts caused by the magnetic field, and shifts associated with the quadratic Doppler effect [1,2].

Frequency shifts associated with the action of a magnetic field are among the dominant ones and determine the uncertainty budget of optical frequency standards based on ytterbium-171. On the other hand, the presence of a controlled nonzero magnetic field is necessary to separate the Zeeman sublevels of the $^2F_{7/2}$ (F=3) state against the background of field shifts resulting from the action of a laser field near the resonance of the interrogated $^2S_{1/2}$ (F=0) → $^2F_{7/2}$ (F=3) octupole transition.

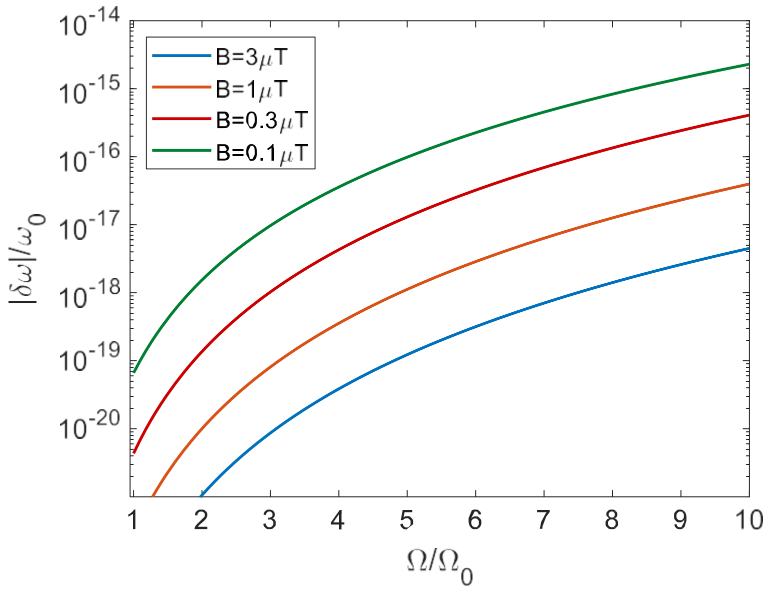

Fig. 1 The dependence of the shift of the central resonance on the logarithmic scale on the Rabi frequency at different values of the magnetic field. Interrogation time T=200 ms, $\Omega_0/2\pi$=10 Hz

In this work, frequency shifts caused by a magnetic field and light shifts during Ramsey spectroscopy of the octupole transition of the ytterbium-171 ion are analyzed. From the obtained dependence (Fig. 1), it is possible to determine the limits of the frequency of Rabi pulses for Ramsey spectroscopy, at which the nonlinear light shift reaches certain levels in the accuracy of determining the position of the resonance.

References
[1] N. Huntemann, et al., Phys. Rev. Lett. **116**, 063001 (2016).
[2] C. Sanner, et al., Nature **567**, 204–208 (2019).

Qudit-based quantum computing using polar molecules

S.Kh. Muminov[1,2], E.O. Kiktenko[1,3] A.S. Nikolaeva[1,4], D.A. Drozhzhin[1,4], S.I. Matveenko [1,5], A.K. Fedorov[1,4] G.V. Shlyapnikov[1,6,7]

[1]*Russian Quantum Center, Skolkovo, Moscow 121205, Russia*
[2]*Moscow Institute of Physics and Technology, Institutsky Lane 9, Dolgoprudny, Moscow Region 141700, Russia*
[3]*Department of Mathematical Methods for Quantum Technologies, Steklov Mathematical Institute of Russian Academy of Sciences, Gubkina Street 8, Moscow 119991, Russia*
[4]*National University of Science and Technology "MISIS", Moscow 119049, Russia*
[5]*L.D. Landau Institute for Theoretical Physics, Chernogolovka 142432, Russia*
[6]*Université Paris-Saclay, CNRS, LPTMS, 91405 Orsay, France*
[7]*Van der Waals-Zeeman Institute, Institute of Physics, University of Amsterdam, Science Park 904, 1098 XH Amsterdam, The Netherlands*

E-mail: gsh@rqc.ru

We propose a scalable qudit-based quantum processor using rotational states of polar molecules. Previously, molecular internal states were used to enlarge Hilbert space, whereas our approach uses optical tweezer arrays to achieve scalable architectures with exponential state-space growth without increasing qudit dimensionality d. Entangling gates are implemented by adiabatically bringing traps together to activate dipole-dipole interactions.

We develop encoding schemes mapping single qubits into qudits with 2 d 5 and pairs of qubits into d= 4, 5 qudits, enabling universal set of quantum gates. Additional levels in d= 3 and d= 5 qudits simplify multiqubit gate decompositions. We analyze experimental parameters for SrF and NaCs molecules. This approach provides a promising route to scalable quantum information processing with multilevel systems using existing experimental platforms.

Amplitude-robust entanglement generation in atomic arrays with individual addressing capability

I. I. Beterov[1,2,3,4], **K. V. Kozenko**[1,2], **V. V. Gromyko**[1,4], **E. A. Yakshina**[1,2,4], **S. A. Spirin**[1,2], **Peng Xu**[5,6], **I. I. Ryabtsev**[1,2]

[1] *Rzhanov Institute of Semiconductor Physics SB RAS, 630090 Novosibirsk, Russia;*
[2] *Novosibirsk State University, 630090 Novosibirsk, Russia;*
[3] *Novosibirsk State Technical University, 630073 Novosibirsk, Russia;*
[4] *Institute of Laser Physics SB RAS, 630090 Novosibirsk, Russia*
[5] *Division of Precision Measurement Physics, Wuhan Institute of Physics and Mathematics,*
[6] *Innovation Academy for Precision Measurement Science and Technology, Chinese Academy of Sciences, Wuhan 430071, China*

E-mail: beterov@isp.nsc.ru

We designed a scheme for a neutral atom Rydberg blockade controlled-Z (CZ) gate based on the double sequence of adiabatic pulses applied symmetrically to both atoms and using counterdiabatic driving for Rydberg excitation [1]. This provides a substantial reduction in the quantum gate operation time compared with previously proposed double adiabatic schemes, and makes our scheme competitive with modern time-optimal protocols for high-fidelity entangling gates with neutral atoms. The use of adiabatic passage reduces the sensitivity of gate fidelity to variations in laser intensity, while counterdiabatic driving provides short gate times. The intensity and phase profiles of the laser pulse acting on the atoms are described analytically depending only on the gate duration. In contrast with many modern CZ gate protocols, our scheme does not generate intrinsic single-qubit phase shifts, although they still appear in two-photon configuration.

We numerically optimized a scheme for a neutral atom Rydberg blockade symmetric CZ gate to increase its robustness to variations in the Rabi frequency [2]. This gate scheme uses analytically defined phase profiles of the laser pulse, illustrated in Fig. 1(a), and demonstrates increased robustness to variations in the Rabi frequency almost by an order of magnitude compared to previous proposals. We demonstrate the applicability of our gate protocol to individual addressing in Rydberg excitation, taking into account the asymmetry of Rabi frequencies for two atoms that are individually excited by tightly focused laser beams. This allows for reducing the effects of residual thermal motion of trapped atoms and beam pointing instability on gate fidelities. We investigated the performance of our gate protocol for single-photon and two-photon Rydberg excitation schemes and showed its advantages for individual addressing at finite temperatures of trapped atoms.

These gate schemes in future will be implemented using a Novosibirsk atomic array, shown in Fig. 1(b).

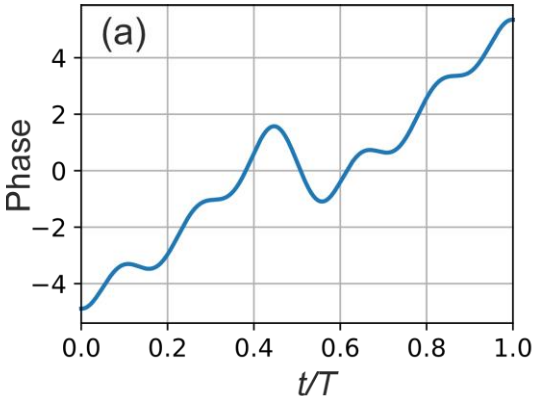

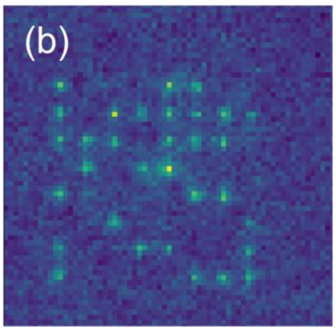

Fig. 1. (a) Phase profile of the laser pulse implementing amplitude-robust CZ gate. (b) Fluorescence image of atomic array in Novosibirsk.

Author thanks Russian Science Foundation Grant No. 23-12-00067-P for their supports.

References

[1] I.I. Beterov et al., Phys. Rev. A **113**, 042614 (2026).
[2] K.V. Kozenko et al., https://arxiv.org/abs/2604.12279.

Lineshape synthesis and contrast enhancement in laser radiation spectroscopy using high-Q resonators

A. Andrianov
A. V. Gaponov-Grekhov Institute of Applied Physics of the Russian Academy of Sciences, Nizhny Novgorod, Russia
E-mail: andrian@ipfran.ru

A novel method for achieving high spectral resolution and high contrast in laser radiation measurement is presented. Characterizing narrow-linewidth optical sources and measuring optical spectra with narrow features is an important task in spectroscopy. Conventional diffraction grating spectrometers do not have sufficient resolution. Optical heterodyning provides high resolution but requires a tunable laser [1], which limits the spectral range. High spectral resolution over a wide wavelength range can be achieved using tunable high-Q optical resonators, but their Lorentzian lineshape with slowly decaying wings results in poor contrast. An improved method using a high-Q resonator and a special signal modulation technique with advanced numerical post-processing allows for the synthesis of the device lineshape (the spectral aperture function) and true optical spectrum measurement with high resolution and improved contrast in a self-heterodyning configuration.

The proposed method was experimentally verified in the telecommunication band (1500-1600 nm) using a fiber ring resonator with a Q-factor of about 10^8 (~2 MHz linewidth at -3 dB level) and a free spectral range of 250 MHz. An example of measured spectra of two narrow-linewidth lasers is shown in Fig. 1.

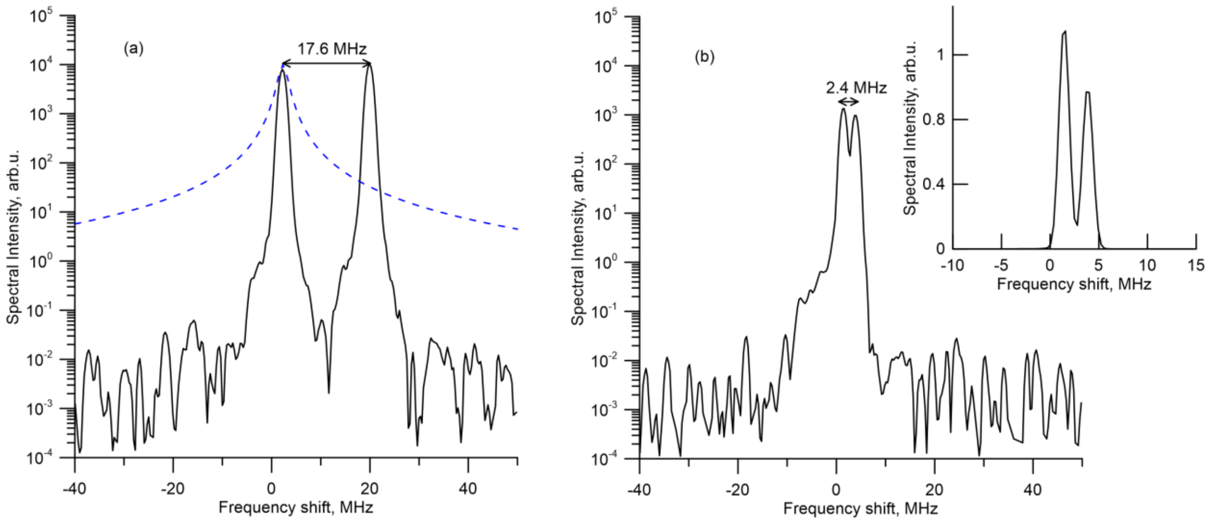

Fig. 1 Measured spectra of two lasers with close optical frequencies: frequency difference 17.6 MHz (a, solid line, logarithmic scale) and 2.4 MHz (b, solid line, logarithmic scale; inset - linear scale). The intrinsic Lorentzian lineshape of the resonator is shown by dashed line in (a). The zero frequency corresponds to an optical frequency of about 193.55 THz (1550 nm).

Spectral resolution of approximately 2 MHz is demonstrated using the synthesized lineshape (aperture function) defined by the Blackman-Nuttall window function. The synthesized aperture function provides much faster wing decay than intrinsic Lorentzian lineshape of the resonator. The resulting close-in contrast exceeds 50 dB at frequency detuning of 20 MHz. It was also shown that two signals from narrow-linewidth lasers with very close optical frequencies and a large difference in intensities can be simultaneously analyzed. Importantly, this method allows one to determine the sign of the frequency difference, i.e. to determine which of the sources has higher optical frequency, which is impossible with standard self-heterodyne methods.

References

[1] H. Mao et al., Opt. Lett. **51**, 748 (2026).

Quantum Spin Liquid State of a Dual-Species Atomic Array on Kagome Lattice

A.M. Farouk[1,†], **I.I. Beterov**[1,2,3,4], **G. Suliman**[1,2], **J. Chen**[1,2], **and I.I. Ryabtsev**[1,2]

[1]*Rzhanov Institute of Semiconductor Physics SB RAS, 630090 Novosibirsk, Russia*

[2]*Faculty of Physics, Novosibirsk State University, 630090 Novosibirsk, Russia*

[3]*Department of Laser Physics, Institute of Laser Physics SB RAS, 630090 Novosibirsk, Russia*

[4]*Faculty of Physical Engineering, Novosibirsk State Technical University, 630073 Novosibirsk, Russia*

[†] E-mail: afarouk@isp.nsc.ru

Dual-species arrays of ultracold neutral atoms have recently attracted increased interest due to the ability to independently control different atomic species and tune interatomic interactions. This capability provides additional flexibility essential for both quantum computing and quantum simulation. In this work we theoretically investigate a quantum spin liquid (QSL) state using a programmable quantum simulator based on a dual-species atomic array of ^{87}Rb and ^{133}Cs neutral atoms, arranged on a Kagome lattice [Fig. 1(a)]. The Kagome lattice is formed from corner sharing triangles, leading to a larger degeneracy, and is often considered as a model for realising QSL states. When the atoms are excited into Rydberg states, long-range interactions result in Rydberg blockade. The geometric frustration of the Kagome lattice, combined with the Rydberg blockade, drives the system into exotic phases with topological order and long-range entanglement.

To drive an array into the QSL state, we use a sweep-quench-sweep protocol [Fig. 1(b)], when the atoms are adiabatically excited into Rydberg state with individually controlled detuning for each atomic species at the end of the protocol. The adiabatic excitation is temporarily interrupted for a variable quenching time t_q. The QSL regime is achieved by tuning the ratio of detunings $\nu = \Delta_{Cs}/\Delta_{Rb}$. The emerging of a QSL phase corresponds to the filling fraction window $\tilde{n} \leq 1/4$. In our calculations this regime is achieved for the relation between the detuning and the Rabi frequency in the range $\mu_i \leq \Delta_{Rb}/\Omega_0 \leq \mu_f$ ($\mu_i = 1.34$, $\mu_f = 4.77$) for interatomic spacing a = 4.0 μm and $\nu = 0.1$ [Fig. 1(c)].

Spatial correlations in the atomic array are quantified via the density-density correlation function $g^{(2)}(r)$, from which the correlation length ξ is extracted. For a = 4.0 μm, we find the maximum correlation length $\bar{\xi}_{max}/a \approx 3.6$ at $\nu = 0.1$ [Fig. 1(d)]. Its peak value coincides with the QSL phase boundary μ_i. The entanglement structure is characterized through mutual information I_{AB} between system subsets, revealing a crossover from area-law to volume-law scaling, as Δ_{Rb}/Ω_0 increases [Fig. 1(e)]. The topological order is confirmed by calculation of the Kitaev-Preskill topological quantum entanglement entropy γ [Figs. 1(f,g)]. It yields $0 < \gamma \leq \log(2)$, which is consistent with a Z_2 toric code phase and provides a promising platform for fault-tolerant quantum computation.

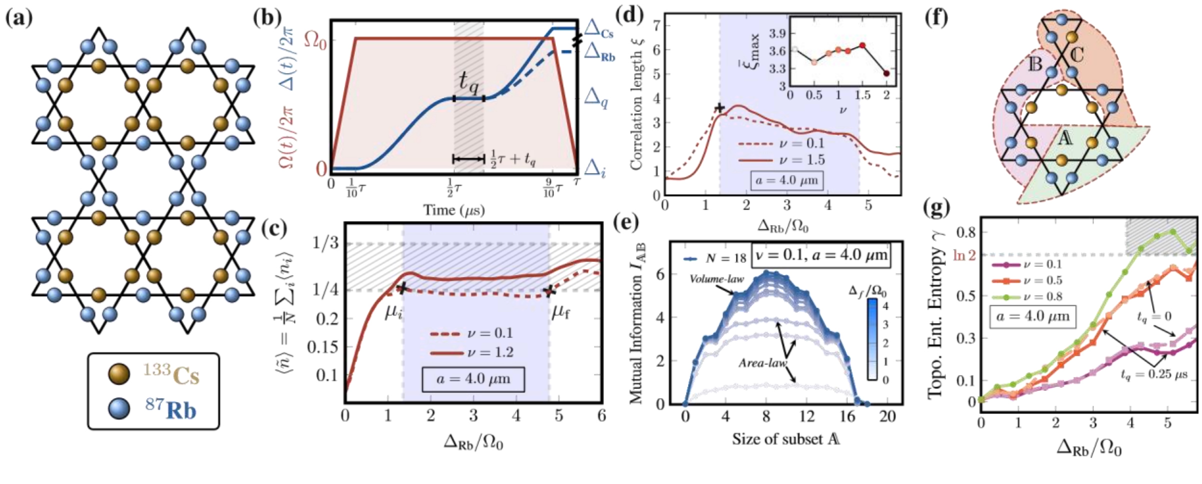

Figure 1: (a) Dual-species ^{87}Rb/^{133}Cs array on a Kagome lattice. (b) Sweep-quench-sweep detuning protocol. (c) Average Rydberg density $\langle\tilde{n}\rangle$ vs. Δ_{Rb}/Ω_0; the shaded region marks the QSL window. (d) Correlation length ξ vs. Δ_{Rb}/Ω_0 for two

values of v; inset shows the peak $\bar{\xi}_{max}$ vs. v. (e) Mutual information I_{AB} vs. subset size for $N = 18$, showing area-law and volume-law regimes. (f) Partition scheme for subsets A, B, C used in the Kitaev-Preskill calculation. (g) Topological quantum entanglement entropy γ vs. Δ_{Rb}/Ω_0 for different v and quench times t_q.

- The preprint of the article is available on arXiv:2605.03579.
- Acknowledgment: This work is supported by the Russian Science Foundation (Grant No. 25-22-00730).

Poster Session B

Polarization state of 89Xnm-range intracavity-contacted oxide-confined VCSELs

M. Bobrov[1], Ya. Kovach[1], A. Blokhin[1], N. Kuzmenkova[1], A. Vasil'ev[1], A. Kuzmenkov[1], N. Maleev[1] and S. Blokhin[1]

[1]*Ioffe Institute, 194021 Saint Petersburg, Russia*

E-mail: blokh@mail.ioffe.ru

There is a lot of attention that has been focused on the development of compact quantum sensors based on gas cells with alkali metal atom vapors for autonomous navigation, secure communication networks, and magnetic reconnaissance [1]. Of particular importance is the polarization stability of compact laser emitters based on single-mode vertical-cavity surface-emitting lasers (VCSELs).

Since VCSELs do not have an intrinsic mechanism of polarization gain anisotropy, to control the polarization state in our 89X nm-range single-mode intracavity-contacted oxide-confined VCSELs (89X nm IC-VCSELs), we induced an asymmetric mechanical stress near the active region by implementing a diamond-shaped selectively oxidized current aperture [2-3]. The realized 89X nm IC-VCSELs based on InGaAs/AlGaAs quantum wells with a characteristic size of the selectively oxidized aperture of 2.5-3 μm can demonstrate efficient lasing with side-mode suppression ratio more than 20 dB and orthogonal polarization suppression ratio more than 15 dB in a fixed current and temperature range [4].

According to the analysis of the 89X nm IC-VCSEL's polarization state, at a fixed current a small change in azimuth (less than 1-2 degrees) is typically observed as ambient temperature increases from 50 to 80°C (see 89X nm IC-VCSEL-A in Fig.1). This can be explained by the piezo-optic effect caused by a mismatch in the thermal expansion coefficients of the laser and the heatsink. However, some lasers exhibit an anomalously large rotation of the polarization plane of up to 30 degrees and a change in ellipticity up to ±2 degrees, despite maintaining the degree of linear polarization (see 89X nm IC-VCSEL-B in Fig.1). The reasons for this require further investigation.

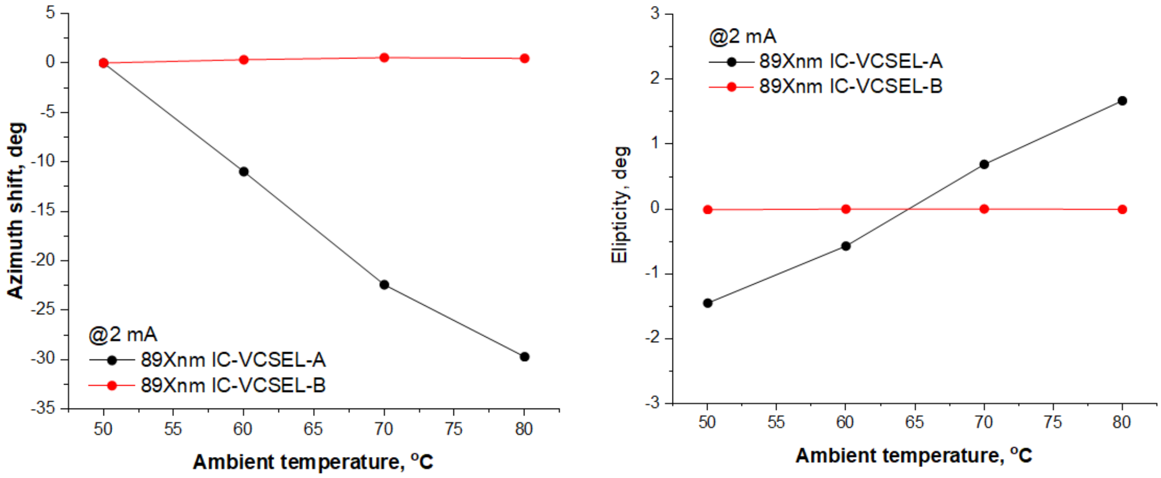

Fig. 1 Dependences of azimuth shift (a) and ellipticity (b) on ambient temperature at a fixed current

Authors acknowledge support in part by the grant of the Russian Science Foundation No. 26-92-20002, https://rscf.ru/project/26-92-20002/ for the study of VCSEL polarization characteristic.

References

[1] J. Kitching., Appl. Phys. Rev. **5** (3), 031302 (2018).
[2] M.A. Bobrov et al., Semiconductors **50** (10), 1390–1395 (2016).
[3] M. Mokhtari et al., Appl. Phys. Lett. **118** (9), 091102 (2021).
[4] S.A. Blokhin et al., SPbPU J. Phys. Math. **16** (3.2), 16-22 (2023).

$^{171}Yb^+$ single ion optical clock development.

S.V. Chepurov, N.S. Lapin, M.I. Nesterenko, D.Y. Primakov, N.A. Kolyada, A.A. Filonov, V.S. Pivtsov, S.A. Kuznetsov

Institute of Laser Physics SB RAS, Novosibirsk, Russia
E-mail: chepurov.sv@yandex.ru

We report recent progress on the development of an optical frequency standard based on the forbidden transition in a single ytterbium-171 ion.

The ion trapping and confinement are performed using a miniature RF trap with endcap electrodes. Laser cooling of the ion and detection of its state are implemented on the quasicyclic dipole transition with a wavelength of 370 nm [1, 2]. The clock transition is excited by a narrow-linewidth probe laser with λ = 436 nm. The preparation and inquiry of ion energy states are performed using a specially chosen sequence of laser pulses. The width of the recorded resonance at the central transition frequency is 30 Hz [3].

Based on the obtained experimental values of the linewidth and drift rate of the probe laser frequency, resonance width, and clock transition excitation probability the daily frequency stability of the developed standard is estimated to be $\sim 10^{-17}$ [4].

$^{171}Yb^+$ single ion optical clock can demonstrate better metrological performance with the use of the highly forbidden octupole transition $^2S_{1/2}$ (F = 0) → $^2F_{7/2}$ (F = 3). To excite this transition we have developed a narrow-linewidth probe system based on the second-harmonic radiation of an external-cavity diode laser with λ = 934 nm. To reduce the spectral linewidth of the laser to ~1 Hz, its frequency is stabilised to a high finesse ($\sim 3{\cdot}10^5$) Fabry – Perot reference cavity, made of glass with a low thermal-expansion coefficient (ULE glass, Corning). To suppress mechanical vibrations, the vacuum chamber with the cavity is installed on a passive vibration-isolation plate. In addition, the cavity is mounted in the chamber using a system of suspensions, reducing its sensitivity to vibrations. The influence of the ambient temperature on the position of cavity resonances is significantly reduced by stabilizing temperature near the 'zero' point (~ 23.7º C), characterized by close-to-zero thermal-expansion coefficient of the cavity base material. The linear drift of the octupole probe laser system is measured to be ~ 20 mHz/s.

We experimentally implemented a novel scheme of deep laser cooling of $^{171}Yb^+$ in a polychromatic field with three frequency components resonant with optical transitions of the $^2S_{1/2} \rightarrow {}^2P_{1/2}$ line. The scheme does not require a strong magnetic field in the laser cooling cycle and allows to precisely control a weak magnetic field used for the clock transition spectroscopy which is important for the deep suppression of quadratic Zeeman shifts of clock transitions [5, 6].

References

[1] S.V. Chepurov et al., Quantum Electronics **44** (6), 527 (2014).
[2] O.N. Prudnikov, et al. Quantum Electronics **47** (9), 806 (2017).
[3] S.V. Chepurov et al. Quantum Electronics **49** (5), 412 (2019).
[4] S V Chepurov et al. Quantum Electronics **51** (6), 473 (2021).
[5] D.S. Krysenko et al. PHYSICAL REVIEW A **108**, 043114 (2023).
[6] O.N. Prudnikov et al. JETP **166**, 4 (10), 556–565 (2024).

Cooling and trapping of neutral atoms in bichromatic optical trap

R.Ya. Ilenkov[1], O. Prudnikov[1], A. Kirpchnikova[1], A. Taicenachev[1,2], V. Yudin[1,2],
, P. Petrov[1,2], and D.V. Brazhnikov[3,4]
[1] *Institute of Laser Physics SB RAS, Novosibirsk, Russia*
[2]*Novosibisk State University, Novosibirsk, Russia*
E-mail: ilenkov.roman@gmail.com

Cold atomic ensembles are recognized as a versatile platform for high-precision metrology, quantum communications, quantum information processing, the development of quantum simulators, and highly sensitive sensors. In the majority of experimental implementations, trapping is accomplished via a magneto-optical trap (MOT), which has become a standard component in virtually all cold-atom experiments. Nevertheless, the presence of an inhomogeneous magnetic field and the associated requirement for its precise control impose fundamental limitations that preclude the attainment of the ultimate sensitivity and accuracy of modern cold-atom-based quantum devices, including optical frequency standards [1], atomic interferometers [2], and quantum logic gates.

We propose a purely optical macroscopic trap (OMT) for atoms for cooling and trapping of atoms without the use of magnetic field. Our idea is based on a combination of two effects. The first is the dipole force rectification in a bichromatic field. The second is dissipative mechanisms of laser cooling in a bichromatic field [3] allowing Doppler and sub-Doppler laser cooling in such a filed. The spatial beating of optical shifts of atomic levels in a bichromatic field forms a macroscopic potential with a period =p/Dk, where Dk=k2-k1 is the difference in the wave vectors of the frequency components of the bichromatic field. When the frequency difference is chosen in the range of ~ 5 - 30 GHz, the macroscopic period of the optical trap has a centimeter scale, enabling sub-millimeter sizes of the trapped atoms cloud. The idea can be realized for various atoms [4,5]. Phase-independent two- and three-dimensional (Fig1) configurations based on a folded light wave have been proposed. These configurations allow the realization of deep purely optical potentials that are resilient to mirror oscillations and that enable sub-Doppler cooling of atoms.

a) b)

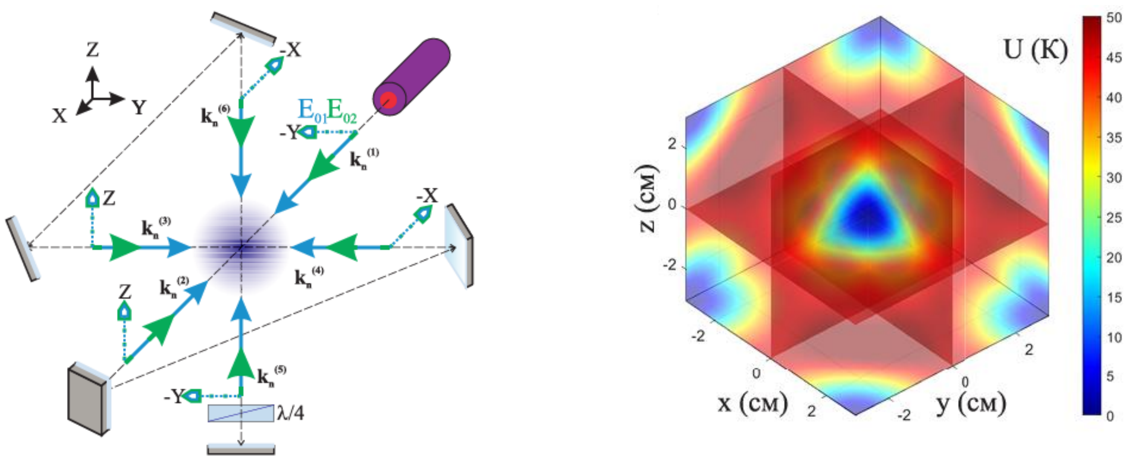

Fig. 1 (a) Three-dimensional configuration of light waves formed by a “folded” wave; (b) Three-dimensional macroscopic deep optical potential.

The work was supported by a grant from the Russian Science Foundation (RSF) № 25-22-00314

References

[1] M. Takamoto et al, Nat. Photonics **14**, 411–415 (2020).
[2] V. Taichenachev et al, J. Phys.: Conf. Ser. **1508**, 012002 (2020).
[3] O. N. Prudnikov et al. JETP **117**, 222–231 (2013).
[4] O. N. Prudnikov et al. Phys. Rev. A **108**, 043107 (2023).
[5] O. N. Prudnikov et. al. Journal of Applied Physics **139**, 114402 (2026).

Structure and surface property response of Ti-6Al-4V alloy to nanosecond UV laser irradiation

M.Yu. Kandaurova, T.Yu. Sablina, I.A. Zyatikov, I.K. Lopatkin, and Yu.N. Panchenko
Institute of High Current Electronics SB RAS, Tomsk, Russia
E-mail: panchenko.marina4@gmail.com

Ti-6Al-4V alloy is widely used in aerospace, chemical and biomedical industries due to its excellent mechanical properties, corrosion resistance and biocompatibility. However, the surface characteristics of this alloy, including chemical and phase composition, topography and morphology, are critical for its performance in applications requiring direct contact with biological tissues. Laser surface modification has emerged as a promising approach to improve the surface properties of titanium alloys [1,2]. Ultraviolet laser treatment is particularly attractive because it enables localized modification of thin surface layers without affecting the bulk properties of the material. In this work, we studied the influence of nanosecond ultraviolet laser irradiation on the structural-phase state and surface properties of Ti-6Al-4V alloy. Specimens of 10×10×1 mm were treated in air using the fourth harmonic of a Nd:YAG laser (λ = 266 nm, $\tau \approx$ 7 ns, 10 Hz) at an energy density of 0.4 J/cm^2, with scanning speeds varied from 200 to 2000 µm/s. The surface before and after treatment was characterized by scanning electron microscopy with energy-dispersive X-ray spectroscopy (SEM/EDS), X-ray diffraction (XRD), nanoindentation, and sessile-drop wettability measurements with subsequent evaluation of the free surface energy by the Owens–Wendt–Rabel–Kaelble method.

UV laser treatment induces oxidation of the surface layer. In addition to the α- and β-Ti reflections, the XRD patterns reveal titanium oxide phases (TiO and TiO_2), while EDS shows a 3–10-fold increase in the oxygen content (up to 12–20 at.%). The oxide phases are localized in a thin surface layer: they are detected by grazing-incidence XRD (analysed depth ≈ 1–2 µm) even at the highest scanning speed. With decreasing scanning speed, the oxide content increases. These changes are accompanied by a decrease of the α-Ti lattice parameter and of the coherent diffraction domain size (from 34 to 30 nm) and by an increase of the microstrain from $\approx 1.5\times10^{-3}$ to 2.7×10^{-3}, indicating a higher defect density in the surface layer. At low scanning speeds, a network of thermal microcracks is formed and the roughness Ra increases from 80 to ≈ 134 nm.

The revealed structural and phase changes lead to a modification of the surface properties. The nanohardness of the surface layer increases by 25–30% compared with the untreated alloy and approaches the substrate value at depths above ≈400 nm, confirming that the hardening is caused by the oxide surface layer rather than by the bulk. The wettability changes significantly: the water contact angle decreases from 80° to 9–13°, and the free surface energy increases from ≈38 to ≈82 mJ/m^2 owing to a considerable increase of its polar component (from 5.6 to ≈78 mJ/m^2). The contact angle and the free surface energy are almost independent of the scanning speed, whereas the oxide content, the substructure and the nanohardness change with it. Therefore, UV laser treatment enables controlled modification of the nanohardness and structural state of the surface layer together with a pronounced increase in its hydrophilicity, which is of interest for surface engineering of Ti-6Al-4V for biomedical applications.

This research was carried out with support from the Russian Science Foundation grant No. 25-29-01116, https://rscf.ru/en/project/25-29-01116/.

References

[1] D.B. Kwidzińska et al., Optics & Laser Technology **184**, 112592 (2025).
[2] J. Stepanovska et al., Biomedical Papers **164**(1), 23-33 (2020).

Developing macroscopic entirely optical trap for Hg atoms

A.A. Kirpichnikova[1], R.Ya. Ilenkov[1], and O.N. Prudnikov[1]
[1]*Institute of Laser Physics, 630090, Novosibirsk, Russia*
E-mail: KirpichnikovaAA@gmail.com

As of today, the mercury atom is one of the heaviest stable atoms for which laser cooling and trapping in magneto-optical traps (MOT) have been developed and implemented. The high atomic number gives distinct advantages for mercury atoms in developing optical frequency standards, namely: a high ionization threshold [1], a low recoil frequency – $\omega_R \approx 14$ kHz for clock transition $^1S_0 \rightarrow {}^3P_0$, and a low BBR clock transition frequency shift amounting to $\Delta\nu_{BBR}/\nu \approx -1.6 \cdot 10^{-16}$ at room temperature [2]. The relatively high vapor pressure at room temperature allows us to avoid heating the atom source, which, on the one hand, eases the process of atom cooling; on the other, does not amplify thermal radiation in the cavity.

Despite extensive study of cooling and trapping Hg atoms, cooling temperatures are usually limited to temperatures on the order of ~ 50 μK. Though according to the theoretical predictions, ground level degeneracy by quantum number for orbital angular momentum is supposed to bring about sub-Doppler cooling in the three-dimensional MOT by means of Sisyphus cooling. The lowest observable temperature 36 μK was stated in [3], but the temperature measuring method leaves a huge scatter. In our opinion, the observation of such relatively high temperatures could be conditioned on an insufficiently small recoil parameter $\varepsilon_R = 1.2 \cdot 10^{-2}$ for the mercury transition under consideration.

In this work we develop an alternative method for laser cooling and trapping mercury atoms without external magnetic field. In our scheme, a deep dissipative potential of macroscopic scale is created by a bichromatic field of collinear light waves. Frequency components of such a field are resonant to different optical transitions allowing forming a macroscopic purely optical trap by fields with relatively low intensities. At the base of such a trap lies two principles. The first one is straightening of dipole force in a bichromatic laser field [4], where spatial beats of light waves allow forming deep potential with macroscopic period $\Lambda = \pi/\Delta k$, where $\Delta k = |\mathbf{k}_2 - \mathbf{k}_1|$ is a difference between wavevectors of frequency components. The second is dissipative mechanisms of laser cooling in a bichromatic light field [5].

It should be noted, that the idea of a macroscopic pure optical trap for the first time was proposed by us for lithium atoms having specific level structure for lines D1 ($2^2S_{1/2} \rightarrow 2^2P_{1/2}$) and D2 ($2^2S_{1/2} \rightarrow 2^2P_{3/2}$) [6]. In this case the difference of light field frequency components amounts to 10 GHz leading to spatial beats and formation of optical potential with macroscopic period $\Lambda = 1.5$ cm. However, for mercury atoms having no hyperfine splitting of the ground level $^1S_0$ such scheme couldn't be directly used [6]. Nevertheless, a general principle of forming a macroscopic optical trap could be applied even in this case. In present work for implementation of a macroscopic potential of centimeter scale for an isotope ^{199}Hg we suggest to use V-scheme for interaction of two frequency components resonant to transitions $^1S_0$ (F=1/2) $\rightarrow$ $^3P_1$(F=3/2) and $^1S_0$ (F=1/2) $\rightarrow$ $^3P_1$(F=1/2) included in structure of intercombination line $^1S_0 \rightarrow {}^3P_1$. At the same time, the frequency difference of light components amounts to tens of GHz allowing forming of macroscopic potential of centimeter scale. Moreover, the resonant nature of interaction of atoms and the field allows ensuring formation of deep potential in fields of relatively low intensity. We conduct numerical analysis of the suggested scheme which could be an alternative to traditional MOT for trapping and laser cooling of mercury atoms without magnetic field.

References
[1] Q. Lavigne et al., Phys. Rev. A. **105**, 033106 (2022).
[2] H. Hachisu et al., Phys. Rev. Lett. **100**, 053001 (2008).
[3] M. Peterson et al., Phys. Rev. Lett. **101**, 183004 (2008).
[4] A.P. Kazantsev et al., JETP Lett. **46**, 264 (1987).
[5] O.N. Prudnikov et al., Quantum Electronics **87**, 806 (2017).
[6] O.N. Prudnikov et al., Phys. Rev.A **108**, 043107 (2023).

Reducing the probability of optical breakdown when passing high-power femtosecond pulses through new-type compressors

E. R. Kocharovskaya[1], E. A. Khazanov[1]
[1]*Federal research center A.V. Gaponov-Grekhov Institute of Applied Physics of the Russian Academy of Sciences (IAP RAS), 46 Ulyanov Street, Nizhny Novgorod, Russia*
E-mail: katya@ipfran.ru

The risk of optical breakdown in lasers is one of the main obstacles preventing the increase of laser output power. The breakdown is caused by local fluctuations in the energy density (fluence) of the laser beam due to spatial noise introduced by reflections from imperfect surfaces and tiny inhomogeneities of the optical elements [1]. According to our previous studies, in linear optical systems, such as free space or femtosecond-pulse compressors on diffraction gratings, spatiotemporal mixing occurs, which leads to self-filtering of the transmitted beam and reduces the probability of optical breakdown [2].

In this work, the probability of locally exceeding the breakdown threshold for a noisy laser beam is found based on analytical [3] and two independent numerical models [2]. It is shown that this probability and entire complex dynamics of noise with spatiotemporal mixing at the compressor output are mainly determined by the equivalent number of noise modes and the ratio, α_0, of the difference between the threshold and average values of the beam fluence to the standard deviation of the spatial fluence noise.

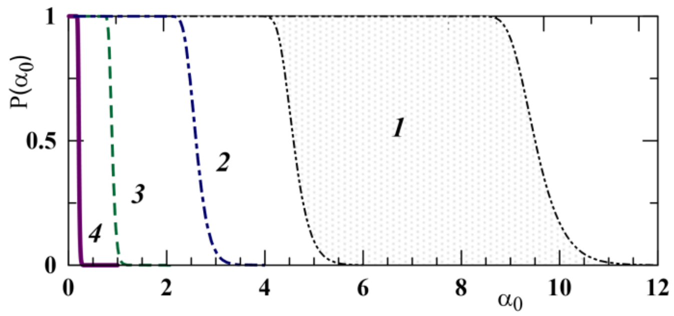

Fig. 1 Probability curves of the optical breakdown as the functions of the ratio α_0 at the compressor input (the shaded region (1) with the left and right boundaries calculated for noise with a threefold difference in spectral width, but depicted for the same, minimal standard deviation) and output (the traditional Treacy compressor (2), the asymmetric compressor (3), the Treacy compressor with one pair of gratings (4)).

The noise spectrum of the laser beam at the compressor input can vary greatly, so that for different noise spectra the probability curves of the optical breakdown at the input as the functions of the ratio α_0 occupy a wide region (zone 1 in the figure, where the left and right boundaries are indicated for noise with a threefold difference in spectral width). However, the probability of breakdown at the compressor output is determined solely by the characteristics of the linear optical system, has a certain profile as a function of the ratio α_0, and does not depend on the spectrum of the input noise if it is wide enough. The effect is demonstrated by curves 2-4 in the figure: compared to the classical Treacy compressor (TC, curve 2), its asymmetric modification (AFGC, curve 3) reduces the breakdown fluence by a factor of 3, and the dual-grating Treacy compressor (2TC, curve 4) by more than an order of magnitude [4].

Detailed modeling of the AFGC and 2TC systems confirms that the laser beam is effectively self-filtered as it passes through these compressors, significantly reducing the probability of breakdown.

The work was supported by the contract No. FFUF-2024-0038 of the Federal Research Center A.V. Gaponov-Grekhov Institute of Applied Physics of the Russian Academy of Sciences.

References

[1] S.Yu. Mironov et al., IEEE Journal of Selected Topics in Quantum Electronics. **18**, 7 (2012)
[2] E. Kocharovskaya et al., Journal of the Optical Society of America B. **42**, 1464 (2025)
[3] A. Kochetkov et al., Journal of the Optical Society of America B. **40**, 2851. (2023)
[4] E.R. Kocharovskaya et al., Radiophysics and Quantum Electronics **69**, (2026) in press

Transition from a class B laser to a class D laser: Transformation of the electromagnetic mode into the polariton mode and the emergence of elements of the superradiant dynamics

E. R. Kocharovskaya[1], **Vl. V. Kocharovsky[1]**
[1]*Federal research center A.V. Gaponov-Grekhov Institute of Applied Physics of the Russian Academy of Sciences (IAP RAS), 46 Ulyanov Street, Nizhny Novgorod, Russia.*
E-mail: katya@ipfran.ru

In the classification of lasers based on the ratios of the relaxation rates of the electromagnetic field, Γ_E, in a cavity and the polarization, Γ_2, of an active medium, as well as its population inversion, Γ_1, traditional lasers belong to class B, where $\Gamma_1 < \Gamma_E << \Gamma_2$, and superradiant lasers belong to class D, where $\Gamma_1 < \Gamma_2 << \Gamma_E$. An intermediate position is occupied by class C lasers, where $\Gamma_E \sim \Gamma_2$; see Fig. 1. For these lasers, changing the parameters of the laser cavity and active medium, as well as continuous-wave pumping, results in a transition from the conventional operating modes of a class B laser, namely, the stationary and self-modulation lasing (left panel in Fig. 1), to various superradiant-like modes. The latter are typical for class D lasing and can contain, e.g., a chaotic sequence of ultrashort superradiance pulses and spontaneous switching to complex multimode asymmetric self-modulation modes (right panel in Fig. 1). In this paper, a set of such transitions is studied for a 2-level active medium in a Fabry-Perot cavity using numerical 1D modeling of the nonlinear semiclassical Maxwell-Bloch equations [1].

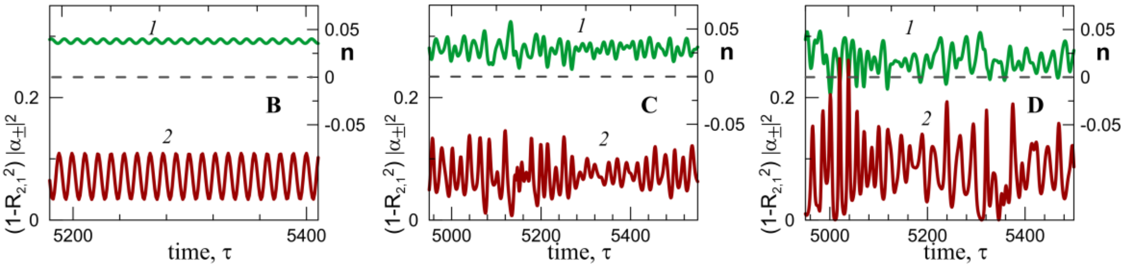

Fig. 1 Changing the laser class with decreasing the polarization relaxation rate, Γ_2: $\Gamma_2 = 6.5\Gamma_E$ - class B (left panel), $\Gamma_2 = 1.3\Gamma_E$ - class C (center panel), $\Gamma_2 = 0.4\Gamma_E$ - class D (right panel). The oscillograms of the sample-averaged population inversion (curves 1) and the radiation intensity from the right end of a cavity (curves 2) are shown for an asymmetric laser with the pumping level $n_p = 0.5$, the length $L = 10$ and the reflection factors of mirrors $R_1 = 0.8$ (left), $R_2 = 0.5$ (right). The time-spatial variables and all relaxation rates are normalized to a so-called cooperative frequency of the active medium [1,2], ν_c, so that $\tau = \nu_c t$ and $\Gamma_E = 0.046$.

It is shown that the transitions are associated with replacement of the dominant role of field dynamics in the cavity by the leading role of the polarization dynamics of the active medium, in particular, with a transformation of the fundamental laser mode from electromagnetic to polariton one [2,3]. For both steady-state and oscillation class C and D lasing, a typical *nonlinear* structure of the polariton mode is described. Unlike the electromagnetic mode, this mode is largely determined by the self-consistent population-inversion grating of the active medium. At high pump levels, the grating becomes localized and acts as an efficient Bragg mirror-amplifier. It is shown that the emergence of superradiant dynamics in the class C and D lasers provides unique opportunity for controlling the qualitative and quantitative features of coherent emission, including the levels of discrete and continuous spectral components, the number of lasing modes and their degree of synchronization, the pulse power and duration, the asymmetry of radiation (which can be many times greater than that of a cold cavity), and others [1-3].

The work was supported by the contract No. FFUF-2026-0003 of the Federal Research Center A.V. Gaponov-Grekhov Institute of Applied Physics of the Russian Academy of Sciences.

References

[1] Vl.V. Kocharovsky et al., Physics Uspekhi **60**, 345 (2017).
[2] E.R. Kocharovskaya et al., Semicond. **57**, 337 (2023).
[3] E.R. Kocharovskaya et al., Radiophysics Quantum Electronics **66**, 167 (2023).

Numerical Modeling of Lasing Dynamics in a Passively Q-Switched Nd:YAG Laser Accounting for Dynamic Thermal Lensing

Hala Diab[1], M.N. Khomyakov[1], A.P. Maiorov[1], P.A. Statsenko[1], N.V. Shahov[1], S.I. Trashkeev[1]
[1]Institute of Laser Physics of the Siberian Branch of the RAS
Email: StatsenkoPA@laser.nsc.ru

This paper presents an advanced numerical model of a pulsed Nd:YAG laser with passive Q-switching operating at wavelengths of 1064 and 1320 nm. The model is based on a system of rate equations[1] and incorporates: the calculated transverse pump distribution within the active element [2], wave propagation in the diffraction approximation [3] (beam-propagation method), and the non-stationary formation of the thermal lens during the pump pulse.

It is demonstrated that stable lasing is achievable only in the presence of a thermal lens, which provides resonator stabilization and improves the overlap between the modal field and the population inversion region.

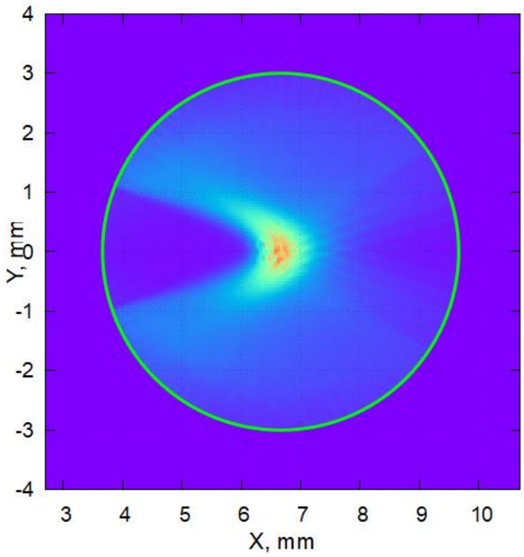

Pump distribution over the active element cross-section.

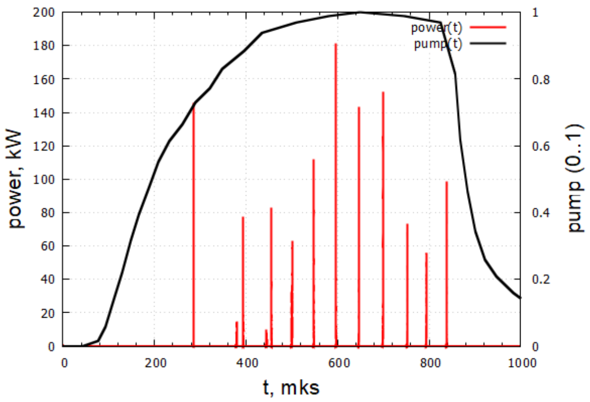

Calculated temporal profile of the pulse trains for passive Q-switching and pulsed pumping.

The thermal lens is shown to have a two-component structure: a stationary component formed by heat accumulation from previous pulses, and a dynamic component that evolves during the current pump pulse. An algorithm for calculating the dynamic thermal lens based on the temperature distribution within the active element was implemented, enabling reproduction of the experimental pulse train with varying amplitudes and durations (~100÷140 ns).

Qualitative and quantitative agreement between calculated and experimental data was achieved for pulse shape, output energy (2.66 W calculated vs. 3 W experimental), and pulse train dynamics.

References

[1] H. Diab et al, JTPh **96**(8), 1618 (2026).
[2] You Wang et al., Optics Communications 226, 303–316 (2003).
[3] M.B. Vinogradova et al, Theory of wave. M., (1979).

New Formulation of Maxwell's Equations for Four Potentials

M.N. Khomyakov[1], P.A. Statsenko[1], S.I. Trashkeev[1]
[1]*Institute of Laser Physics of the Siberian Branch of the RAS*
Email: StatsenkoPA@laser.nsc.ru

Radar research methods are based on the solution of Maxwell's equations [1]. The development and improvement of scientific and technical approaches leads to the need to consider increasingly complex problems of electromagnetic radiation propagation, which cannot be solved using approximate methods or simplifications of the original formulation. This is most clearly demonstrated in issues related to pulsed electromagnetic sounding of the geological environment [2,3]. This work is devoted to a method for the numerical solution of Maxwell's equations in media with a complex structure for direct geophysical problems, based on the potential formalism proposed and substantiated in [4].

The paper considers a new method based on the formalism of introducing two 4-potentials, which initially eliminates the need to take into account non-evolutionary conditions in the form of divergences from the sought fields [4]. This method leads to the solution of first-order hyperbolic equations equivalent to the original Maxwellian formulation. Based on the principles of constructing a wave propagation model in a potential formulation, the equations considered in [4] can be generalized to take into account conductivity and external sources. The required system of equations takes the form

$$\begin{aligned} &\varepsilon\left(\frac{\partial \mathbf{A}}{\partial t}+\nabla\varphi\right)+\sigma\mathbf{A}-rot\mathbf{S}=\mathbf{P}, && \frac{\partial \mathbf{S}}{\partial t}+\nabla\psi+\mu^{-1}rot\mathbf{A}=\mathbf{M},\\ &\varepsilon\mu\frac{\partial\varphi}{\partial t}+div\mathbf{A}=0, && \varepsilon\mu\frac{\partial\psi}{\partial t}+div\mathbf{S}=0. \end{aligned} \tag{1}$$

In general, all coefficients may depend on time and coordinates. Here, a stationary scalar medium is considered in which the permittivity $\varepsilon = \varepsilon(r)$, magnetic permeability $\mu = \mu(r)$, and conductivity $\sigma = \sigma(r)$ are specified. In addition, external sources are specified in the medium in the form of the density of the dielectric dipole moments $P = P(t,r)$ and magnetic dipole moments $M = M(t,r)$. System (1) is written in dimensionless form (the speed of light in a vacuum is $c = 1$), and the coefficients 4π are omitted. The scalar φ and vector A functions are classical potentials, ψ and S are introduced, auxiliary potentials necessary for writing first-order equations.

The system of equations for potentials (1) is equivalent to the original Maxwell equations for an arbitrary medium, which for comparison are solved by the FDTD method [5].

References

[1] Botov M.I., Vyakhirev V.A. Fundamentals of the Theory of Radar Systems and Complexes. Krasnoyarsk, SFU, 2013.
[2] Shtabel N.V. et al., Geology and Geophysics, **55**(1), 108—118 (2014).
[3] Cheremisin A.A. et al., Geology and Geophysics, **59**(2), 256—267 (2018).
[4] Trashkeev S.I. et al., Computational Mathematics and Mathematical Physics, **53**(11), 62-73 (2013).
[5] Taflove A., Hagness S. C. Computational electrodynamics. The finite-difference time-domain method. 3rd ed. Boston / New York: Artech House, 2005.

Maxwell's form of relativistic quantum equations

S.I. Trashkeev

[1] *Institute of Laser Physics of the Siberian Branch of the RAS, Russia, Novosibirsk, 630090*

E-mail: sitrskv@mail.ru

A new form of the equations of relativistic quantum mechanics is proposed, cast as linear complex Maxwell equations for the potentials. In the approach considered here, starting from Dirac's postulates [1], the relativistic quantum-mechanical equations are formulated in the form of complex Maxwell equations for four-vector potentials, proposed for other purposes in [2]. In doing so, the basic requirements that Dirac took as the foundation of his equation are satisfied. In essence, for a particle in free space, these requirements are [1]: linearity of the equations, first order in the derivatives, Lorentz invariance, and satisfaction of the relativistic energy-conservation law. If, following de Broglie, a particle is regarded as a wave, then it seems natural to seek the required model among wave equations—for instance, of Maxwellian type—with the source terms replaced by linear terms so as to satisfy the relativistic energy-conservation law.

Mathematically, Dirac reduced the second-order Klein–Gordon–Fock (KGF) equation to a system of first-order equations. Formally, the same procedure was carried out in deriving the Maxwell equations for the potentials [2]. The order reduction of the partial differential equations, accounting for all possible cases, was carried out computationally. The resulting equations for the two four-vectors ψ^α and η^α constitute a system of eight coupled equations (as opposed to four in the Dirac formulation), which contain constant, independent four-vectors of two types. The result can be written in various forms, the most transparent of which is the Maxwellian form of the equations:

$$\begin{cases} \dot{\psi} + div\boldsymbol{\psi} = in_0\psi - i\mathbf{n}\boldsymbol{\psi}, \\ \dot{\boldsymbol{\psi}} + \nabla\psi - rot\boldsymbol{\eta} = -in\boldsymbol{\psi} + i\mathbf{n}\psi + i\left[\mathbf{n}\boldsymbol{\eta}\right], \\ \dot{\eta} + div\boldsymbol{\eta} = -in_0\eta + i\mathbf{n}\boldsymbol{\eta}, \\ \dot{\boldsymbol{\eta}} + \nabla\eta + rot\boldsymbol{\psi} = in\boldsymbol{\eta} - i\mathbf{n}\eta + i\left[\mathbf{n}\boldsymbol{\psi}\right]. \end{cases} \tag{1}$$

For brevity, one of the possible choices of the constant four-vector $n^\alpha = (n_0, n_1, n_2, n_3) = (n_0, n_x, n_y, n_z)$, satisfying $n^\alpha n_\alpha = \mu^2 c^2/\hbar^2$, ($\mu$ being the particle mass), is presented here. Equations (1) are written in dimensionless form, with $\mu = c = \hbar = 1$, and an overdot denotes differentiation with respect to time. By means of a unitary transformation, the two four-vectors ψ^α and η^α can be transformed into two bispinors. After this transformation, Eq. (1), for $\mathbf{n}=0$, reduces to two independent Dirac equations.

As a result:

1. The resulting equations are more general than the Dirac equations and describe a broader class of particles and other quantum objects.
2. The equations involve complex pairs of four-vector or four-tensor quantities, which are intuitively more transparent than the spinors and bispinors of the Dirac formalism.
3. The form of the equations makes it possible to use the extensive mathematical framework developed for Maxwell's equations, including numerical methods.

References

[1] Dirac P. A. M. The Relativistic Electron Wave Equation. Preprint K.FKI-1977-62. – Budapest: Hungarian Academy of Sciences. Central Research Institute for Physics, 1977 – 19p.

[2] Kudryavtsev A.N. et al., S.I. Computational Mathematics and Mathematical Physics, **53** (11), 1653–1663 (2013).

Organic structured media – a new type of nonlinear optical materials

S.I. Trashkeev[1]*, L.V. Kulik[2]
[1]*Institute of Laser Physics SB RAS.630090, Novosibirsk, 13/3 Akademika Lavrentyeva Ave.*
[2]*Institute of Chemical Kinetics and Combustion SB RAS. 630090, Novosibirsk, 3 Institutskaya St.*
*E-mail: sitrskv@mail.ru

Organic optoelectronics is an important field of research and development of new technologies. Until recently, the application of organic media was mainly limited to photovoltaics, information display devices, and other areas that can be classified as linear optics systems. Among the wide variety of organic materials, a special class of substances can be distinguished and collectively referred to as soft media [1]. This concept should encompass not only the crystal lattice but also the “softness” of the states of the outer electronic structures responsible for interaction with radiation. At present, this “classification” includes only liquid crystals (LCs) and semiconducting polymers (SPs), i.e., the materials that have been investigated as new nonlinear-optical media at the Institute of Laser Physics, Siberian Branch of the Russian Academy of Sciences, and the Institute of Chemical Kinetics and Combustion, Siberian Branch of the Russian Academy of Sciences, Novosibirsk.

Evidence for the possibility of highly efficient frequency conversion of coherent radiation [see 2 and the references therein] has been obtained for the following materials: nematic LCs (5CB, 8CB, and commercial mixtures) and semiconducting polymers (RR-P3HT, PCDTBT, PBDBT, F8T2).

The most important experimental results showed that all the organic materials listed above were capable of frequency conversion of coherent radiation with an efficiency of 0,5% to 15% at thicknesses of 10–100 μm for LCs and 0,5–10 μm for SPs. The threshold pump powers for the onset of nonlinear generation were on the order of tens of milliwatts, at a power density of 10^4 W/cm². The estimated second-order nonlinear susceptibility, for example $\chi^{(2)}$, was on the order of 10^{-6}–10^{-5} m/V. Simultaneous generation of two harmonics was observed, and for 5CB, under certain temperature conditions, generation of three harmonics was observed. In the nematic phase of LCs, generation of even harmonics and difference-frequency generation involved the breaking of centrosymmetry.

Analysis of the obtained data led to the conclusion that the mechanism of nonlinear nonresonant radiation generation in soft media is quadrupolar in nature. The quadrupolar nature of the mechanism is confirmed by second-harmonic generation in the isotropic phase of a nematic LC. In the experiment on third-harmonic generation (THG) in P3HT [2], the pump-beam width w (and, consequently, grad(I)) was varied while maintaining the average pump-radiation power density I. The THG intensity decreases by approximately one order of magnitude when w is increased or grad(I) is decreased by a factor of 1,7. The average gradient is 10^7–10^8 W/cm³.

The studies performed and the qualitatively consistent data obtained on highly efficient nonlinear frequency conversion of radiation in certain types of soft organic media (liquid crystals and semiconducting polymers) provide grounds for asserting that a new type of nonlinear-optical materials has been identified. These materials are promising for the development of highly efficient miniature generators and converters of coherent radiation at moderate power levels.

State assignment of the ILP SB RAS, topic code FWGU-2021-0010.

References

[1] 1. M. Kleman et al., Soft Matter Physics. NewYork: Springer-Verlag, 680, (2003).
[2] 2. N.T. Vasenin, et.al. Quantum Electronics **51**(5), 437–445 (2021).

Recent progress of the dual-species 10-m atom interferometer

Si-Tong Yan[1], Lu Zhou[1,2], Chuan He[1], Jun-Jie Jiang[1,2], Jia-Qi Lei[1,2], Run-Dong Xu[1], Zhuo Hou[1,2], Zhi-Xin Li[1,2], You-Meng Hu[1,2], Jia-Ming Wei[1,3], Lin Zhou[1,3]*, Jin Wang,[1,3,4]* and Ming-Sheng Zhan[1,3,4]

[1]*State Key Laboratory of Magnetic Resonance and Atomic and Molecular Physics, Innovation Academy for Precision Measurement Science and Technology, Chinese Academy of Sciences-Wuhan National Laboratory for Optoelectronics, Wuhan 430071, China*

[2]*School of Physical Sciences, University of Chinese Academy of Sciences, Beijing 100049, China*

[3]*Hefei National Laboratory, Hefei 230088, China*

[4]*Wuhan Institute of Quantum Technology, Wuhan 430206, China*

*E-mail: lzhou@apm.ac.cn, wangjin@wipm.ac.cn

Long-baseline atom interferometers serve as powerful platforms for exploring fundamental physics. We have built a 10-meter dual-species atom interferometer platform based on ^{87}Rb and ^{85}Rb in Wuhan, which is used for tests of the equivalence principle (EP) and other investigations [1]. For the single-species ^{87}Rb atom interferometer, the maximum free evolution time reaches 2.86 s with the newly developed phase shear readout method [2, 3], corresponding to a gravity measurement resolution of 4.1×10^{-11} g per shot. By developing the four-wave double-diffraction Raman scheme, we have achieved a dual-species atom interferometer, with maximum free evolution time of 2 s and a differential measurement resolution of 4.5×10^{-12} g. To prepare for ultracold atom fountain of our atom interferometer, we have also developed the coherent acceleration technology by using Bloch oscillation. With the combination of a two-stage acousto-optic modulator and a tapered amplifier, the sweeping frequency reaches up to 90 MHz. Accordingly, the atomic cloud can be accelerated to 70 m/s, with the momentum transfer efficiency exceeding 99.9%. Collectively, these advances pave the way for higher precision EP tests in upcoming research.

References:

[1] L. Zhou et al., Phys. Rev. A **104**, 022822 (2021).
[2] S.-T. Yan et al., Phys. Rev. A **108**, 063313 (2023).
[3] L. Zhou, et al., Front. Phys. **10**, 1039119 (2022).

Limitations in the Use and Processing of Speckle Interferograms for Deformation and Residual Internal Technological Stress Analysis

S. Cheremushkin[1] and K.A. Nikitin[2]
[1,2]Novosibirsk State Technical University
[1]E-mail: semen.cheremushkin@mail.ru
[2]E-mail: ni-ki-ti-n2000@mail.ru

Modern non-destructive testing tasks require non-contact methods for measuring microdeformations of objects with complex geometry. Digital speckle pattern interferometry (DSPI) is one of the most informative methods, but its practical implementation is associated with the need for precise adjustment of the optical system and consideration of the limitations imposed on the spatial resolution of the recording system. The paper presents an optimization of the configuration of a two-beam laser speckle interferometer to obtain speckle interferograms with a given speckle size. It has been experimentally confirmed that for correct spectral separation, the speckle radius must be at least 6 pixels. A prototype software for automatic processing of speckle interferograms has been developed, including noise filtering, phase reconstruction, and mapping of deformations. A method of localization of an external impact point based on gradient analysis of phase maps with reference to a CAD model of the object is proposed.

The purpose of this work is to identify the parameters affecting speckle interferograms, and further develop software for constructing deformation maps with the possibility of subsequent localization of the point of external influence on the studied objects. The main objectives of the study are: to optimize the configuration of a two-beam laser speckle interferometer to obtain speckle interferograms with a specified speckle size; to develop algorithms for the digital processing of speckle interferograms to construct deformation maps confirming the correctness of the selected parameters; to create a prototype of a software module for comparing deformation maps with the CAD model of the object and automatically determining the coordinates of the load application.

The work implements a two-beam scheme with reference and object beams, which is shown in Fig. 1. The laser radiation (λ=532.8 nm) is expanded and directed to a beam splitter, where it is divided into reference and object beams, with the object beam being directed at the sample under study. The reflected object radiation passes through the lens and enters the CMOS camera (pixel size 13.7×13.7 µm, resolution 2210×3002 pixels). The reference beam passes through a system of mirrors and interferes with the object beam on the camera sensor.

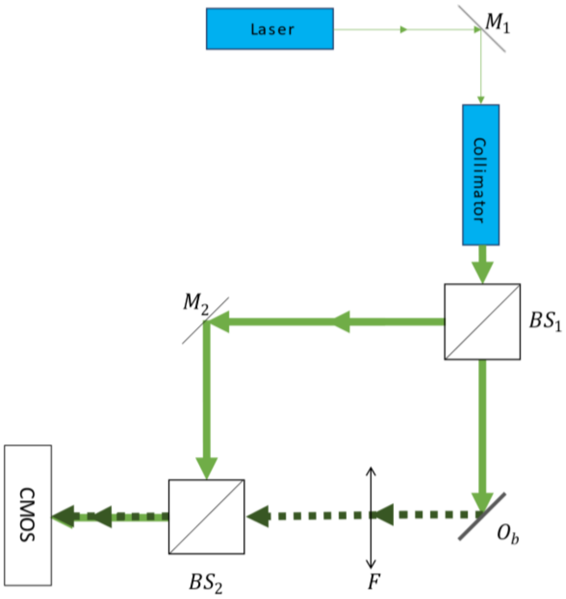

Fig. 1. Scheme of a speckle interferometer: M_i – mirrors, BS_i – beam splitter cubes, F – lens with adjustable aperture, L_F – light filter, O_b – object of study

The key condition for obtaining an interference pattern with maximum contrast is the equalization of the intensities of the reference and object beams. For this purpose, a selection of optical glasses (light filters) is used. The size of the speckles in the DSPI system does not depend on the microstructure of the object's surface but is determined solely by the parameters of the recording optics. According to [1], the average radius of the speckle can be estimated as:

$$r_{sp}=1{,}22\lambda(1+M)f \tag{1}$$

$$f= F/D \tag{2}$$

where M is the optical magnification, λ is the laser wavelength, f is the f-number of the lens, F is the focal length of the lens, and D is the effective diameter of the aperture.

In digital recording, the speckle size must be consistent with the pixel pitch of the sensor. According to the criterion established in reference [1], the following condition must be met for the correct separation of spectral components in the frequency domain:

$$4\ f_s \leq f_c\ \leq 2f_{max}/3 \tag{3}$$

$$fs = 1/(2r_{sp}) \tag{4}$$

$$f_{max} = 1/(2d_{pixel}) \tag{5}$$

where f_s is the spatial resolution of the speckle image, f_{max} is the maximum spatial frequency of the camera. This is equivalent to:

$$r_{sp} \geq 6\ d_{pixel} \tag{6}$$

i.e., the speckle radius must be at least 6 pixels.

Over the course of a year, a series of experiments were conducted with three different speckle sizes: ~1 pixel, ~2 pixels, and ~6 pixels. A steel plate with one edge rigidly fixed was used as the test object; the other edge was displaced using a micrometric screw (Fig. 2). The speckle size was varied by adjusting the optical magnification, which was due to the limited power of the laser source.

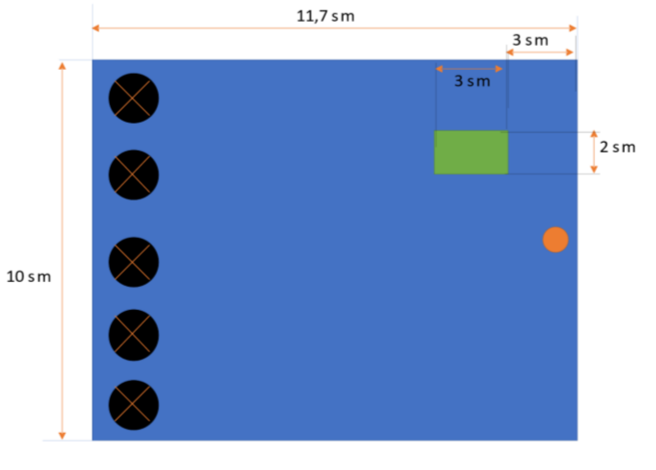

Fig. 2. Schematic representation of a metal plate: black circles indicate the plate's attachment to the base stand with bolts; the green rectangle represents the illumination spot of the objective beam; the orange circle indicates the point where pressure from the micrometer is applied.

The experiments confirmed the theoretical requirement: the speckle radius must be at least 6 pixels to ensure spectral separation and correct phase recovery. If the speckle size is less than 6 pixels, spectral components overlap, which leads to a significant deterioration in the quality of phase maps. If the speckle size is ≳6 pixels or more, the necessary spectral separation is achieved, and the quality of the phase maps improves significantly, as shown in Fig.3.

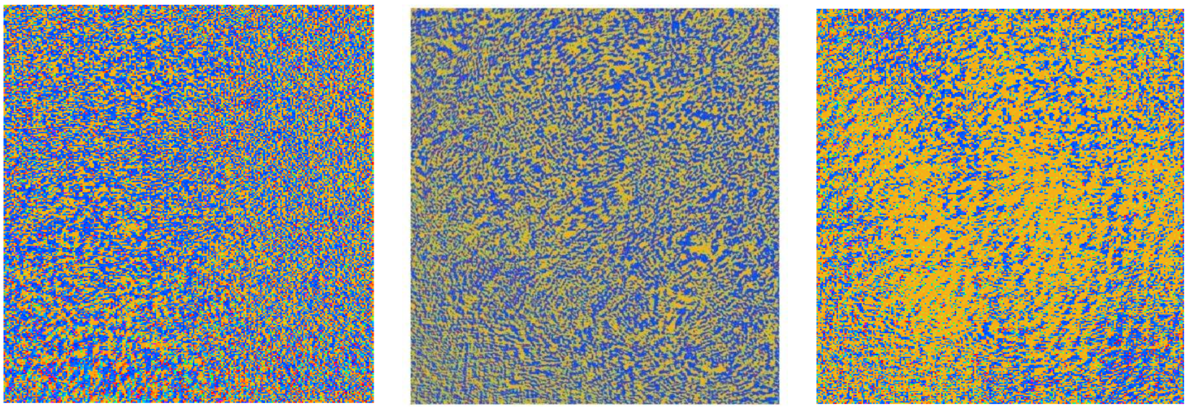

a b c

Fig. 3. Speckle interferograms of a metal plate with different speckle sizes: a) rs≈1px; b) rs≈2px; c) rs≈6px.

A set of algorithms for the preliminary processing of speckle images has been developed, including digital noise filtering while preserving phase boundaries. The developed algorithmic complex provides: calculation of the phase difference (interferograms) between the deformed and undeformed states of the object; phase recovery and phase unwrapping; conversion of phase shifts into physical strain values (μm), taking into account the geometry of the optical system and the sensitivity vector. A working prototype of a software module has been created, featuring an interface for visualizing the resulting stress and strain fields. The software enables automatic processing of speckle image sequences and the creation of deformation maps (Fig. 4).

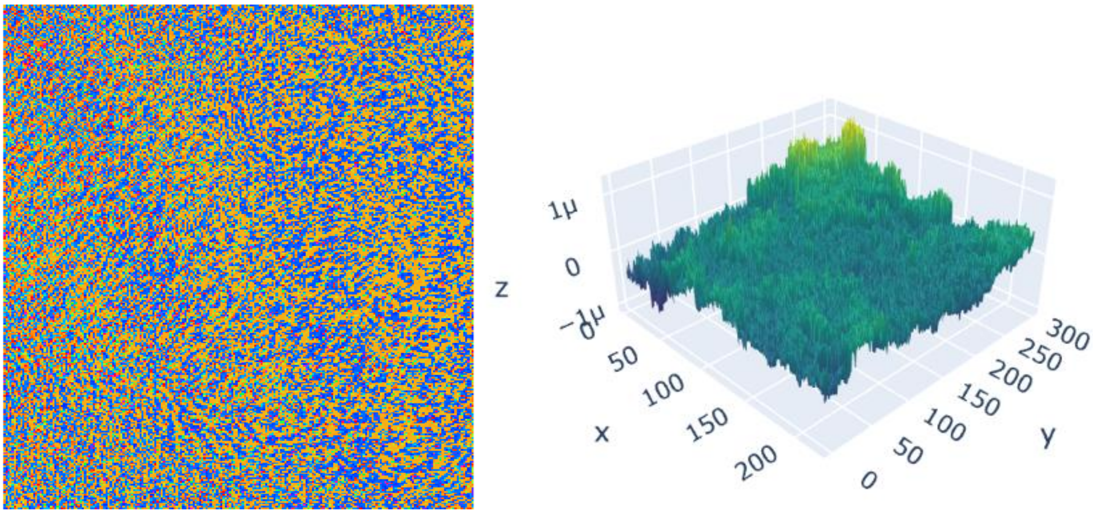

a b

Fig. 4. a) Phase diagram for bending of a metal plate; b) Deformation diagram for bending of a metal plate.

A method has been developed for loading and software representation of the CAD model of the object under study, which makes it possible to compare the results of speckle interferometric measurements with the geometry of the part. A method for searching for the epicycle of deformation based on gradient analysis of the phase shift map has been proposed. The algorithm uses information about the spatial distribution of phase shifts to determine the point of application of the external load. A method has been developed for converting the planar coordinates of the speckle pattern into the 3D space of the part, which ensures accurate localization of the point of force application.

A scheme has been created and the parameters of an experimental speckle interferometry setup based on a two-beam configuration have been identified. The intensities of the reference and object beams have been aligned to obtain an interference pattern with high contrast. It has been experimentally confirmed that for correct spectral separation, the speckle radius must be ≳6 pixels. A working prototype of software for automatic processing of speckle interferograms has been developed, including algorithms for speckle noise filtering, phase recovery, and construction of deformation maps. A prototype has been developed for automatically determining the load point on the objects under study, incorporating methods of gradient analysis of phase maps and mapping the plane coordinates of the speckle pattern to the 3D geometry of the part.

The authors thank the staff of TDI SIE SB RAS for providing the high-speed camera and specialized software for speckle interferogram recording, and acknowledge the Optical Laboratory of NSTU for the opportunity to conduct experimental research on its premises.

References

[1] Li, Zhisong & Zhong, Ping & Tang, Xin & Ling, Jiayao & Chen, Jiawei & He, Guoxing. (2019). Effect of the Speckle Size on the Quality of Speckle Pattern in DSPI System. IEEE Access. 7. 115010-115022. 10.1109/ACCESS.2019.2935754.

Online Session

On the prospects of laser-coolable molecular cations

T. Isaev[1,2]
[1]*Shenzhen MSU-BIT University, Shenzhen, P. R. China.*
[2] *M.V. Lomonosov Moscow State University, Moscow, Russia*

Among molecular systems amenable for direct cooling with lasers, laser-coolable polyatomic molecular cations present particular interest. Even the design of such species is challenging. In small molecules (up to six atoms) just increasing the charge of optical circulation center (OCC) carrying atom, whether in the core of ligand, normally leads to compounds with forbidden optical transitions between ground and first excited electronic states [1-3]. In Ref. [4] we proposed using OCC-functionalized zwitterions as laser-coolable molecular cations with allowed working optical cooling transitions, providing examples of such compounds. We are discussing properties of these compounds and their prospects for use in searches for effects of space parity- and time-reversal symmetry violations.

References

[1] M.V. Ivanov et al., Phys. Chem. Chem. Phys., **22**, 17075 (2020).
[2] A.V. Oleynichenko, et al., Phys. Rev. A, **105**, 022825 (2022).
[3] T. Isaev et al., Chem. Phys. Lett., **845**, 141301 (2024).
[4] H. Sinenka et al., J. Phys. Chem. Lett., **14,** 5784 (2023).

BOTDA-based eavesdropper localization procedure in 100 km fiber-optic communication link

A. Bezruchenko[1,2], **V.Shilov**[1,3], **and G. Lesovik**[1,2]
[1]*Moscow Institute of Physics and Technology, Dolgoprudny, Moscow Region, 141701, Russia*
[2]*LLC "P.I.R.S.", Dolgoprudny, Moscow Region, 141701, Russia*
[3]*Project Center for Applied Photonics, Skoltech, Moscow, 121205, Russia*
E-mail: bezruchenko.as@phystech.edu

Physical layer security of fiber-optic channels is essential for quantum key distribution (QKD) systems. Evanescent tapping via fiber bending is particularly challenging to detect. Correlation-based BOCDA [1] offers cm-scale resolution but is limited in range, while OTDR does not provide additional information such as temperature and strain. Hence, detecting eavesdropper with brillouin scattering-based techniques in long-haul networks remains an open problem. We propose a BOTDA-based approach with bidirectional EDFAs, probe signal depolarization and Lorentzian curve fitting (LCF). The test line consisted of two 50-km SMF spans connected by a 10-dB amplifier. A local bend, installed at the far end (100 km), simulates 5% power leakage. Measurements used pulsed pump and CW probe with frequency detuning around 10.86 GHz.

The measured Brillouin frequency shift spectrum with applied LCF clearly shows a localized perturbation at the bend position. This perturbation manifests as narrowing and intensity reduction of the spectrum, caused by the reduced opto-acoustic interaction amplitude due to power leakage. The achieved spatial resolution was 40 m, enabling reliable localization of the bend. Thus, we demonstrate for the first time the detection of 5% evanescent tapping at 100 km using BOTDA, which significantly extends the applicability of Brillouin sensors for real-world network security.

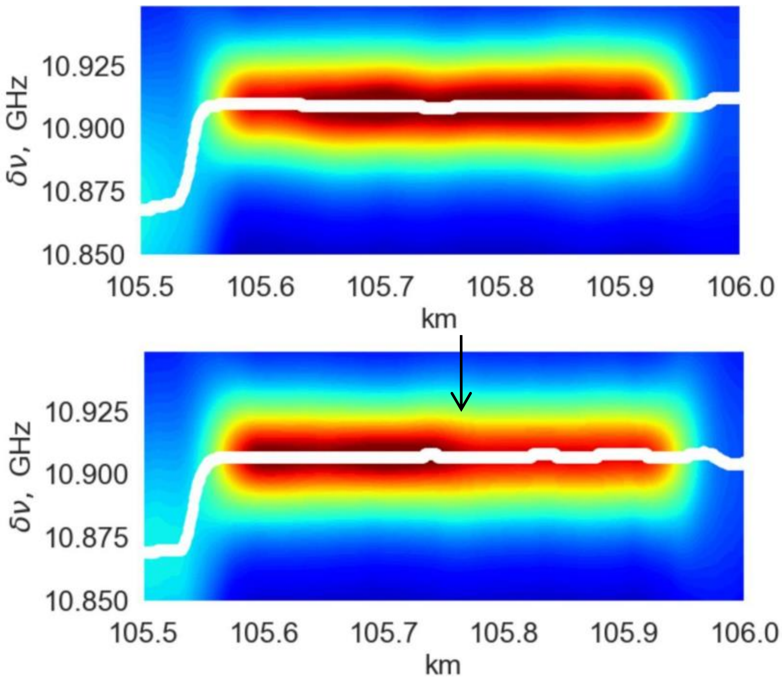

Fig. 1. Brillouin frequency shift with 5% bend (lower) compared with the reference fiber (upper). The spectrum distortion near 105.75 km marks the location of the 5% bend.

References

A. Popp et al., Optica Quantum **2**, 21-28 (2024).

LaserPhys

Лекторы

Phase-switching and unravelling-based feedback control of quantum-optical systems

V.A. Tomilin
Institute of Automation and Electrometry SB RAS, 630090 Novosibirsk, Russia, Ac. Koptyuga ave. 1
E-mail: tomilin@iae.nsk.su

Quantum control theory is a rich and emerging field – a synthesis of ideas from physics, mathematics and engineering sciences [1]. It has become most topical with the development of experimental techniques allowing manipulation of single quantum systems, such as individual atoms, molecules, quantum dots, etc. In classical control theory most efficient control strategies are based on feedback – the control action is deduced from the outcome of the measurement performed on the system. Evidently, such strategies cannot be directly translated to quantum systems, since the back-action from a measurement performed on a quantum system irreversibly changes its state. However, this drawback can be turned into advantage – a whole class of quantum state engineering methods relies on the so-called measurement-based control techniques [2].

The general framework of describing quantum systems with measurement-based feedback control under Markov approximation is be derived. We will focus on particular realizations in quantum optics, in which the systems of interest are individual atoms, their coherent ensembles or cavity QED systems (see Fig. 1(a)). It is shown that in such systems, control can be implemented via external classical fields by varying their amplitudes and phases.

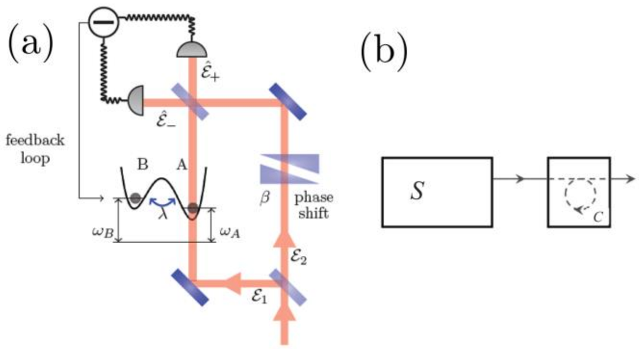

Fig. 1 (a) Control of a two-mode atomic Bose-Einstein condensate subject to interferometric probing. The trapping potentials are adjusted based on the detections in the output channels of the Mach-Zehnder interferometer. (b) Controlling the system S by feedback loop that modifies its interaction with environment.

A quantum system subject to external control via feedback loop inevitably becomes an open one. It exchanges information and energy with the environment. There are particularly important cases in which this energy and information exchange can be represented by a series of time-resolved events registered by a detector array. An obvious example from quantum optics is detecting photons emitted from the system or scattered from it. This situation presents two possibilities. First, it is useful to bind the feedback action to the time instances of detecting these events. The specific action can be chosen based on the partial history of previously detected events. Second, the feedback action can modify the very way the system interacts with environment by changing the informational content of the registered events (see schematics in Fig. 1(b)) [3,4]. This can be described formally by controlling the unravelling [5] of quantum operation corresponding to system-environment interaction. Several interesting and promising consequences and implications of this novel approach to quantum control are demonstrated.

This work was supported by the State Order (project 124041700105-5) at the Institute of Automation and Electrometry SB RAS.

References

[1] H.M. Wiseman, G.J. Milburn, *Quantum Measurement and Control* (Cambridge, Cambridge University Press, 2010).
[2] J. Zhang et al., Phys. Rep. **679**, 1 (2017).
[3] V.A. Tomilin, L.V. Il'ichov, JETP Lett. **116**, 649 (2022).
[4] V.A. Tomilin, L.V. Il'ichov, Front. Phys. **19**, 41201 (2024).
[5] C.M. Caves, Phys. Rev. Lett. **47**, 4010 (1993).

Нарушение равенства вторых коэффициентов Эйнштейна для поглощения и вынужденного испускания. Физические следствия.

А. М. Шалагин
Институт автоматики и электрометрии СО РАН. 630090 Новосибирск, просп. Акад. Коптюга, 1.
E-mail: shalagin@iae.nsk.su

В начале XX века Альберт Эйнштейн рассмотрел задачу взаимодействия излучения с атомами среды в квазирезонансных условиях. Атомы моделировались двухуровневыми квантовыми системами, а излучение полагалось широким по спектру, но близким по частоте к частоте квантового перехода. Им установлено, что процесс взаимодействия содержит три ключевых физических составляющих: акты спонтанного испускания с верхнего уровня энергии (рис. 1а), акты поглощения, вызывающие переход с нижнего уровня на верхний (рис.1б) и акты вынужденного испускания, вызывающие переход с верхнего уровня на нижний с рождением фотона, обладающего характеристиками воздействующего излучения (рис. 1в). Эйнштейном

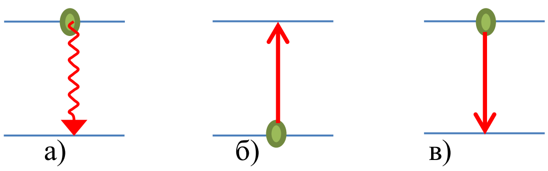

Рис. 1

выявлены соотношения между этими физическими характеристиками. В частности, установлено, что вероятности поглощения и вынужденного испускания (так называемые вторые коэффициенты Эйнштейна) в точности равны друг другу. Этот вывод длительное время воспринимался исследователями как универсальный и не подвергался сомнению даже с развитием лазерной физики. Однако в конце концов было установлено [1 - 3], что существуют условия, при которых вторые коэффициенты Эйнштейна отличаются друг от друга. В частности, это реализуется для частиц газа в условиях частых столкновений и при отстройке частоты излучения ω от частоты квантового перехода ω_0 на величину, сопоставимую с частотным интервалом для средней энергии теплового движения kT, где k – постоянная Больцмана, T – температура среды. Соотношение между вторыми коэффициентами Эйнштейна в данных условиях будет определяться множителем $\exp\{i\Omega / kT\}$, где $\Omega = \omega - \omega_0$.

Неравенство вторых коэффициентов Эйнштейна приводит к ярким физическим проявлениям. При воздействии на частицы газа достаточно интенсивным излучением в далеком синем ($\Omega > 0$) крыле спектральной линии формируется инверсия населенностей на квантовом переходе частиц и, как следствие, возникает генерация излучения на резонансной частоте перехода. Этот эффект надежно зарегистрирован экспериментально [2]. Если же возбуждающее излучение настроено в резонанс и достаточно интенсивно для выравнивания населенностей уровней, то в этом случае в далеком красном ($\Omega < 0$) крыле спектральной линии осуществляются условия для усиления пробного излучения [4]. В [4] показано, что таким способом можно получить лазер очень высокой мощности.

Исследование выполнено в рамках государственного задания (проект №124041700105-5) в Институте автоматики и электрометрии СО РАН.

Литература

[1] Ю.К. Земцов и др., ЖЭТФ **110**, 1654 (1996).
[2] Р.В. Марков и др. ,ЖЭТФ **120**, 1185 (2001).
[3] А.М. Шалагин, Письма в ЖЭТФ **75**, 301 (2002).
[4] А.И. Пархоменко, А.М. Шалагин, Квантовая электроника **51**, 915 (2021).

Участники постерной сессии

Investigation of systematic shifts in a quantum interferometer gravimeter

D. N. Kapusta[1], K. N. Adamov[1,2], A. E. Bonert[1], A. N. Goncharov[1,2,3], M. A. Nelin[1,3], K. E. Rekhtin[1,2], V. I. Yudin[1,2,3], A. V. Taichenachev[1,2,3], O. N. Prudnikov[1]

[1]*Institute of Laser Physics SB RAS, Novosibirsk, Russia*
[2]*Novosibirsk State University, Novosibirsk, Russia*
[3]*Novosibirsk State Technical University, Novosibirsk, Russia*

E-mail: ofadamovkirill@gmail.com

High-precision measurements of the gravity acceleration g are of fundamental importance for the refinement of fundamental physical constants, experimental tests of fundamental physical theories, and a wide range of practical applications, including navigation, geodesy, and mineral exploration [1]. Such measurements are performed using gravimeters. Among the various types of gravity sensors, absolute quantum gravimeters (QGs) based on atom interferometry with ultracold atoms have emerged as one of the most advanced technologies. These instruments combine high accuracy, sensitivity, and long-term stability with immunity to instrumental drift, portability, and high data-rate.

For achieving high absolute accuracy of a gravimetric sensor, correction of systematic shifts is required. The systematic shifts in a QG include the first-order light shift [2], the two-photon light shift (TPLS) [3], the shift induced by additional laser lines of the raman beams formed using an electro-optic modulator (EOM) [4], interference line asymmetry caused shift (LACS) [5,6] and others.

The present report describes the results of studies devoted to the measurement and compensation of the systematic shifts mentioned above in a QG (for a typical interrogation time of T = 10 ms). Compensation of the first-order light shift improved the absolute measurement accuracy by approximately 100 mGal for our QG. It was implemented using an algorithm [7] based on alternating the direction of the raman beams effective wave vector. An investigation of the shift induced by additional laser lines of raman beams and TPLS was carried out. It was shown that the magnitude of these shifts can reach up to 10 mGal for our setup. Furthermore, this work presents an analysis of the TPLS induced by EOM sidebands. Calculations showed that this shift could reach up to 400 μGal for our QG.

In addition, an experimental investigation of the LACS was performed for the first time. It was demonstrated that the magnitude of this shift decreases proportionally to T^{-3} with increasing T. For T values in the millisecond range, the LACS magnitude reaches 0.1–1 mGal. The obtained experimental results are in good agreement with our theoretical predictions [5].

This work was carried out with the financial support of the Russian Science Foundation (Grant № 23-12-00182-P).

References

[1] J. Vovrosh et al., Sensors **23**, 7651 (2023).
[2] A. Peters et al., Metrologia **38**, 25 (2001).
[3] O. Carraz et al., Phys. Rev. A **86**, 033605 (2012).
[4] A. Gauguet et al., Phys. Rev. A **78**, 043615 (2008).
[5] V. Yudin et al., JETP Lett. **122**, 737-742 (2025).
[6] D. Kapusta et al., JETP Lett. **123**, 388-392 (2026).
[7] Y. Bidel et al., Appl. Phys. Lett. **14**, 144107 (2013).

Создание двухкаскадного параметрического преобразователя частоты на длине волны 6,45 мкм

<u>М.В. Вострикова</u>[1,2], С.Э. Сере[2], Е.Ю. Ерушин[1,2], А.А. Бойко[1,2], Г.С. Шевырдяева[3], Д.В. Бадиков[3], А.А. Карапузиков[4], Н.Ю. Костюкова [1,2]

[1]Новосибирский государственный университет, г. Новосибирск, Россия
[2]Институт лазерной физики СО РАН, г. Новосибирск, Россия
[3]Кубанский государственный университет, г. Краснодар, Россия
[4]ООО «Специальные технологии», г. Новосибирск, Россия
e-mail: m.vostrikova@g.nsu.ru

В настоящее время источники излучения среднего-ИК диапазона пользуются особой популярностью во многих областях науки. Для разных применений требуются источники излучения различных и иногда специфических спектральных диапазонов. Создание таких источников может оказаться очень сложной и экономически не выгодной задачей. Например, в лазерной хирургии применяют метод лазерной абляции с использованием источников излучения с длиной волны 6,45 мкм. Выбор спектрального диапазона, в данном случае, определяется исходя из соотношения между эффективностью абляции и размером области повреждения соседних тканей [1]. Одним из возможных способов генерации излучения с указанной выше длиной волны является параметрическое преобразование частоты, то есть реализация параметрического генератора света (ПГС). Возможность непрерывной перестройки длины волны ПГС в широком спектральном диапазоне (например, ~5–9 мкм для ПГС на основе кристалла $BaGa_2GeS_6$ (BGGS) [2]) позволяет осуществлять тонкую настройку длины волны излучения в соответствии с требованиями конкретного приложения.

В данной работе пойдет речь о создании двухкаскадного параметрического преобразователя частоты на длине волны 6,45 мкм на кристаллах BGGS, где в роли первого каскада выступает ПГС, излучение которого вводится во второй кристалл BGGS, где происходит оптическое параметрическое усиление. Накачка осуществлялась излучением Nd:YAG лазера на длине волны 1,064 мкм. Были определены выходные энергетические характеристики данного источника излучения. Максимальная энергия холостой волны на выходе второго каскада составила 7,5 мДж при энергии накачки усилителя 174,4 мДж (эффективности преобразования 4,2 %). Во время проведения эксперимента было замечено, что при увеличении энергии накачки длительность импульса сигнальной волны изменялась с 14,4 до 16,3 нс, что свидетельствует об увеличении эффективности преобразования, а ширина спектральной линии возрастала с 1 до 1,6 нм. Также, были измерены пространственные характеристики выходного излучения, а именно параметр качества пучка, который по оси X составил 53,7, а по оси Y – 79,4 при энергии усилителя 110 мДж и энергии накачки ПГС 50 мДж. В сравнении с ранее разработанной однокаскадной схемой параметрического генератора света [2] реализованная конфигурация характеризуется более высоким уровнем выходной энергии источника излучения.

Работа выполнена при поддержке государственного задания ИЛФ СО РАН (грант FWGU-2026-0005).

Литература

[1] Edwards G., Logan R., Copeland M. et al., Nature. 371, 416-418 (1994)
[2] Erushin E.Yu., Sere S.E., Vostrikova M.V., et al., Infrared Phys. Technol. 154, 106393 (2026)